



# O-GlcNAc modification of casein kinase 2 alpha alters the phosphoproteome

## Citation

Schwein, Paul Andrew. 2022. O-GlcNAc modification of casein kinase 2 alpha alters the phosphoproteome. Doctoral dissertation, Harvard University Graduate School of Arts and Sciences.

## Permanent link

<https://nrs.harvard.edu/URN-3:HUL.INSTREPOS:37372195>

## Terms of Use

This article was downloaded from Harvard University's DASH repository, and is made available under the terms and conditions applicable to Other Posted Material, as set forth at <http://nrs.harvard.edu/urn-3:HUL.InstRepos:dash.current.terms-of-use#LAA>

## Share Your Story

The Harvard community has made this article openly available. Please share how this access benefits you. [Submit a story](#).

[Accessibility](#)

HARVARD UNIVERSITY  
Graduate School of Arts and Sciences




DISSERTATION ACCEPTANCE CERTIFICATE

The undersigned, appointed by the  
Department of Molecular and Cellular Biology  
have examined a dissertation entitled  
O-GlcNAc modification of casein kinase 2 alpha alters the phosphoproteome

presented by Paul Andrew Schwein

candidate for the degree of Doctor of Philosophy and hereby  
certify that it is worthy of acceptance.

Signature  \_\_\_\_\_

Typed name: Prof. Rachele Gaudet

Signature  \_\_\_\_\_  
Brian Liau (Apr 20, 2022 12:00 EDT)

Typed name: Prof. Brian Liau

Signature  \_\_\_\_\_

Typed name: Prof. Suzanne Walker

Signature \_\_\_\_\_

Typed name: Prof.

Signature \_\_\_\_\_

Typed name: Prof.

Date: April 19, 2022

*O-GlcNAc modification of  
casein kinase 2 alpha alters the phosphoproteome*

A dissertation presented

by

Paul Andrew Schwein

to

The Department of Molecular and Cellular Biology

in partial fulfillment of the requirements for the degree of

Doctor of Philosophy

in the subject of

Biology

Harvard University

Cambridge, Massachusetts

April 2022

© 2022 Paul Andrew Schwein

All rights reserved

## **O-GlcNAc modification of casein kinase 2 alpha alters the phosphoproteome**

### **Abstract**

Post-translational modifications govern protein function and are paramount to many signaling networks in cells. How different post-translational modifications intersect to result in complex signaling outcomes represents a fascinating field of study. O-GlcNAc is an essential carbohydrate post-translational modification that intersects with phosphorylation signaling pathways in two major ways – via crosstalk on protein substrates, or by direct modification of the kinases that write the phosphate modification. Disparate cellular pathways are tuned to the nutritional state of the cell through the O-GlcNAc modification by the highly promiscuous enzyme pair that regulates it. In Chapter 1, I discuss the history of the O-GlcNAc modification, methods to manipulate it, and how O-GlcNAc intersects with phosphorylation and with kinases. In Chapter 2, I discuss the role of O-GlcNAc in T cell activation, and efforts to identify the glycosite of tyrosine kinase Zap-70 using site-directed mutagenesis, mass spectrometry, and techniques based in Western blotting to visualize O-GlcNAc stoichiometry. In Chapter 3, I discuss another O-GlcNAcylated kinase, casein kinase 2 alpha, the catalytic subunit of the ubiquitously expressed and constitutively active kinase CK2. Here, complementary targeted O-GlcNAc editors, nanobody-OGT and -splitOGA, are applied to selectively write and erase O-GlcNAc from a tagged CK2 $\alpha$ . These tools effectively and selectively edit the S347 glycosite on CK2 $\alpha$ . Using quantitative phosphoproteomics, we report 51 proteins whose enrichment changes as a function of editing O-GlcNAc on CK2 $\alpha$ , including HDAC1, HDAC2, ENSA, SMARCD1, and PABPN1. Specific phosphosites on HDAC1 (S393) and HDAC2 (S394), both reported CK2 substrates, are significantly enhanced by O-GlcNAcylation of CK2 $\alpha$ . Chapter 4 contains a discussion on how these data will propel future studies on the crosstalk between O-GlcNAc and phosphorylation.

## Acknowledgements

While the work presented in this dissertation is primarily associated with my name, the cast of characters who have provided me with academic and emotional support during my graduate school experience is what made all of it happen. I'll begin by thanking those involved in my academic experience at Harvard. What I was able to accomplish with CK2 $\alpha$  would not have been possible without the herculean efforts of Dr. Daniel Ramirez and Dr. Yun Ge in leading the development of the nanobody-OGT and nanobody-splitOGA systems respectively. I am equally grateful to the coauthors of my *ACS Chemical Biology* manuscript – Dr. Yun Ge again, Dr. Bo Yang, Alexandria D'Souza, Alison Mody, and Dr. Dacheng Shen. Conducting this work in the Woo lab has been a joy since day one. I am especially appreciative of past members Dr. Erin Heim, Dr. Chant Aonbangkhen, Erik Owen, and Dr. Hope Flaxman, as well as current members David Miyamoto, Alexander West, Zhi “Lindsey” Lin, and Farah Kabir for their genuine friendship in addition to their scientific insights. I am also thankful for the unimpeachable insights of my Dissertation Advisory Committee – Dr. Rachelle Gaudet, Dr. Suzanne Walker, and Dr. Brian Liao – on the CK2 $\alpha$  work and on my personal development. Finally, I am immensely grateful for the support of the fearless leader of the Woo lab, my advisor Dr. Christina Woo. I will never forget her patience, her sagacity, or her unwavering belief in me to see this PhD through to the end.

Before arriving at Harvard, several past teachers and mentors left a lasting impact with me that contributed to my love of education and commitment toward scholarship. Mrs. Weingartner, my teacher for both 4<sup>th</sup> and 5<sup>th</sup> grade, devoted memorable time outside of school to train me for external competitions that challenged my knowledge. Mrs. Golden, thank you for being a fantastic first science teacher. At Cypress Bay High School, Mr. Boswell, Mrs. Russo, and Mr. Rose taught me honors chemistry, AP Chemistry, and AP Physics C respectively. Their dedication as teachers inspired me to pursue science, while my AP English Language and

Literature teachers, Dr. Amparo and Mrs. Waite, refined my rhetorical analysis skills and writing style to make me a better communicator. I am eternally grateful to them all.

At the Massachusetts Institute of Technology, multiple instructors and advisors played memorable roles in my scientific development. To Dr. Hazel Sive, my first biology professor and academic advisor, I can't wait to show you that I have my PhD in hand. To my 7.02 instructors Dr. Vanessa Cheung and Dr. Ayce Yesilaltay, thank you for a fantastic class. 7.02 was such a positive environment to learn research fundamentals. To my three research advisors, Dr. Laurie Boyer, Dr. Jean-Francois Hamel, and Dr. Jing-Ke Weng, thank you all for making space in your laboratories for me and devoting resources toward refining my research techniques such that I felt ready for graduate school. In the Weng lab, Dr. Olesya Levsh was a fantastic mentor, and I'll never forget her patience and generosity with her time.

I'd finally like to acknowledge those who have supported me in other ways during my time in graduate school. Teaching LS1a and MCB60 was my favorite part of my time as a graduate student, and I am grateful to all of the undergraduate students I had the privilege to instruct. To fellow GSAS community members Dr. Garth Coombs and Romaine Campbell, thank you for the fun times and glorious banter. To my fellow MCO cohort members Nicole Bush, Alexander McQuown, Cassidy Madison, Elizabeth May, and Stephania Irwin, you were some of my first connections at Harvard, and I thank you for your friendship. I am eternally grateful for the emotional support of my parents, Ana Gomez-Schwein and Paul D. Schwein, and my sister, Gabriella Schwein. They consistently checked in on me to let me know I am capable and I am loved. Finally, to my partner Thomas G. O'Neill... you're one of a kind. Since moving in together during my G3 year, you have gone above and beyond as a significant other in the ways you provide me with emotional support, keep me focused, and maintain our life together, all while advancing your own career. I genuinely admire your work ethic and resilience, and appreciate your presence in my life more than I can express in words.

## Table of Contents

<i>Title Page</i> .....	<i>i</i>
<i>Copyright Page</i> .....	<i>ii</i>
<i>Abstract</i> .....	<i>iii</i>
<i>Acknowledgements</i> .....	<i>iv</i>
<i>Table of Contents</i> .....	<i>vi</i>
<i>List of Figures</i> .....	<i>vii</i>
<i>List of Tables</i> .....	<i>viii</i>
<b>Chapter 1: Regulation of phosphorylation by the O-GlcNAc modification</b> .....	<b>1</b>
1.1 The O-GlcNAc modification .....	3
1.2 Methods for detecting and mapping O-GlcNAc .....	7
1.3 Methods for manipulating O-GlcNAc in cells.....	10
1.4 Phosphorylation and kinases .....	13
1.5 Intersection of O-GlcNAc and phosphorylation .....	15
1.6 O-GlcNAc regulation of kinases .....	17
<b>Chapter 2: O-GlcNAc in T cells</b> .....	<b>27</b>
2.1 O-GlcNAc and T cell activation.....	29
2.2 Zap-70 .....	36
2.3 Discussion .....	44
2.4 Materials and Methods .....	46
<b>Chapter 3: O-GlcNAc on CK2<math>\alpha</math></b> .....	<b>51</b>
3.1 Introduction to CK2 .....	53
3.2 Manipulating glycosylation of CK2 $\alpha$ .....	56
3.3 CK2 $\alpha$ is glycosylated at S347 in human cells.....	60
3.4 CK2 $\alpha$ glycosylation affects the phosphoproteome.....	64
3.5 Limitations .....	74
3.6 Materials and Methods .....	75
<b>Chapter 4: Discussion</b> .....	<b>81</b>
<b>Appendix</b> .....	<b>85</b>
Supplementary Figures .....	85
Supplementary Tables.....	97
<b>References</b> .....	<b>100</b>



## List of Figures

Figure 1.1.1 The O-GlcNAc post-translational modification .....	3
Figure 1.1.2 Structure and isoforms of human OGT .....	5
Figure 1.1.3 Structure and isoforms of human OGA.....	7
Figure 1.2.1 Workflow for isotope-targeted glycoproteomics (IsoTaG).....	10
Figure 1.3.1 Methods for regulating O-GlcNAc at global, protein-selective, and site-specific scales .....	11
Figure 1.3.2 Diagram of nanobody-OGT and -splitOGA system for protein-selective O-GlcNAc manipulation .....	12
Figure 1.4.1 The phosphate post-translational modification .....	13
Figure 1.5.1 Modes of crosstalk between O-GlcNAcylation and .....	16
Figure 1.5.2 Sequence motif for O-GlcNAc/phosphorylation crosstalk.....	17
Figure 1.6.1 The AGC Kinase family.....	18
Figure 1.6.2 The CMGC Kinase family.....	20
Figure 1.6.3 The CAMK Kinase family .....	21
Figure 1.6.4 The STE Kinase family.....	23
Figure 1.6.5 The CK1 Kinase family .....	23
Figure 1.6.6 TK and TKL Kinase families .....	24
Figure 2.1.1 Summary and timeline of influential publications in the field of O-GlcNAc in T cell activation.....	29
Figure 2.1.2 O-GlcNAcylated proteins in the T cell activation pathway.....	32
Figure 2.1.3 TCR-mediated T cell activation is hampered by OGT inhibition.....	34
Figure 2.1.4 Tyrosine phosphorylation of early T-cell activation proteins changes with OGT inhibition.....	36
Figure 2.2.1 Zap-70 is not glycosylated at S497 .....	38
Figure 2.2.2 PEG blot analysis of Zap-70 domains reveals multiple potential glycosites .	39
Figure 2.2.3 PEG blot analysis of candidate glycosites from mass spectrometry analysis .....	41
Figure 2.2.4 Additional negative controls in GalT1 labeling and PEG blot workflow reveal glycosylation levels comparable to background, unaffected by TMG treatment.....	42
Figure 2.2.5 Lentiviral transduction of Zap-70 in P116 cells results in lower Zap-70 expression compared to Jurkat cells.....	43
Figure 3.1.1 Graphical representations of (A) CK2 holoenzyme crystal structure and (B) CK2 $\alpha$ monomer primary sequence.....	54
Figure 3.2.1 – Endogenous CK2 $\alpha$ levels decrease following OGA inhibition.....	57
Figure 3.2.2 – Approach for selectively manipulating glycosylation on tagged CK2 $\alpha$ .....	58
Figure 3.2.3 Nanobody system selectively alters glycosylation of CK2 $\alpha$ .....	59
Figure 3.3.1 Experimental design to map the glycosite(s) of GFP-FLAG-CK2 $\alpha$ -EPEA .....	60
Figure 3.3.2 GFP-FLAG-CK2 $\alpha$ -EPEA is O-GlcNAcylated at Ser347 .....	61
Figure 3.3.3 GFP-FLAG-CK2 $\alpha$ -EPEA binds to endogenous CK2 $\beta$ .....	63
Figure 3.4.1 – Phosphoproteomics Workflow.....	64
Figure 3.4.2 O-GlcNAc on GFP-FLAG-CK2 $\alpha$ -EPEA affects the phosphoproteome.....	66
Figure 3.4.3 STRING network of phosphoproteins with a moderate/major increase in the nanobody-OGT condition, or moderate/major decrease in the nanobody-OGA condition	68
Figure 3.4.4 Further phosphoprotein analysis .....	70
Figure 3.4.5 O-GlcNAc on GFP-FLAG-CK2 $\alpha$ -EPEA affects specific phosphosites .....	73
Supplementary Figure 1 – EThcD spectrum assigned to Zap70-FLAG-EPEA T155 glycosite from HEK293T cells.....	85

Supplementary Figure 2 – EThcD spectrum assigned to Zap70-FLAG-EPEA T156 glycosite from HEK293T cells.....	86
Supplementary Figure 3 – EThcD spectrum assigned to Zap70-FLAG-EPEA S257 glycosite from HEK293T cells.....	87
Supplementary Figure 4 – EThcD spectrum assigned to Zap70-FLAG-EPEA S258 glycosite from HEK293T cells.....	88
Supplementary Figure 5 – Nanobody-OGT Phosphoprotein Level Normalization Box Plot .....	89
Supplementary Figure 6 – Nanobody-OGT Phosphoprotein Level Principal Component Analysis.....	90
Supplementary Figure 7 – Nanobody-splitOGA Phosphoprotein Level Normalization Box Plot .....	91
Supplementary Figure 8 – Nanobody-OGA Phosphoprotein Level Principal Component Analysis.....	92
Supplementary Figure 9 – Nanobody-OGT Phosphosite Level Normalization Box Plot ...	93
Supplementary Figure 10 – Nanobody-OGT Phosphosite Level Principal Component Analysis.....	94
Supplementary Figure 11 – Nanobody-splitOGA Phosphosite Level Normalization Box Plot .....	95
Supplementary Figure 12 – Nanobody-splitOGA Phosphosite Level Principal Component Analysis.....	96

## List of Tables

Table 2.4.1 Transfection reagents used for lentiviral production in HEK293T cells .....	50
Supplementary Table 1 – MS Data (protein level hits) .....	97
Supplementary Table 2 – MS Data (site level hits) .....	99

# **Chapter 1: Regulation of phosphorylation by the O-GlcNAc modification**

## **Adaptation**

Parts of this chapter are adapted from Schwein, P. A.; Woo, C. M., The O-GlcNAc Modification on Kinases. *ACS Chem Biol* **2020**, 15 (3), 602-617.

## **Contributions**

Both this chapter and the cited literature review were written in collaboration with Dr. Christina Woo.

## **Introduction**

Protein post-translational modifications (PTMs) significantly expand the chemical complexity of the proteome beyond what is encoded by the human genome to facilitate the regulation of proteins, integration of metabolic pathways, and transduction of biological signals. PTMs range in size and function and serve to integrate signals from discrete pathways. PTM precursor molecules are synthesized by the cell from various metabolic inputs. These are used as co-substrates by enzymes designed to install the PTM to specific proteins, resulting in one or many biological outcomes. Common examples of PTMs include phosphorylation, glycosylation, acetylation, methylation, and ubiquitination, each of which tune protein function and/or stability in different ways. Furthermore, one PTM may affect the occupancy of another PTM on the same protein to integrate signals and tailor protein function in a phenomenon termed PTM crosstalk.

O-linked N-Acetyl glucosamine (O-GlcNAc), a monomeric glycan, and phosphorylation are two PTMs that occur on serine and threonine residues of nuclear and cytoplasmic proteins. Both are reversible and are regulated by separate writers and erasers. Phosphate groups are installed by >500 kinases and removed by ~200 phosphatases,<sup>1</sup> resulting in a broad repertoire of substrates whose phosphosites are regulated independently. By contrast, O-GlcNAc is regulated by only one enzyme pair – O-GlcNAc transferase (OGT) installs O-GlcNAc, and O-GlcNAcase (OGA) removes O-GlcNAc from protein substrates. O-GlcNAc sites often occur in close proximity

(within 1–9 residues) to known phosphosites, and many examples of Ser/Thr residues that serve as glycosites or phosphosites exist.<sup>2, 3</sup> Considerable evidence describing the relationship between O-GlcNAc and phosphorylation in the context of how they regulate the occupancy of one another on the same protein, i.e. PTM crosstalk, has been described.<sup>3, 4</sup> An additional form of phosphorylation regulation by O-GlcNAc is through direct modification of the writers of the phosphate modification, kinases. This chapter will briefly introduce the O-GlcNAc and phosphorylation modifications, respectively, and describe two models for their crosstalk, first with respect to competitive or cooperative occupancy on protein substrates and second with respect to regulation of kinases by O-GlcNAc.

### 1.1 The O-GlcNAc modification

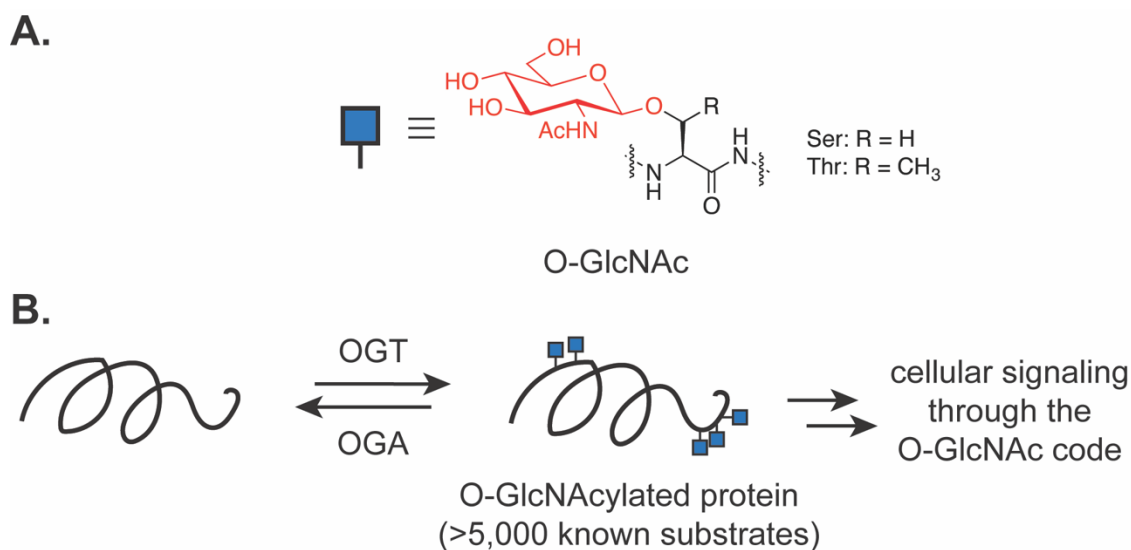


**Figure 1.1.1 The O-GlcNAc post-translational modification. (A)** Chemical structure of O-GlcNAc as it exists when covalently attached to serine or threonine residues of proteins. O-GlcNAc is represented as a blue square here and in subsequent figures. **(B)** O-GlcNAc occupancy on proteins is mediated by the OGT/OGA enzyme pair. To date, over 5,000 proteins have been identified as O-GlcNAc modified.<sup>5</sup>

O-GlcNAc is a monomeric glycan found on serine or threonine residues of thousands of nuclear, cytosolic, and mitochondrial proteins<sup>5</sup> (Figure 1.1.1A). O-GlcNAc was first discovered from mammalian cells in 1984.<sup>6</sup> The O-GlcNAc modification on proteins is regulated by only one

enzyme pair (Figure 1.1.1B). The enzyme O-GlcNAc transferase (OGT) installs O-GlcNAc onto proteins, while O-GlcNAcase (OGA) removes it. Following the discovery of OGT from rat liver extracts in 1997,<sup>7</sup> other intracellular O-GlcNAc transferase genes were discovered in plants<sup>8</sup> and fungi. O-GlcNAc is essential as deletion of the gene encoding OGT in mice leads to embryonic lethality,<sup>9</sup> while deletion of the OGA gene results in perinatal death.<sup>10</sup> The molecular precursor to O-GlcNAc, UDP-GlcNAc, is derived from the hexosamine biosynthetic pathway. Adequate flux through this pathway, requiring inputs from metabolism of glucose, nucleotides, amino acids, and fatty acids, is necessary to maintain homeostatic levels of UDP-GlcNAc – therefore, a function of O-GlcNAc is to tune disparate cellular pathways to the nutritional state of the cell.<sup>11</sup> Another function is to tune the occupancy of other PTMs on the same protein, like phosphorylation.<sup>4, 12</sup>

Like the O-GlcNAc modification itself, the enzymes OGT and OGA that install or remove O-GlcNAc have multifaceted roles that are still under investigation. OGT is a glycosyltransferase that is expressed in all mammalian tissues and possesses a tetratricopeptide repeat (TPR) domain and a catalytic domain (Figure 1.1.2). OGT is expressed in three isoforms that vary by the length of the TPR domain, termed the nucleocytoplasmic or full-length OGT (ncOGT, 13.5 TPRs), the mitochondrial isoform (mOGT, 9 TPRs), and the short isoform (sOGT, 2.5 TPRs) (Figure 1.1.2A).<sup>13</sup> The TPR domain mediates protein–protein interactions (PPIs) of OGT, affecting substrate and glycosite selection.<sup>14-17</sup> Structurally, the TPR domain forms a series of stacked alpha-helical domains that form a coiled tube-like structure that funnels polypeptide sequences to the catalytic domain primarily through associations with asparagine and aspartate residues lining the domain.<sup>14, 18</sup> The catalytic domain transfers the sugar from a UDP-GlcNAc donor to serine or threonine residues that are positioned by the TPR domain (Figure 1.1.2B). Mutation of H508 or K852 reduce binding of UDP-GlcNAc and thus impair catalytic activity. The catalytic domain catalyzes additional chemistries, including transfer of UDP-GlcNAc to cysteine residues,<sup>19</sup> transfer of glucose,<sup>20</sup> proteolysis,<sup>21</sup> and deamidation.<sup>22</sup> In cells, OGT forms dimers through associations in the TPR domain that also alter UDP-GlcNAc binding constants.<sup>23-25</sup> OGT possesses three of

its own O-GlcNAc sites and is modified by other PTMs, including phosphorylation, ubiquitinylation, and sumoylation.<sup>26</sup> OGT appears to require accessory proteins to modify protein substrates efficiently, as reduction or removal of the TPR domain reduces activity with full length proteins, but retains catalytic activity with synthetic peptides *in vitro*.<sup>13, 18</sup> Further exploration of the substrate selection mechanisms for OGT will improve the understanding of the regulatory role of O-GlcNAc and its dynamic cycling.

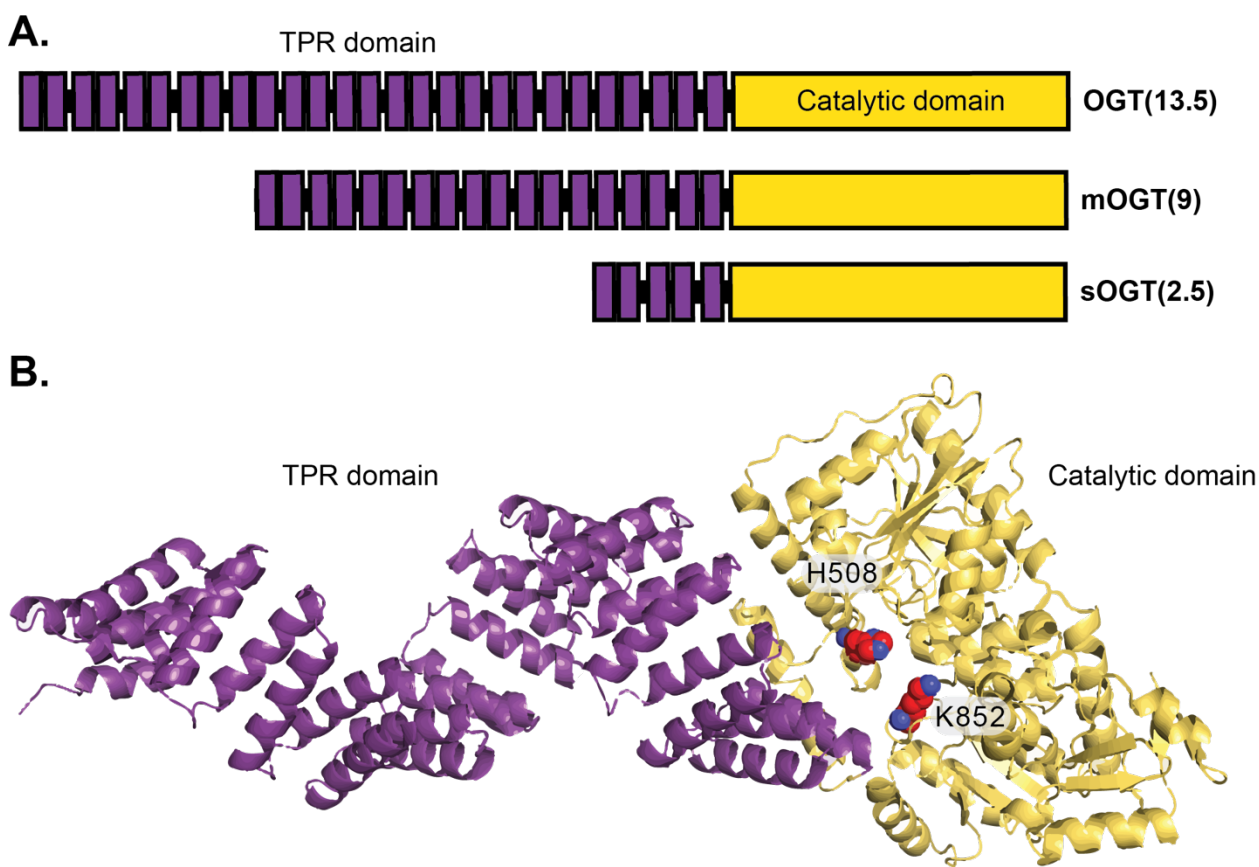


**Figure 1.1.2 Structure and isoforms of human OGT. (A)** Linear representation of the full-length (OGT(13.5)), mitochondrial (mOGT(9)) and short (sOGT(2.5)) isoforms of OGT. Each is distinguished by the indicated number of repeats in their TPR domains. **(B)** Tertiary structure of full-length OGT with the TPR domain in purple and catalytic domain in yellow. Point mutations at the highlighted residues H508 or K852 decrease catalytic activity.

O-GlcNAc is catalytically removed from proteins by OGA. Similar to OGT, the mechanisms of how OGA selects from numerous O-GlcNAc substrates and the functions of the separate

domains of OGA are still emerging. OGA is composed of three domains: a catalytic domain and a histone acetyltransferase (HAT)-like domain connected by a stalk domain (Figure 1.1.3A).<sup>27</sup> The stalk domain is interspersed with an unstructured region that forms a binding interaction with OGT.<sup>28</sup> OGA is encoded by a single gene that is expressed as two main isoforms in vertebrates, the full length isoform, OGA(I), and a short isoform lacking the C-terminal HAT-like domain, OGA(II).<sup>29</sup> Full-length OGA(I) is a nucleocytoplasmic enzyme, while OGA(II) is found predominantly in the nucleus and in lipid droplets.<sup>30</sup> The crystal structure of human OGA had eluded definition until recently (Figure 1.1.3B).<sup>31-33</sup> These structures of OGA(II) revealed a remarkable homodimer, wherein the stalk domain of one monomer covers the catalytic domain of the other monomer to create a substrate-binding cleft.<sup>32</sup> A series of contacts between the stalk domains stabilize the homodimer. OGA is regulated at least in part by an O-GlcNAc-related feedback mechanism that triggers gene expression; inhibition of OGA by Thiamet G treatment causes a compensatory increase in OGA expression and decrease in OGT expression.<sup>34</sup> Large-scale profiling studies have revealed several sites for ubiquitination and phosphorylation of OGA, including an O-GlcNAc site at S405, indicating possible regulation by OGT.<sup>35</sup> The biochemical characterization of these modification sites may illuminate additional mechanisms of OGA regulation.



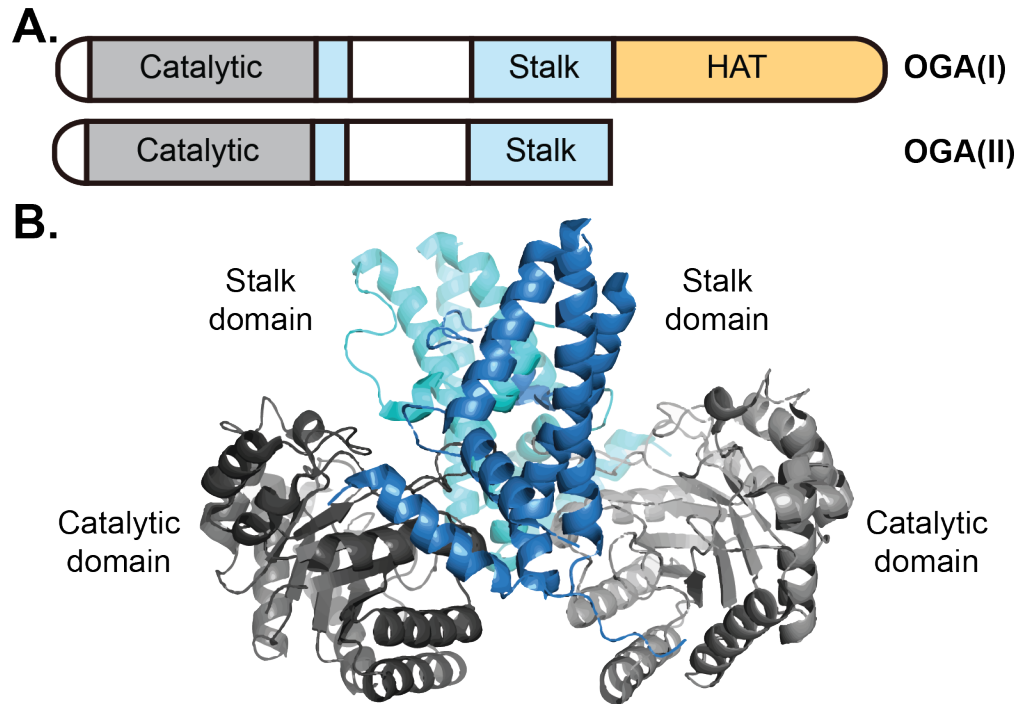


**Figure 1.1.3 Structure and isoforms of human OGA.** (A) Linear representation of the OGA(I) and OGA(II). OGA(II) lacks the C-terminal HAT domain. (B) Quaternary structure of the OGA(II) homodimer with the catalytic domain in gray and the stalk domain in blue (PDB ID: 5UN9).<sup>32</sup>

## 1.2 Methods for detecting and mapping O-GlcNAc

Compared to other PTMs, O-GlcNAc has historically been difficult to detect.<sup>36</sup> In general, changes in O-GlcNAc levels do not affect glycoprotein migration during gel electrophoresis, and O-GlcNAc is enzymatically labile and rapidly removed from proteins when the cell is damaged or lysed. Furthermore, O-GlcNAc is also chemically labile to common mass spectrometry (MS)-based mapping techniques to analyze PTMs, such as collision-induced dissociation (CID) during secondary MS.<sup>37</sup> Analysis of O-GlcNAc by MS pushes detection limits due to occurrence of O-GlcNAc at substoichiometric levels on the protein, ion suppression of the glycopeptide in the presence of unmodified peptides, and facile fragmentation of the glycan from the peptide during ionization processes in the mass spectrometer.<sup>38, 39</sup> Recently, advances in chemical glycoproteomics have drastically accelerated the ability to map modification sites in the global proteome. These advances have recently been reviewed.<sup>40</sup>

Although O-GlcNAc is found widely throughout the nucleocytoplasmic proteome, its substoichiometric modification site occupancy necessitates the combination of an efficient enrichment method and a sensitive analytical detection method. The enrichment of O-GlcNAc has been achieved by several means. Lectin weak affinity column chromatography using wheat germ agglutinin (WGA) enables the enrichment of O-GlcNAc and other sugars. Alternatively, the introduction of bioorthogonal handles via metabolic labeling<sup>41, 42</sup> or chemoenzymatic labeling<sup>43</sup> results in the selective installation of an azido-sugar as a reporter for O-GlcNAc on proteins, enabling the further functionalization with a variety of reporting strategies (e.g., fluorescence microscopy, anti-biotin Western blot, mass spectrometry). Metabolic labeling involves the addition of a sugar carrying a bioorthogonal handle, like an azide, to living systems that metabolically incorporate the azido-sugar to protein substrates. Several sugar reporter molecules for O-GlcNAc have been developed, including Ac<sub>4</sub>GalNAz or Ac<sub>4</sub>GlcNAz, or O-GlcNAc-specific reporters 6AlkGlcNAc,<sup>44</sup> 6AzGlcNAc,<sup>45</sup> 1,3-Ac<sub>2</sub>GalNAz, and 1,3-Pr<sub>2</sub>GalNAz.<sup>46</sup> The latter two were validated to reduce background conjugation to cysteine residues (S-glycosylation) from other metabolic reporters.<sup>47</sup> Chemoenzymatic labeling uses a mutant GalT1 enzyme that accepts azido- or keto-sugars for enzymatic labeling of the O-GlcNAc residue itself.<sup>48</sup> The azide introduces a handle that is selectively tagged with reporter molecules using copper-catalyzed azide–alkyne cycloaddition (CuAAC) chemistry. Reaction of the azide groups with cleavable biotin tags and isolation of the O-GlcNAc peptide enables maps of O-GlcNAc modification sites throughout the proteome. Both metabolic labeling and chemoenzymatic labeling may produce off-target labeling products due to the addition of reactive azido-sugar intermediates or promiscuity of the labeling for additional glycan types.<sup>47, 49</sup> Thus, the assignment of O-GlcNAcylated proteins is best performed at glycosite-level confirmation.

Analysis of the O-GlcNAc modification is commonly achieved by Western blot or MS-based proteomics. Visualization of O-GlcNAcylated proteins by Western blot is commonly performed using the O-GlcNAc CTD110.6, RL2, or 18B10.C7 primary antibodies. If the glycoprotein is

labeled by an azido-sugar, a mass shift assay using a 5-kilodalton PEG mass tag carrying an alkynyl functional group may be performed to determine the stoichiometry of the O-GlcNAc modification on individual proteins.<sup>50</sup> The intensity of the shifted bands relative to the unshifted band allows for determination of O-GlcNAc stoichiometry. To characterize protein glycosite(s), mass spectrometry-based proteomics has emerged as the primary mechanism for site-specific mapping of the O-GlcNAc modification site on individual proteins to the complex proteome. However, due to the chemical lability of the O-linked glycosidic bond from the peptide backbone by CID or higher-energy CID (HCD) resulting in altered fragmentation mechanisms for glycopeptides, the assignment of the glycopeptide species is challenging. In cases of successful identification of the glycopeptide, the glycosite may only be localized to the serine and threonine residues in the peptide sequence. Solutions to this challenge included determination of the modification site using a sequence of induced beta-elimination of O-GlcNAc from the peptide backbone, followed by controlled Michael addition of dithiothreitol as a reporter for the glycosite (BEMAD), yielding early insight to the O-GlcNAc proteome.<sup>51</sup> The further development of electron-transfer dissociation (ETD) and electron-transfer higher energy collision induced dissociation (EthCD) methods on high resolution mass spectrometers enabled the detection of O-GlcNAcylated peptides via a fragmentation method that leaves the glycosidic bond intact. Chemical glycoproteomics methods, such as Isotope Targeted Glycoproteomics (IsoTaG), combine metabolic labeling with enrichment to map exactly when and where O-GlcNAc is modifying the protein network (Figure 1.2.1).<sup>52</sup> The development of efficient enrichment methods for O-GlcNAc coupled to advances in MS technology have drastically increased the number of O-GlcNAc sites that have been identified from the whole proteome of multiple species.<sup>35, 53-55</sup>

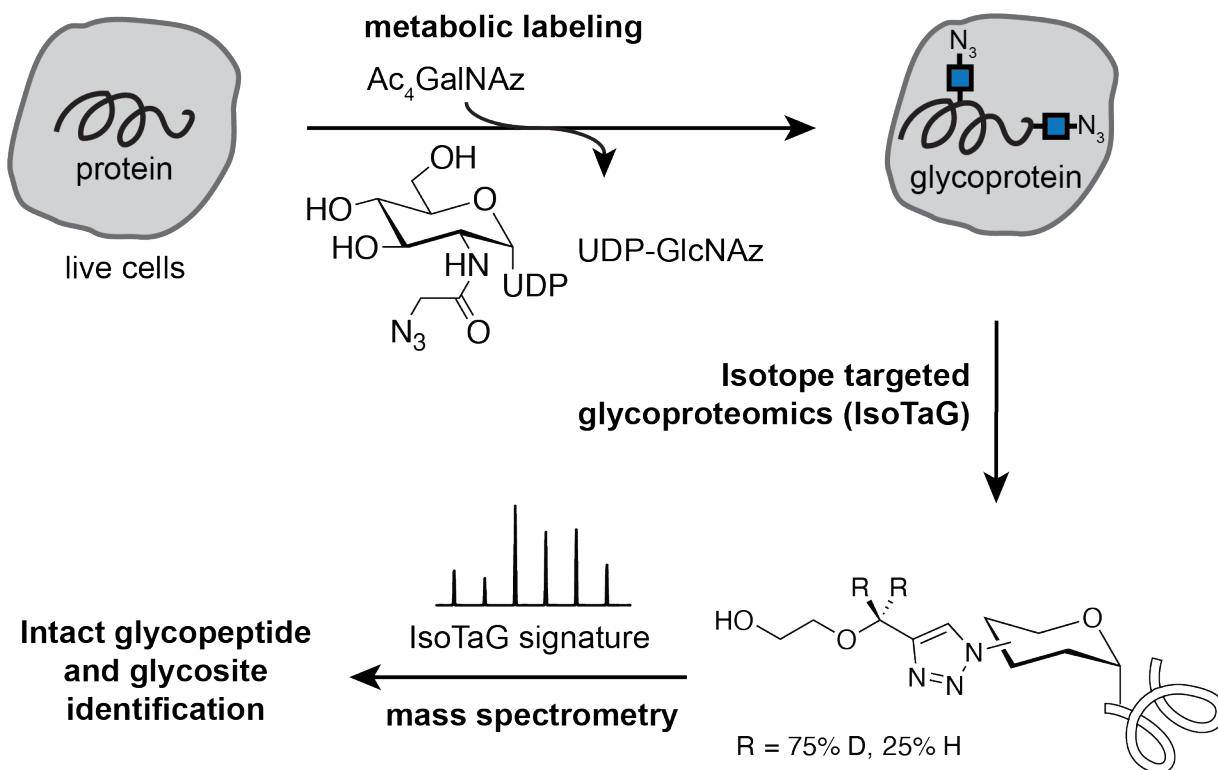


**Figure 1.2.1 Workflow for isotope-targeted glycoproteomics (IsoTaG).** Live cells are labeled with an azido sugar (e.g.,  $Ac_4GalNAz$ ) as a reporter for the O-GlcNAc modification. Enrichment, digestion, and acid cleavage of the tag release the modified glycopeptides for characterization by MS.

### 1.3 Methods for manipulating O-GlcNAc in cells

In addition to the array of methods for detection of O-GlcNAc, a number of techniques are available for regulating O-GlcNAc in cells across scales (Figure 1.3.1). Global O-GlcNAc levels can be manipulated through genetic and chemical methods. Global O-GlcNAc levels can be increased through OGT overexpression, knockout of the OGA gene, or treatment with a chemical inhibitor of OGA. For chemical OGA inhibition, the general N-acetylhexosaminidase inhibitor PUGNAc<sup>27</sup> was used prior to the development of Thiamet G by Vocadlo and co-workers.<sup>56</sup> Comparatively, Thiamet G has less toxicity and higher specificity to OGA than PUGNAc. Conversely, global O-GlcNAc levels can be decreased through OGA overexpression, genetic OGT knockout, or treating cells with a chemical OGT inhibitor, such as  $Ac_4-5S-GlcNAc$ <sup>57</sup> or OSMI.<sup>58</sup> The first OSMI compound, OSMI-1, was discovered by Walker and co-workers though

high-throughput screening. Structure-based evolution led to the development of OSMI-4, which is cell-permeable and possesses a  $\sim 3\mu\text{M}$   $\text{EC}_{50}$  in HEK293T cells. All OSMI molecules demonstrate higher specificity toward OGT compared to 5S-GlcNAc. These chemical tools are useful for studying the holistic effects of O-GlcNAc on the cell, but additional studies are needed to correlate observations made at the cellular level to specific glycoproteins or glycosites.

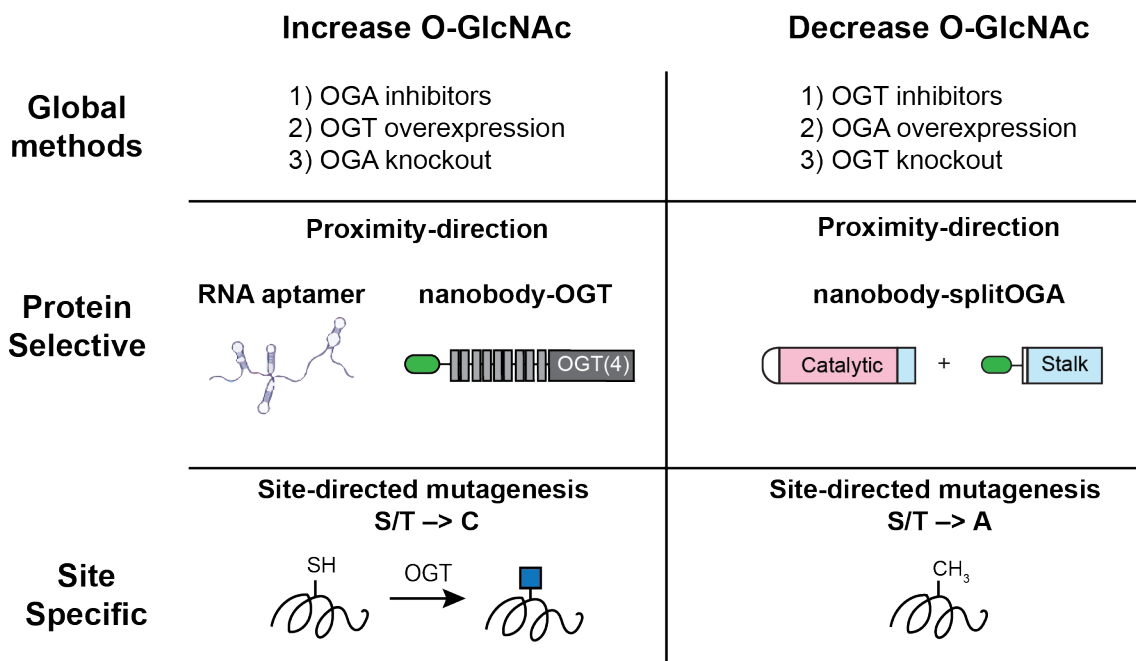


**Figure 1.3.1 Methods for regulating O-GlcNAc at global,<sup>56, 58</sup> protein-selective,<sup>59-61</sup> and site-specific<sup>62</sup> scales.** Figure is adapted from *Current Protocols* Vol. 1, e117.<sup>61</sup>

To ascertain glycoprotein- or glycosite-level detail, more specific O-GlcNAc tuning methods are appropriate. If the glycosite of interest is known, site-directed mutagenesis can be employed to convert the site to alanine to eliminate glycosylation, or to cysteine to introduce an S-GlcNAc site modifiable by OGT, but unable to be hydrolyzed by OGA.<sup>62</sup> Van Aalten and co-workers report

that the CTD110.6 antibody is best for detecting mutagenized S-GlcNAc sites, as well as the GalT1 labeling protocol followed by an orthogonal detection method.

If the glycosite is not known, or there are multiple glycosites on the protein of interest, recently reported proximity-directed mutants of OGT and OGA can be used (Figure 1.3.2).<sup>61</sup> In these systems, a truncated OGT<sup>59</sup> or truncated and split OGA<sup>60</sup> is fused to a nanobody directed toward the protein of interest. Nanobodies are small, single-domain protein fragments derived from the antigen-binding domain of camelid antibodies.<sup>63</sup> They bind specific epitopes with high specificity, similar to canonical antibodies. Nanobodies in the nanobody-OGT/splitOGA system engage their targets through direct binding to the endogenous glycoprotein, if a nanobody for it is commercially available, or to a short tag (e.g., EPEA, Ubc) on an engineered version of that protein. Protein-selective O-GlcNAcylation has also been tested with OGT using an RNA aptamer fusion instead of a nanobody. This was described by Yi Zhu at Johns Hopkins University, and is discussed in Dr. Zhu's thesis.<sup>64</sup>

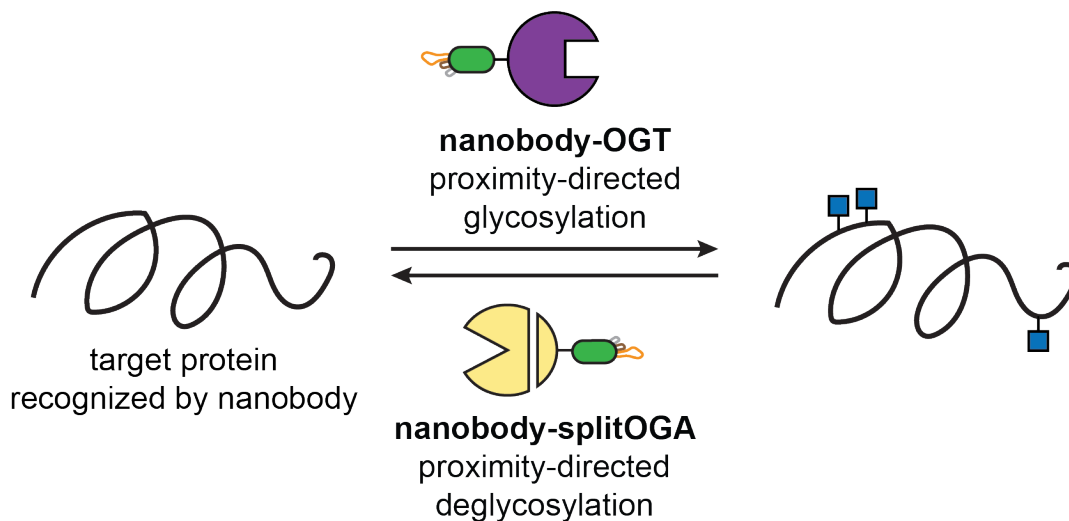


**Figure 1.3.2 Diagram of nanobody-OGT and -splitOGA system for protein-selective O-GlcNAc manipulation.**

## 1.4 Phosphorylation and kinases

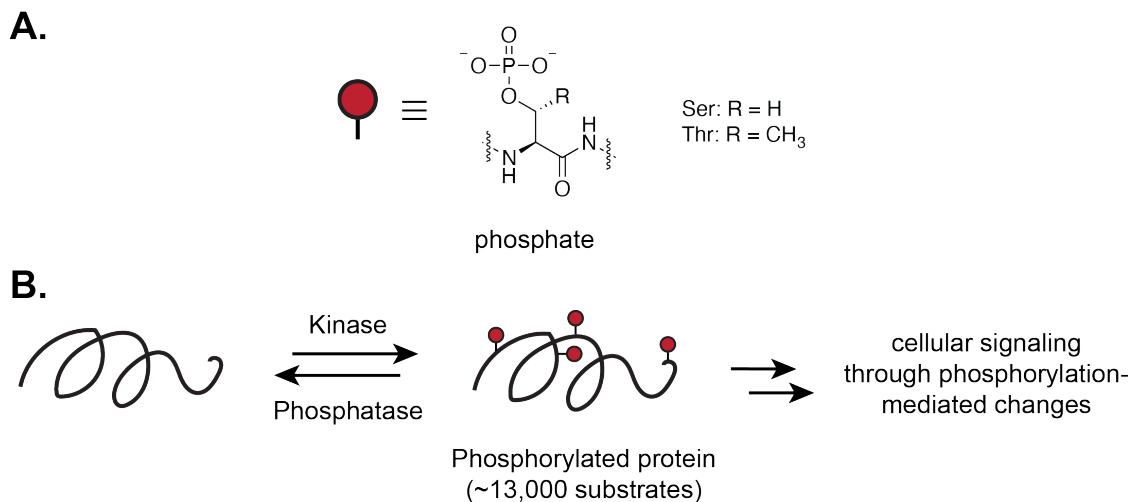


**Figure 1.4.1 The phosphate post-translational modification. (A)** Chemical structure of a phosphate group on serine or threonine residues of proteins. Phosphate is represented as a red circle here and in subsequent figures. **(B)** Phosphorylation of proteins is catalyzed by kinases. Dephosphorylation is catalyzed by phosphatases. It is estimated that ~13,000 proteins in humans are phosphorylated.<sup>65</sup>

Phosphorylation is arguably one of the most well-studied PTMs to proteins (Figure 1.4.1A). The discovery that transfer of a phosphate group to an enzyme could convert it from an inactive to an active state occurred in 1955 in the case of phosphorylase.<sup>66</sup> Previous work demonstrated that phosphorylase, the enzyme responsible for converting glycogen to glucose-1-phosphate, existed in two forms after purification from rabbit musculoskeletal extracts<sup>67</sup> – phosphorylase *a*, an active form, and phosphorylase *b*, an inactive form. Fischer and Krebs subsequently confirmed that conversion from phosphorylase *b* to phosphorylase *a* was possible in the presence of musculoskeletal extract supplemented with a divalent metal ion and ATP.<sup>66</sup> Later studies led to the discovery of phosphorylase kinase, the enzyme responsible for phosphorylase phosphorylation, and that this enzyme is also activated via phosphorylation, in this case by PKA.<sup>68</sup> Thus, protein phosphorylation became acknowledged as a key regulatory mechanism for tuning enzyme activity.

Two families of enzymes regulate the phosphate PTM. The phosphorylation reaction is catalyzed by protein kinases, and the reverse reaction, dephosphorylation, is catalyzed by phosphatases (Figure 1.4.1B). 518 protein kinases and approximately 200 phosphatases are encoded in the human genome.<sup>1</sup> Both families of enzymes work independently to regulate the phosphoproteome. The canonically phosphorylated amino acids in eukaryotes are serine, threonine, and tyrosine. Of the canonical phosphosites, the distribution of pSer, pThr, and pTyr sites is estimated to be 79.3%, 16.9%, and 3.8% respectively.<sup>69</sup> Phosphorylation of histidine, arginine, lysine, aspartate, glutamate, and cysteine have also been reported.<sup>70</sup> Further work is necessary to determine if these noncanonical phosphosites play a functional role, result from promiscuous kinase activity, or serve as intermediates for further chemical manipulation.

The kinase superfamily is divided into eight groups based on phylogeny – TK (tyrosine kinases), TKL (tyrosine kinase-like, but phosphorylate Ser/Thr sites), STE (MAPK family members), CK1, CAMK (Calmodulin/Calcium regulated), CMGC (CDK, MAPK, GSK3, and CLK families), AGC (PKA, PKC, PKG families), and atypical. Over 100 kinases are modified by O-GlcNAc, and glycosylated kinases are represented in each family.<sup>71</sup>

Several methodologies exist for detection of protein phosphorylation. Classically, cultured cells were supplemented with <sup>32</sup>P-orthophosphate, a phosphate group containing a radiolabeled phosphorus atom. This phosphorus isotope becomes incorporated into cellular ATP and subsequently leads to radiolabeled phosphosites. Phosphoproteins from these labeled cells could be detected by autoradiography following sodium dodecyl sulfate polyacrylamide gel electrophoresis (SDS-PAGE).<sup>72</sup> In 1981, the first phosphorylation-specific antibody was produced from rabbits.<sup>73</sup> This antibody broadly recognized phosphotyrosine. Following the development of both broadly-recognizing, protein-specific, and site-specific phosphosite antibodies, Western blotting and enzyme-linked immunoassays (ELISAs) became the most common methods for phosphorylation detection.



When proteome-level phosphorylation detail is sought, phosphoproteomics by mass spectrometry allows for analysis of entire signaling pathways from a single cell lysate. Phosphopeptides are often enriched by immobilized metal affinity chromatography (IMAC) before analysis to reduce the number of non-phosphorylated peptides, which are ordinarily in high abundance compared to phosphopeptides. CID, and later ETD, are both common MS/MS fragmentation methods for achieving phosphosite-level precision.

### **1.5 Intersection of O-GlcNAc and phosphorylation**

O-GlcNAcylation and phosphorylation are frequently studied in the context of one another as both are reversible PTMs that occur on Ser/Thr residues of nuclear and cytosolic proteins. Furthermore, many O-GlcNAc sites occur on or in close proximity to protein sites that are likewise modified by phosphorylation.<sup>2, 12</sup> Many biochemical characterizations of the role O-GlcNAc plays on a protein of interest involve phosphorylation changes (Figure 1.5.1A). If O-GlcNAc inhibits subsequent phosphorylation on the same protein, or vice versa, this is considered competitive modification. If O-GlcNAc promotes subsequent phosphorylation on the same protein, or vice versa, this is considered cooperative modification. Cases of competitive modification, where the presence of one PTM precludes the installation of the other at a nearby site, are most common.<sup>74, 75</sup> The competitive modification of a protein by O-GlcNAc or phosphorylation has been described for the tumor suppressor p53,<sup>76</sup> the oncoprotein c-Myc,<sup>77</sup> and the Alzheimer's associated-protein tau,<sup>78</sup> among others. For example, the structural effects of modification on a region of tau revealed that the addition of phosphate drove helical formation, while the addition of O-GlcNAc opposed helical formation by NMR solution structure.<sup>79</sup> Conversely, modification of the murine estrogen receptor with O-GlcNAc increased the helical turn propensity while phosphorylation decreased helicity.<sup>80</sup> A case of cooperative modification, where one PTM promotes the presence of the other, has been reported in the case of cyclin-dependent kinase inhibitor p27(Kip1).<sup>81</sup> Mutation of the three O-GlcNAc sites of p27(Kip1) to alanine significantly decreased phosphorylation at S10;

conversely, a S10A mutation decreased O-GlcNAcylation, while the S10E mutation acted as a phosphomimetic that increased O-GlcNAcylation.

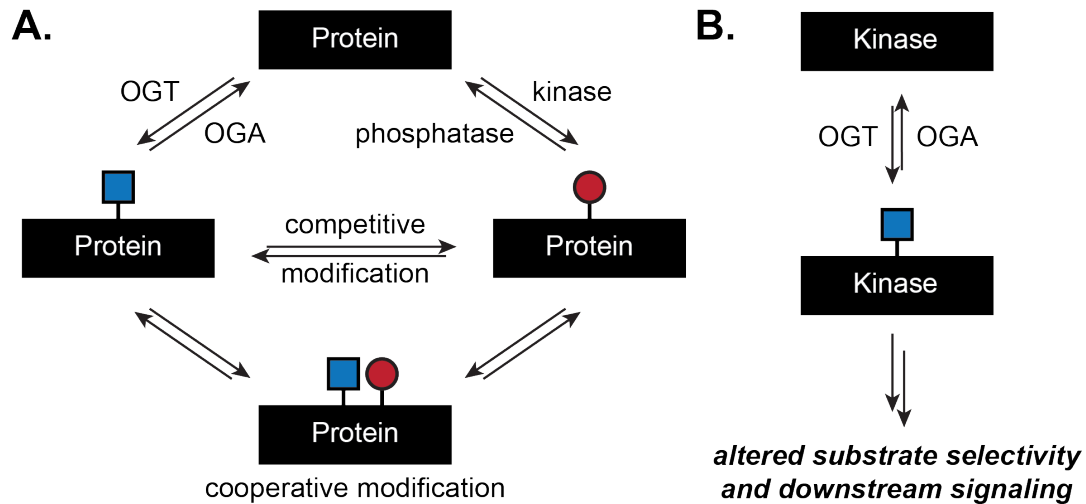


**Figure 1.5.1 Modes of crosstalk between O-GlcNAcylation and phosphorylation.**

**(A)** Post-translational modification of a protein with O-GlcNAc or phosphorylation may be competitive, where one modification precludes the other, or cooperative, where one modification enhances the propagation of others. **(B)** Modification of a kinase with O-GlcNAc can alter downstream substrate selection and signaling through phosphorylation.

The possibility of O-GlcNAc blocking proximal phosphosites was first suggested by Hart and coworkers in 1987.<sup>82</sup> In 2008, a large-scale phosphosite profiling study in mouse fibroblasts revealed roughly half of the 711 mapped phosphosites changed in abundance in response to a global increase in O-GlcNAc glycosylation via chemical inhibition of OGA.<sup>83</sup> Furthermore, inhibition of phosphatases by okadaic acid decreased global O-GlcNAc levels by Western blot in NIH/3T3 cells.<sup>84, 85</sup> In primary human T cells, 45% of O-GlcNAc sites occur in close proximity to a previously mapped phosphorylation site (within 10 amino acids).<sup>2</sup>

While many possible modalities for O-GlcNAc and phosphorylation to lead to synergistic signaling outcomes exist, the Heck group has identified an amino acid motif that results in consistent regulation of O-GlcNAc by phosphorylation.<sup>86</sup> In an attempt to characterize O-GlcNAcylation kinetics on phosphopeptides, Heck and co-workers identified a four-residue

sequence (S/T-P-A/T/V-S/T) wherein phosphorylation at the N-terminal S/T prevented subsequent glycosylation at the C-terminal S/T by OGT (Figure 1.5.2). This result was replicated on eight phosphopeptides derived from human protein sequences, and the reciprocal case was true at the protein level in cells. HeLa cells treated with a global OGA inhibitor showed decreases in phosphorylation at the -3 position in the same set of phosphoproteins. Further evaluation of O-GlcNAc and phosphorylation maps from cellular or *in vivo* systems may reveal additional instances of PTM crosstalk.



**Figure 1.5.2 Sequence motif for O-GlcNAc/phosphorylation crosstalk.** Identified by Heck and co-workers.<sup>86</sup> Phosphorylation of Ser/Thr at the -3 position prevents subsequent O-GlcNAcylation at the 0 position. All permutations of this sequence are enriched in the proteome compared to other random 4-mer sequences, indicative of evolutionary convergence.

## 1.6 O-GlcNAc regulation of kinases

While several studies have uncovered crosstalk between O-GlcNAcylation and phosphorylation on individual protein substrates and pathways, an understanding of the role of O-GlcNAc in regulating kinases is emerging (Figure 1.5.1B). Both OGT and OGA have been immunoprecipitated in protein complexes containing kinases and phosphatases.<sup>87, 88</sup> *In vitro* glycosylation of a kinase microarray with OGT found that approximately 39% of these kinases are substrates.<sup>89</sup> Here, I examine the current O-GlcNAcylated kinome based on large-scale O-GlcNAc

maps sorted by kinase group,<sup>2, 4, 52, 90-96</sup> as well as more detailed biochemical characterizations of the O-GlcNAc modification regulating kinase activity. Phosphatases are also examined. This serves to highlight the central role of O-GlcNAc in regulating phosphorylation on protein substrates through the phosphate writers and erasers themselves.

## AGC

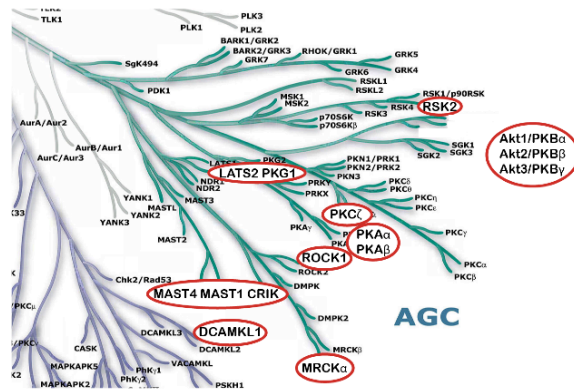


**Figure 1.6.1 The AGC Kinase family.** 15 members are glycosylated.

The AGC kinase family (Figure 1.6.1) contains Ser/Thr protein kinases named after three representative families, the cAMP-dependent protein kinase (PKA), the cGMP-dependent protein kinase (PKG) and the protein kinase C (PKC) families. The AGC family contains more than 60 human protein kinases. Seven members of this kinase family have been identified as O-GlcNAc modified.

PKA plays a role in CREB signaling and additionally modifies tau. O-GlcNAcylation of PKA subunit PKA $\alpha$  and PKA $\beta$  alters their subcellular localization and enhances their kinase activity.<sup>97</sup> Protein kinase B (AKT) is a serine/threonine kinase involved in multiple cellular processes, including the insulin response, apoptosis, and cell migration. AKT was found to be modified by O-GlcNAc in 2006.<sup>98</sup> Enrichment of AKT by wheat germ agglutinin increased under high glucose conditions or when dosing the OGA inhibitor PUGNAc, indicative of higher O-GlcNAc levels on AKT. Follow up experiments demonstrated that elevated global O-GlcNAc levels

correlate with AKT translocation from the cytoplasm to the nucleus. Two separate laboratories later reported distinct glycosites on AKT.<sup>99, 100</sup> Hart and co-workers used tyrosine as a glycomimetic mutation to show that O-GlcNAcylation at T305 and/or T312 on AKT inhibits phosphorylation at T308, a residue in the activation loop of AKT whose phosphorylation is necessary for AKT activation.<sup>101</sup> These studies implicated glycosylation as a mechanism to downregulate AKT activity using an in vitro AKT activity assay.<sup>99</sup> Gong and co-workers later report that increased O-GlcNAcylation on AKT positively correlates with markers for apoptosis and overexpression of AKT alleviates this phenotype.<sup>100</sup> AKT2 has also been identified as O-GlcNAc modified.<sup>102</sup> Treatment of rat adipocytes with the OGA inhibitor PUGNAc increased glycosylation and decreased insulin-induced phosphorylation of AKT2 by Western blot.

O-GlcNAc may be linked to regulation of cancer cell migration via another member of the AGC kinase family, ROCK.<sup>103</sup> Chemical inhibition of OGA resulted in accelerated migration that was found to be mediated by the RhoA/ROCK/MLC (myosin light chain) interaction in SKOV3 and 59M ovarian cancer cells. Knockout RhoA or inhibition of ROCK eliminates the change in cell migration caused by OGA inhibition. While direct O-GlcNAcylation of RhoA or ROCK was not established in this study, a glycosite on ROCK has recently been identified in a large-scale glycoproteomics study.<sup>2</sup> Biochemical confirmation and characterization of this glycosite will lead to further conclusions about the role of O-GlcNAc in regulating ROCK and cell migration.

## CMGC

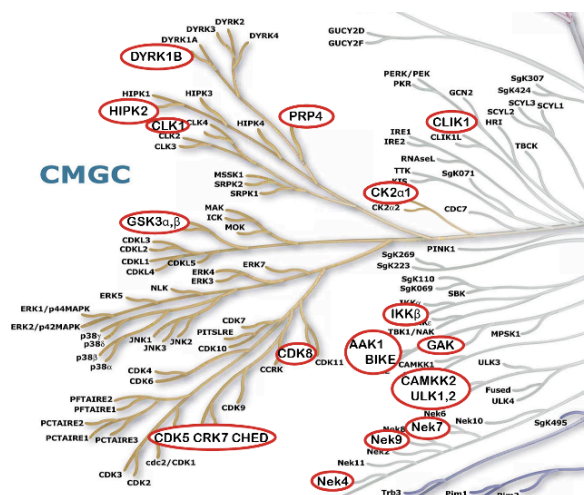


**Figure 1.6.2 The CMGC Kinase family.** 12 members are glycosylated.

The CMGC family (Figure 1.6.2) contains the cyclin-dependent kinases (CDK), mitogen-activated protein kinases (MAPK), glycogen synthase kinases, and the CDC-like kinases (CLK). These kinases are involved in cell-cycle regulation and signaling, cell communication, and cell growth.

GSK3 $\beta$  regulates OGT via phosphorylation and is likewise regulated by OGT through O-GlcNAc. Inhibition of GSK3 $\beta$  alters the abundance of several O-GlcNAc sites on GSK3 $\beta$  in the mouse and monkey proteomes, a result that could be attributed to the loss of phosphorylation on OGT or other GSK3 $\beta$  substrates.<sup>104, 105</sup> In addition, the O-GlcNAc modification on GSK3 $\beta$  results in regulation of the molecular chaperones that are stably expressed under heat-shock conditions.<sup>106</sup> Specifically, knockout of OGT in MEF cells results in altered expression of HSP72, a heat shock protein that is governed by the GSK3 $\beta$ -substrate HSF1.

Several studies additionally report regulation of CMGC complexes by O-GlcNAc. In these examples, members of the CMGC kinase complex are glycosylated, leading to alteration of the kinase function and substrate selectivity that affect essential cellular processes, including motility



modified by OGT, with the effects on CAMKIV being best studied.<sup>74</sup> CAMKIV is O-GlcNAcylated at several sites. Modification of CAMKIV with O-GlcNAc at the active site reduces the level of stimulatory phosphorylation at T200 and results in inhibition of the kinase activity.

Unc-51-like-kinase 1 (ULK1) is an important gatekeeper of the autophagy pathway. ULK1 is glycosylated at T754. Glycosylation of ULK1 can only occur once ULK1 has been dephosphorylated by PP1 to remove a phosphosite installed by mTOR.<sup>108</sup> O-GlcNAcylation of ULK1 at T754 promotes binding to substrate ATG14L, which results in phosphatidylinositol-(3)-phosphate production and initiation of autophagy. In this example, dephosphorylation by PP1 represents a gatekeeping step for subsequent O-GlcNAcylation, and illustrates key regulatory mechanisms by O-GlcNAc in the autophagy pathway.

AMPK is a heterotrimeric kinase that has a protective function from cellular metabolic stress. AMPK activity is strongly associated with depleted cellular energy levels as the kinase is activated by 5'-AMP and ADP, but inhibited by ATP. Stimulation with 5'-AMP or ADP yields a net upregulation of catabolic and downregulation of anabolic processes. The kinase complex is further activated by phosphorylation of T172 in the AMPK alpha subunit. During differentiation of C2C12 mouse skeletal muscle myotubes, AMPK activity is closely associated with OGT translocation to the nucleus. The altered localization of OGT results in increased O-GlcNAcylation of nuclear proteins and H3K9 acetylation<sup>109</sup> and results in phosphorylation of OGT at T444. Phosphorylation of OGT by AMPK alters the O-GlcNAc landscape. All  $\alpha$  and  $\gamma$  subunits of AMPK substrates for OGT, and active AMPK shows increased O-GlcNAcylation of the  $\gamma$ 1 subunit.



## STE

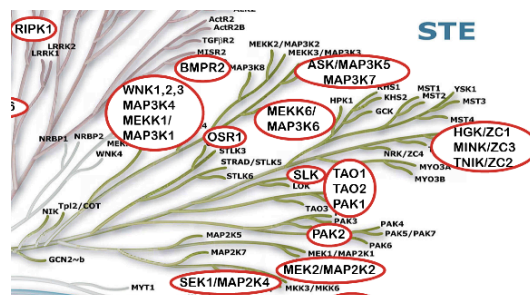


**Figure 1.6.4 The STE Kinase family.** 19 members are glycosylated.

The homologs of yeast Sterile 7, 11, and 20 (STE) kinase family (Figure 1.6.4) contains many kinases involved in cell growth, differentiation, oxidative damage, and apoptosis, including many MAP and serine/threonine protein kinases.<sup>110, 111</sup> PAK, GCK, MEK, and MKK kinases are also part of the STE family. Prominent O-GlcNAcylated members of this family include WNK1-3, PAK1-2, TAO1-2, SLK, OSR1, and several MAP3K proteins, all revealed in large-scale proteomics experiments. The functional outcomes of glycosites on kinases in the STE family have yet to be biochemically characterized.

## CK1

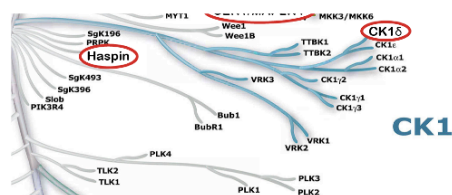


**Figure 1.6.5 The CK1 Kinase family.** Two members are glycosylated.

Despite the limited number of kinases in the CK1 family (Figure 1.6.5), these kinases are involved in important cellular processes, including regulation of membrane transport, cell division, DNA repair, and nuclear localization. CK1 $\delta$  and CK2 $\alpha$  have been discovered to be O-GlcNAc

modified to date. The O-GlcNAcylation of CK1 $\delta$  was discovered in a large-scale murine synaptosome proteomics study at multiple potential sites that remain to be functionally characterized.<sup>90</sup> Glycosylation of human CK2 $\alpha$  was evaluated by Cole and coworkers.<sup>75</sup> The mapped glycosite S347 was found proximal to multiple known phosphosites on CK2 $\alpha$ . By semi-synthesis, O-GlcNAcylation of CK2 $\alpha$  was found to inhibit phosphorylation at T344, which decreased the interaction of CK2 $\alpha$  with Pin1 and produced a net destabilization of CK2 $\alpha$ .

## TK/TKL

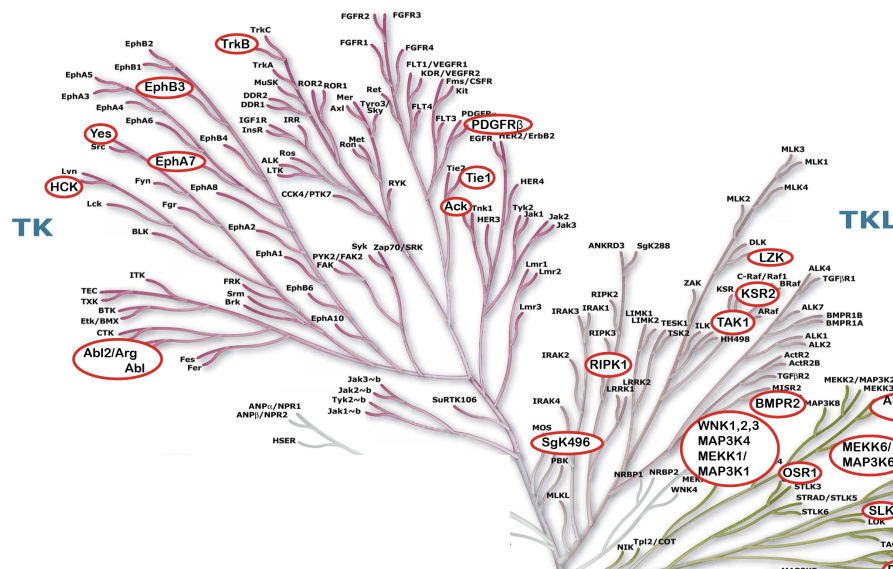


**Figure 1.6.6 TK and TKL Kinase families.** Ten TK and six TKL family members are glycosylated.

The protein tyrosine kinase family (Figure 1.6.6) can be subdivided into two main groups: cytosolic tyrosine kinases (CTKs) (e.g., Src, JAK, Abl) and receptor tyrosine kinases (RTKs) (e.g., EGFR, VEGFR, FLT3). Receptor tyrosine kinases are transmembrane proteins that are activated by the binding of an extracellular ligand that induces dimerization and subsequent autophosphorylation of two RTK monomers, followed by phosphorylation of downstream signaling proteins. Since tyrosine kinases regulate many key processes including cell growth and survival,

their dysregulation has been found in the development and progression of a wide range of cancers. The tyrosine kinase-like family (TKL) is closely related to TK, but its members are serine/threonine kinases instead (e.g. Raf). Diverse members of this kinase family are shown to be glycosylated, including those involved in cell differentiation (BMPR2).<sup>2, 90, 112</sup> Regulatory functions for the O-GlcNAc sites on kinases in this family await biochemical characterization.

### **Other kinases**

Kinases that phosphorylate non-protein targets are also privy to regulation by O-GlcNAc. GNE is an epimerase/kinase responsible for converting UDP-GlcNAc to ManNAc-6P.<sup>113</sup> A GNE point mutation at M743T, commonly observed in GNE myopathy, results in significantly higher O-GlcNAcylation of GNE than its wildtype counterpart. Elevated O-GlcNAcylation on GNE was found to inhibit the epimerase activity of both the wildtype enzyme and the M743T mutant. One hypothesis for why GNE is regulated by O-GlcNAc is due to its role in the consumption of UDP-GlcNAc, the donor sugar used by OGT from the hexosamine biosynthesis pathway.

OGT modifies kinases involved in sugar metabolism and glycolysis in addition to GNE, including pyruvate kinase M2 and phosphofructokinase 1.<sup>114, 115</sup> Phosphofructokinase 1 (PFK1) is an enzyme in glycolysis responsible for converting fructose-6-phosphate to fructose-1,6-bisphosphate, a committal step that sends the product through the rest of the glycolytic pathway as compared to the hexosamine biosynthetic pathway. OGT installs O-GlcNAc at S529 of PFK1, attenuating its kinase activity.<sup>115</sup> This modification increases in abundance under hypoxic conditions, leading to the redirection of glycolytic flux from the glycolysis pathway toward the pentose phosphate pathway, a glucose-consuming metabolic pathway necessary for synthesis of nucleotides and other sugars.

## Phosphatases

Human cells express approximately 200 phosphatase enzymes that remove phosphorylation from protein substrates. Several examples of interplay between O-GlcNAc and dephosphorylation have been reported, including the identification of a functional complex between OGT and protein phosphatase 1.<sup>116</sup> For example, priming phosphorylation of folliculin-interacting protein 1 (FNIP1) at S938 by CK2 leads to many subsequent phosphorylation events of FNIP1, ultimately resulting in binding to Hsp90 to inhibit its ATPase activity. If this priming phosphorylation does not occur, OGT can glycosylate FNIP1 at S938, blocking subsequent phosphorylation steps, and consequently lead FNIP1 to be ubiquitinated and degraded.<sup>117</sup> Activation of the transcription factor Sp1 is enhanced on dephosphorylation by phosphatase 2A and may be additionally controlled by reciprocal O-GlcNAc and phosphate modification.<sup>118</sup>

A number of phosphatases are also privy to modification by O-GlcNAc (e.g., MYPT1, PPFIA2–4, PPP6R2, PTPN6, PTPN7, PTPRC, TNS2, SIRPA).<sup>2, 91, 92, 119</sup> Direct regulation of phosphatase activity by O-GlcNAc has been reported in a few instances. O-GlcNAcylation of protein tyrosine phosphatase 1B (PTP1B) at S104, S201, and S386 inhibits PTP1B activity, which leads to an increase in AKT and GSK3 $\beta$  activity and therefore insulin response in HepG2 cells.<sup>120</sup> Human small CTD phosphatase 1 (hSCP1) was identified as O-GlcNAc modified by Western blot, and its glycosite at S41 was confirmed by Q-TOF MS and site-directed mutagenesis.<sup>121</sup> Additionally, the phosphatase myosin phosphatase target subunit 1 (MYPT1) may regulate the substrate specificity of OGT.<sup>88</sup> MYPT1 and OGT can be co-immunoprecipitated, MYPT1 is modified by O-GlcNAc, and depletion of MYPT1 alters OGT substrate selectivity in Neuro-2a neuroblastoma cells. These studies highlight additional mechanisms of cellular integration of the O-GlcNAc modification and phosphorylation signaling and represent a significant opportunity for further study.

## Chapter 2: O-GlcNAc in T cells

## Contributions

Erik Owen, Dr. Daniel Ramirez, Dr. Chanat “Jay” Aonbangkhen, Dr. Yun Ge, Dr. Erin Heim, and Dr. Christina Woo all made valuable contributions to the work presented in this chapter. Erik Owen assisted with cloning, tissue culture, and Western blotting. Dr. Daniel Ramirez, Dr. Chanat “Jay” Aonbangkhen, and Dr. Yun Ge provided experimental support throughout and were involved in helpful discussions at subgroup meetings. Dr. Erin Heim assisted with lentiviral work in Jurkat cells. Finally, Dr. Christina Woo conceived the study and taught me techniques for T cell activation, culturing primary T cells, and Western blotting.

## Introduction

The physiological roles for O-GlcNAc in cellular signaling can be attributed to a few principles. First, O-GlcNAc serves as a metabolic reporter as core metabolic pathways are involved in the biosynthesis of the donor molecule UDP-GlcNAc. Thus, global O-GlcNAc levels can fluctuate according to nutrient availability and flux through the hexosamine biosynthetic pathway. Second, O-GlcNAc on proteins can affect protein–protein interactions and PTM occupancy at nearby sites, which tunes outcomes of other signaling pathways. Third, the high promiscuity of OGT and OGA underlies the broad repertoire of substrates and pathways in which O-GlcNAc may play a regulatory role. T cell activation is one such pathway.

Compared to most cell types, activated T cells require elevated levels of glucose and glutamine.<sup>122, 123</sup> Activated T cells incorporate ten times more glutamine than other amino acids, implying an increased need to fuel glutamine-metabolizing pathways.<sup>124</sup> In addition to its role in protein composition, glutamine feeds into the citric acid cycle, where it is ultimately converted to acetyl-CoA once transported out of the mitochondria.<sup>125</sup> Acetyl-CoA is a central component of fatty acids and cholesterol.<sup>126</sup> Notably, all of the aforementioned metabolites serve as substrates in the hexosamine biosynthetic pathway (HBP), enabling the production of UDP-GlcNAc.<sup>127</sup>

In this chapter, I will highlight previous studies that examine the role of O-GlcNAc in T cell activation, report my own findings, and discuss efforts to identify the glycosite of one putative glycoprotein in the T cell activation pathway – tyrosine kinase Zap-70.

## 2.1 O-GlcNAc and T cell activation

1991	2007	2016	2018
Kearse et al., <i>Proc Natl Acad Sci</i>	Golks et al., <i>EMBO J</i>	Lund et al., <i>J Immunol</i>	Woo et al., <i>Mol Cell Proteomics</i>
First study to suggest a role for O-GlcNAc in early T cell activation	siRNA-mediated knockdown of OGT led to reduced IL2 and CD69 production in $\alpha$ -CD3/CD28-stimulated Jurkat cells	Used mass spectrometry-based methods to identify glycoproteins in $\alpha$ -CD3/CD28-mediated activation in primary T cells	Improved upon 2016 study to map over 2,000 glycosites in primary T cells over both $\alpha$ -CD3/CD28-mediated and PMA/I-mediated T cell activation
Stimulated primary T cells with ConA	Also observed reduced NFAT and NF $\kappa$ B activation in OGT knockdown cells	Metabolic labeling + biotin click chemistry + streptavidin enrichment for protein-level analysis; BEMAD + thiol affinity enrichment for site-level analysis	Isotag workflow, simultaneous protein-level and site-level analysis
Observed increased O-GlcNAc on many nuclear proteins, decreased O-GlcNAc on subset of cytosolic proteins		>200 glycoproteins identified, many involved in RNA metabolism	Many glycosites assigned to proteins in T cell activation pathway (Zap-70, LAT, NFAT), and transcription factors (c-JUN, JUNB)

**Figure 2.1.1 Summary and timeline of influential publications in the field of O-GlcNAc in T cell activation**

The study of the function of O-GlcNAc in the T cell activation pathway has been ongoing for the past 31 years (Figure 2.1.1). A role for O-GlcNAc in T cell activation was first posited by Hart and colleagues in 1991.<sup>128</sup> They reported dynamic O-GlcNAc changes two hours after activating primary splenic T cells with concanavalin A (ConA), a lectin that binds glycoproteins on the T cell surface and results in activation. After a rapid increase of O-GlcNAc in the proteome, O-GlcNAc levels returned to baseline after six hours, suggesting that O-GlcNAc acts at the beginning of the activation process. In particular, increased O-GlcNAc was observed on nuclear proteins and decreased O-GlcNAc on a subset of cytosolic proteins. For detection of glycosylated

proteins, the Hart group used a GalTase labeling technique to label O-GlcNAc sites with [<sup>3</sup>H]galactose, and detected the <sup>3</sup>H-labeled proteins after 2D electrophoresis.

In 2007, Golks and colleagues reported that siRNA-mediated knockdown of OGT in Jurkat cells impairs activation.<sup>129</sup> After siRNA transfection of Jurkat cells, they measured T cell activation in two ways – IL-2 expression by luciferase reporter, and CD69 at the cell surface by flow cytometry. Both outputs were significantly reduced by OGT siRNA transfection compared to control conditions. Interestingly, they observe that transfection of siRNA for Lck, a key kinase involved in early T cell activation, impairs IL-2 expression, but not CD69 expression, implying a mechanism for CD69 expression that is Lck-independent.

Further insights to the specific O-GlcNAc proteome involved in T cell activation were subsequently reported across two publications from the Davis lab.<sup>2, 55</sup> As described in Chapter 1, advancements in mass spectrometry were paramount for rapid identification of O-GlcNAc sites from biological samples. In their 2016 publication, Davis and colleagues reported the utilization of two different techniques for enrichment and derivatization of O-GlcNAc sites to identify glycoproteins, and later map glycosites at different timepoints during CD3/CD28-mediated primary T cell activation, and compared this to cells exposed to isotype control antibodies (Figure 2.1.2).<sup>55</sup> For protein-level analysis, primary T cells were metabolically labeled with Ac<sub>4</sub>GalNAz, which is enzymatically converted to UDP-GlcNAz as a reporter for O-GlcNAc. After stimulation and lysis, O-GlcNAz-modified proteins were labeled with biotin through the Staudinger ligation reaction using biotin phosphine. This method enabled facile enrichment of glycosylated proteins through the biotin tag, but glycosite-level analysis was not possible. To detect specific glycosites, Davis and colleagues employed beta-elimination coupled with Michael addition of dithiothreitol (BEMAD<sup>51</sup>) with heavy or light dithiothreitol isotopes to enable sample pooling of control and treatment conditions. They combined BEMAD with thiol affinity enrichment. To reduce the number of false positives, they added a β-N-acetylglucosaminidase treatment step in a parallel



experiment – glycopeptides that were lost during enrichment as a result of glycosidase treatment were regarded as true O-GlcNAc sites.

A follow up study from Davis and co-workers reported a significant increase in the number of high-confidence glycopeptides due to several changes to the glycoproteomics methodology.<sup>2</sup> First, in collaboration with the Bertozzi and Pitteri groups, the Isotope-Targeted Glycoproteomics (IsoTaG) workflow was adopted for enrichment and derivatization of glycopeptides. This enabled simultaneous protein-level and site-level analysis, and resulted in a reduced false positive rate compared to the previous BEMAD-dependent workflow. Performing proteolysis with both trypsin and chymotrypsin, running the LC-MS/MS on an LTQ-Orbitrap Elite capable of HCD/CID/ETD fragmentation, and the ability to distinguish labeled glycopeptides from unlabeled, regular peptides through the isotopic tag all helped to broaden the total number of true positives assigned. Key conclusions from this study include a detailed breakdown of the subcellular localization of the glycoproteins identified. Nuclear proteins made up 42% of total glycoproteins identified, followed by cytosolic proteins at 31%. Most importantly, this study found that 399 unique glycosites identified were within 0-9 residues of a known phosphosite. This high rate of glycosite–phosphosite co-localization may suggest evolutionary convergence toward PTM crosstalk between O-GlcNAc and phosphorylation. A few of the glycosites identified occur on phosphoproteins with characterized functions in the T cell activation cascade, including tyrosine kinase Zap-70, scaffolding protein LAT, and transcription factors c-JUN and JUNB. These findings motivated our further investigation into the role of O-GlcNAc in T cell activation.

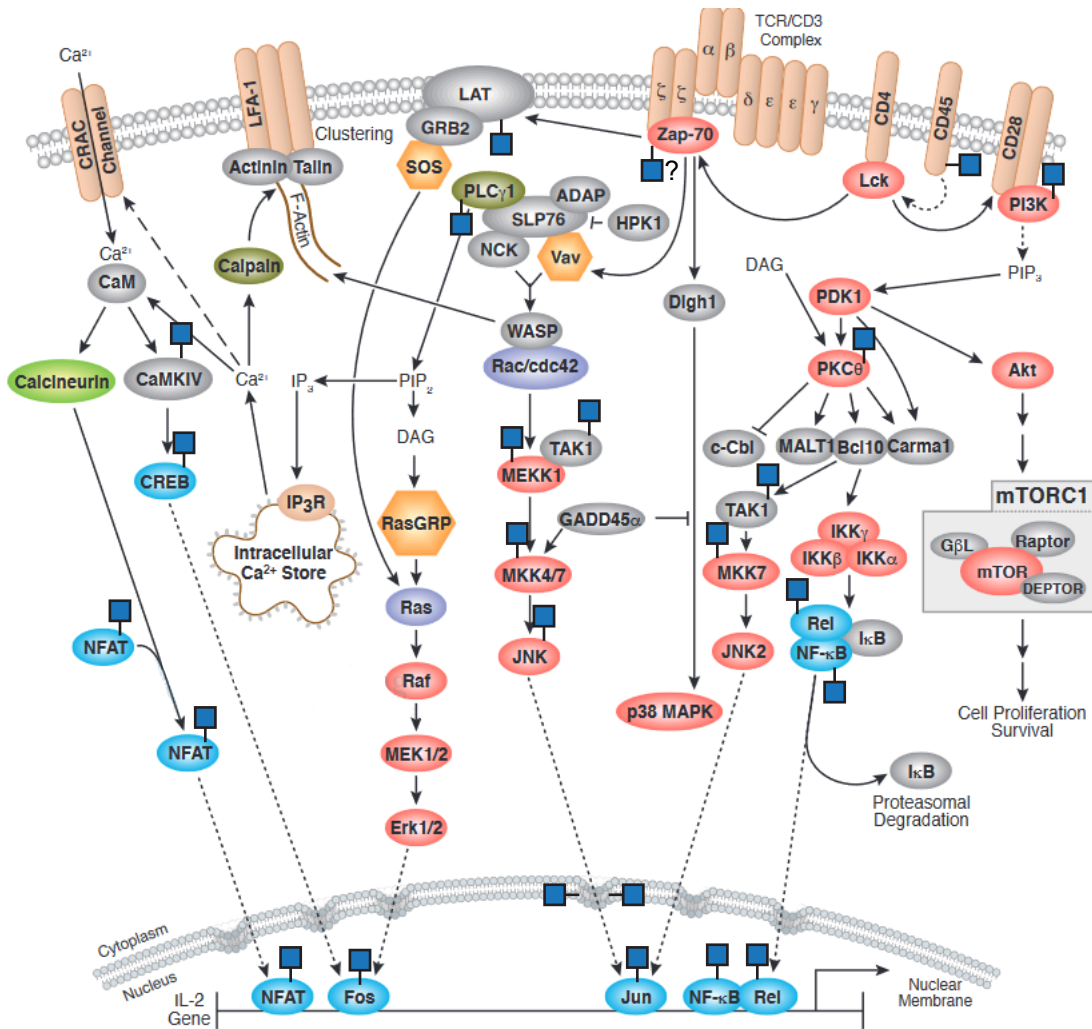


**Figure 2.1.2 O-GlcNAcylated proteins in the T cell activation pathway<sup>2, 55</sup>**

O-GlcNAcylated proteins identified by Woo et al. are marked with a blue square. Figure adapted from CellSignaling Technology.

These two publications from Davis and colleagues clarified key findings from the aforementioned Hart and Golks studies. In agreement with the Golks study, Davis and co-workers observed decreased IL-2 production in primary activated T cells treated with Ac<sub>4</sub>-5S-GlcNAc prior to stimulation, suggesting that OGT activity is necessary for proper T cell effector function. Contrary to the Hart study, the Davis studies found that global O-GlcNAc levels increased throughout T cell activation, which was measured up to 18 hours after stimulation. Both Davis studies drew their conclusions about global O-GlcNAc levels from immunoblotting-based assays;

however, the Davis study employed commercially available  $\alpha$ -O-GlcNAc primary antibodies that was not available when the Hart study was published. Additionally, the T cells used in each study differed in origin. The Hart study's enzymatic labeling technique utilized GalTase to label O-GlcNAc sites with [ $^3$ H]galactose. The sensitivity of the  $^3$ H detection compared to current Western blotting detection techniques, the differences in T cell origin, and the specificity of the GalTase for O-GlcNAc compared to the primary antibodies all contribute to the different results obtained by the two studies.

The aforementioned studies all suggest O-GlcNAc is most important early in T cell activation,<sup>2, 55, 128, 129</sup> Since chemical stimulation of Jurkats with PMA/ionomycin bypasses the early steps of T cell activation through the T-cell receptor (TCR) complex,<sup>130</sup> we sought to confirm whether chemical inhibition of OGT or OGA would affect PMA/ionomycin-mediated T-cell activation in the same way as TCR-mediated T cell activation through  $\alpha$ -CD3/CD28 antibody exposure (Figure 2.1.3). In this experiment, Jurkat cells were treated with 40  $\mu$ M OSMI-4b, 100  $\mu$ M TMG, or an equivalent volume of DMSO for 24 hours before activation by  $\alpha$ -CD3/CD28 antibodies for 18 hours or PMA/I treatment for four hours. Cells were washed with PBS and stained with a FITC-conjugated  $\alpha$ -CD69 antibodies. CD69 positive cells were used as a readout for the percentage of activated T cells in each sample and were detected via fluorescence-activated cell sorting (FACS).

In the  $\alpha$ -CD3/CD28 stimulation condition, OSMI-4b-treated Jurkat cells had significantly lower CD69 expression than Thiamet G-treated and control cells. TMG-treated cells were comparable to control cells. By contrast, PMA/I stimulated cells all showed high levels of CD69 expression regardless of OGT or OGA inhibition. These results suggest chemical inhibition of OGT, but not OGA, suppresses CD3/CD28-mediated activation in Jurkat cells, and that PMA/I-mediated activation is unaffected. This aligns with the literature precedent set by the Golks study, where OGT siRNA was used instead of chemical inhibition.<sup>129</sup>

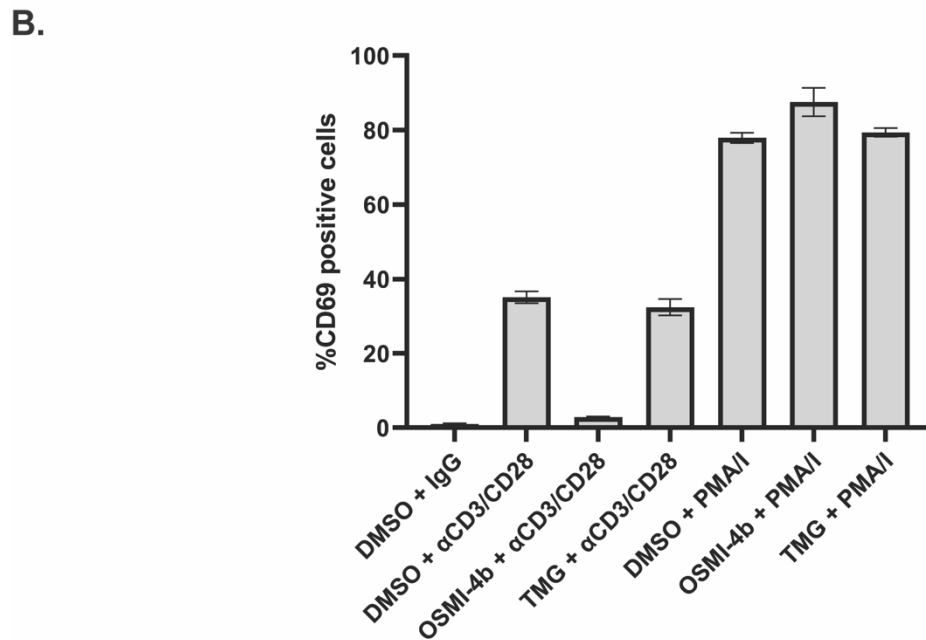
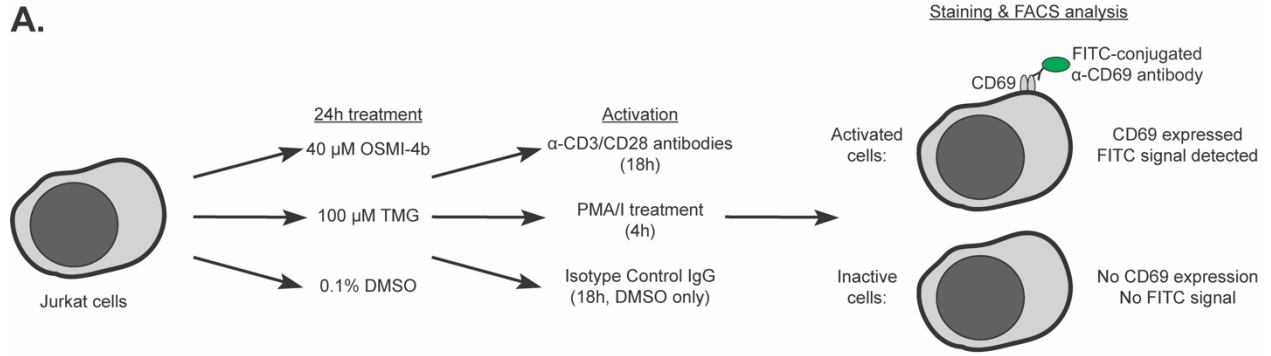


**Figure 2.1.3 TCR-mediated T cell activation is hampered by OGT inhibition.**

**(A)** Jurkat cells were treated with 40  $\mu$ M OSMI-4b, 100  $\mu$ M Thiamet G (TMG), or an equivalent volume of DMSO for 24 hours before activation by  $\alpha$ -CD3/CD28 antibody treatment for 18 hours or PMA/ionomycin treatment for 4 hours. Cells were stained with  $\alpha$ -CD69 FITC-conjugated antibody prior to FACS analysis. **(B)** Results of FACS analysis. Averages are based on 3 independent replicates, and error bars are representative of  $\pm$  one standard deviation.

We next examined the initial steps of T cell activation to understand which glycoproteins are potentially essential for the early T cell activation process. The initial steps of T cell activation involve convergence of two transmembrane protein complexes. Through extracellular contacts with the major histocompatibility complex (MHC) of an antigen-presenting cell, the multimeric T cell receptor is brought into contact with CD4. On the intracellular side, CD4-linked tyrosine kinase

Lck phosphorylates the immunoreceptor tyrosine-based activation motifs (ITAMs) of CD3 $\zeta$  on the cytosolic side of the T cell receptor (TCR). The Src homology 2 (SH2) domains of Zap-70 have high affinity for these phosphorylated ITAMs on CD3 $\zeta$ . The binding event between these two proteins brings the kinase domain of Zap-70 to the activated TCR, where it in turn becomes activated through phosphorylation by Lck and autophosphorylation. Activated Zap-70 phosphorylates scaffolding proteins LAT and SLP76, leading to downstream events in the T cell activation cascade.

With the aforementioned early T cell activation proteins in mind, we sought to visualize how phosphosites on Lck, Zap-70, and LAT change over the first 15 minutes of TCR-mediated T cell activation, and if chemical inhibition of OGT or OGA caused any changes (Figure 2.1.4). The Jurkat cells were treated with 40  $\mu$ M OSMI-4b, 100  $\mu$ M Thiamet G (TMG), or an equivalent volume of DMSO for 24 hours before activation by  $\alpha$ -CD3/CD28 antibody treatment. Cells were lysed in Mammalian Protein Extraction Reagent (MPER) supplemented with protease and phosphatase inhibitors. As expected, Jurkat cells showed noticeable increases in phosphorylation of Zap-70 Y352 and LAT Y191 after 15 min of stimulation. Phosphorylation of Zap-70 and LAT proteins at the same 15 min timepoint is noticeably reduced in the OSMI-4b condition compared to DMSO. Phosphorylation of the same sites is at comparable levels in the Thiamet G condition. These results likely imply a functional role for OGT activity, but not OGA activity, in early T cell activation. Differences in OGT or OGA gene expression may also play a role, as treatment with chemical inhibitors of OGT or OGA rapidly affects expression of both genes within 2 hours,<sup>131</sup> and as observed in lanes 7–9 of the  $\alpha$ -OGT blot.

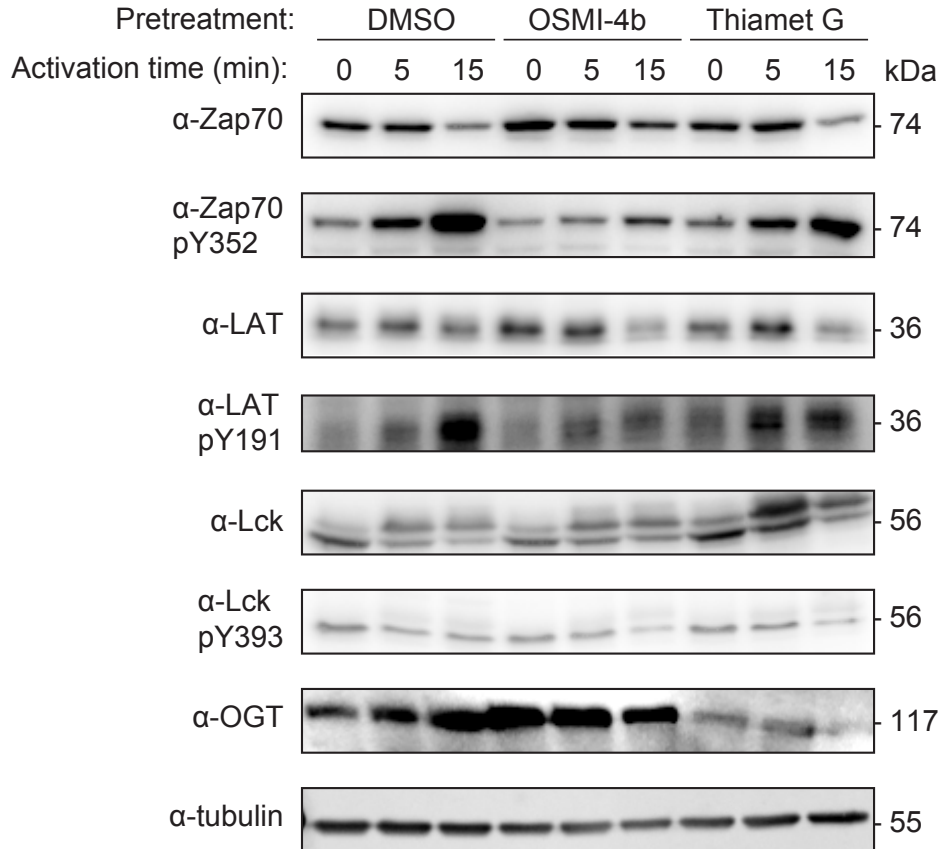


**Figure 2.1.4 Tyrosine phosphorylation of early T-cell activation proteins changes with OGT inhibition.** Jurkat cells were treated with 40 $\mu$ M OSMI-4b, 100 $\mu$ M Thiamet G (TMG), or an equivalent volume of DMSO for 24 hours before activation by  $\alpha$ -CD3/CD28 antibody treatment and lysis.

## 2.2 Zap-70

With substantial evidence that OGT activity is necessary for proper initiation of T cell activation, we consulted the dataset of glycoproteins from the *Molecular & Cellular Proteomics* study by Woo, Davis, and colleagues<sup>2</sup> for suitable candidates. We elected to study Zap-70 in more detail as the singular glycopeptide assigned and the clearly characterized role of tyrosine kinase Zap-70 made it our preferred candidate for closer study. The name Zap-70 comes from the initial discovery by Weiss and colleagues in 1992 that a 70 kDa protein associated with the zeta chain of CD3 during T cell activation – henceforth referred to as zeta-associated protein 70 (Zap-70).<sup>132</sup>

Zap-70 is one of two family members of the Syk tyrosine kinase family, the other being spleen tyrosine kinase Syk itself.<sup>133</sup> Syk is expressed in B cells, while Zap-70 is expressed in T cells. Syk and Zap-70 share 56% sequence identity across two N-terminal SH2 domains, a C-terminal kinase domain, and two short intervening domains which connect the two SH2 domains, and the second SH2 domain to the kinase domain. Both Syk and Zap-70 require upstream phosphorylation by Src family kinases for activation – more specifically, a Src kinase (Lyn in B cells or Lck in T cells) must phosphorylate ITAMs on the intracellular side of immunoreceptor proteins. The SH2 domains of Syk family kinases have high affinity for these phosphorylated ITAMs. Their binding results in a conformational change in the Syk family kinase that promotes stimulatory autophosphorylation, as well as activating phosphorylation by Src family kinases.<sup>134</sup> The active Syk family kinase then propagates the immunoreceptor activation signal through downstream phosphorylation events.

To initiate study of Zap-70 glycosylation, our first objective was to determine what cell line was most suitable for expression and analysis. Jurkat and HEK293T cells were both strong candidates for different reasons. As immortalized lymphocytes, Jurkat cells express the entire CD3/28 T cell activation pathway, and would enable examination of Zap-70 activity in its native environment. However, Jurkat cells are readily not amenable to transfection by lipofectamine, which is a major method for exogenous gene expression in human cells. By contrast, HEK293T cells are highly amenable to transfection, and would allow us to probe transiently expressed Zap-70 point mutants for glycosylation in cells. However, study of biological applications in HEK293T cells would be impossible, and glycosite validation in T cells would still be important, as OGT in HEK293T cells may not modify the same glycosite(s) as in T cells. Because of the desirable features of both cell lines, both were used in our analysis.

Since we first sought to confirm the S497 glycosite assigned to Zap-70 in the Woo et al. study,<sup>2</sup> we began our studies in HEK293T cells. Facile lipofectamine transfection enabled us to overexpress an S497A mutant of FLAG-tagged Zap-70 and compare its level of glycosylation to

wild-type Zap-70. For detection of glycosylation, we used a well-established method to attach 5 kDa poly(ethylene glycol) to azide-labeled O-GlcNAc sites,<sup>135</sup> and visualized the proportion of mass-tagged Zap-70 via Western blot (Figure 2.2.1). In this experiment, HEK293T metabolically-labeled with Ac<sub>4</sub>GalNAz were transfected with wild-type Zap-70 or S497A Zap-70 overexpression constructs. Following lysis and alkylation, O-GlcNAz labeled proteins were bound to 5kDa PEG groups through a copper-free click reaction with dibenzocyclooctyne (DBCO)-PEG-5kDa. Western blot analysis indicates both wild-type (WT) and S497A Zap-70 show a mass-shifted band in lanes 2 and 4, implying both are glycosylated. Surprisingly, the S497A Zap-70 shows a stronger mass-shifted band than the wild-type Zap-70, implying greater glycosylation. The lack of additional higher molecular weight bands implies Zap-70 is only glycosylated once in HEK293T cells.

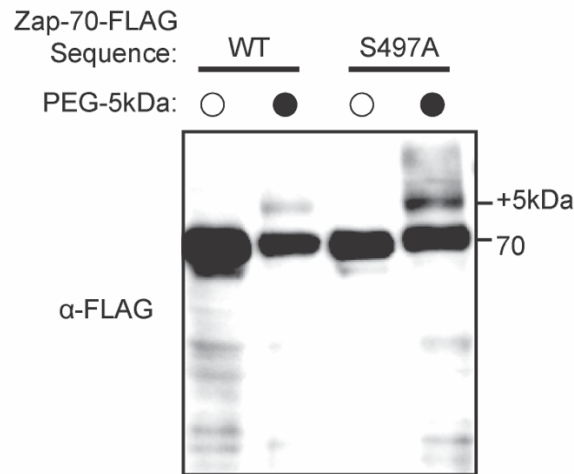


**Figure 2.2.1 Zap-70 is not glycosylated at S497.** FLAG-tagged Zap-70 was overexpressed in metabolically labeled HEK293T cells carrying its wild-type sequence, or with an alanine mutation at S497. Cell lysates were alkylated, then reacted with DBCO-PEG5kDa, which bound to O-GlcNAz-modified proteins and allowed visualization of O-GlcNAc stoichiometry by Western blot.

Although S497 was not the Zap-70 glycosite, the data from mass shift assay suggests that Zap-70 carries a glycosite. Rather than sequentially mutate each Ser/Thr in Zap-70 and look for loss of glycosylation, we instead expressed each Zap-70 domain with C-terminal FLAG and EPEA



tags, and analyzed each for glycosylation by Western blot (Figure 2.2.2). Zap-70 has two tandem SH2 domains, which recognize phosphorylated ITAMs on CD3 $\zeta$ . Short intervening sequences separate the N-terminal SH2 domain (N-SH2) from the C-terminal SH2 domain (C-SH2), and C-SH2 from the kinase domain (Figure 2.2.2A). From our original Zap-70 construct, we generated expression constructs for the N-SH2 domain (residues 1-160), the C-SH2 domain (161-337), and the kinase domain (338-620) by PCR and Gibson assembly. We generated samples using the same workflow as Figure 2.2.1 and looked for mass-shifted bands from each Zap-70 domain by Western blot (Figure 2.2.2B). We observed mass-shifted bands from both the N-SH2 and C-SH2 FLAG-tagged Zap-70 domains, indicative of multiple potential glycosites. Additionally, the mass-shifted bands appear ~10kDa higher than the unmodified protein, although this could be attributed to differences in protein mass resolution on a 12% tris-glycine gel in this molecular weight range.

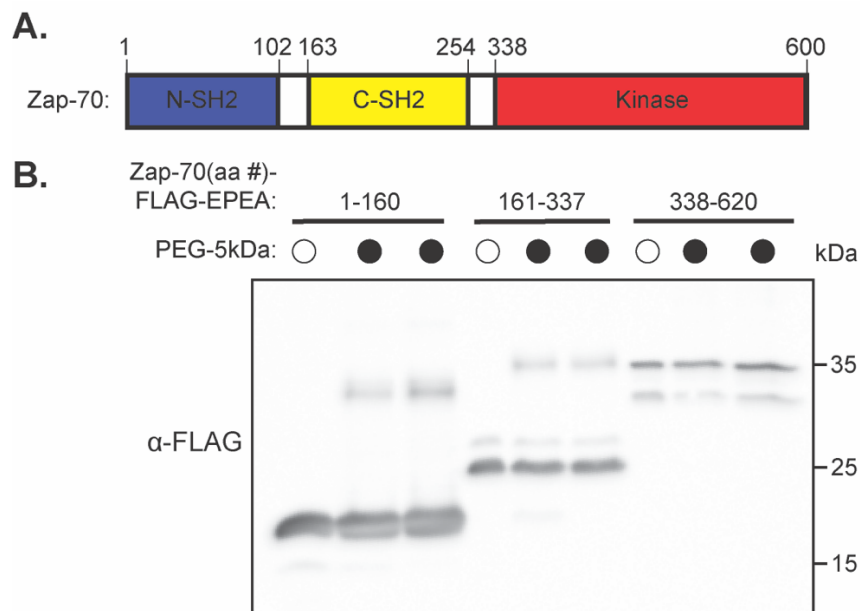


**Figure 2.2.2 PEG blot analysis of Zap-70 domains reveals multiple potential glycosites.**

**(A)** Diagram of Zap-70 primary sequence showing the two SH2 domains that precede the kinase domain. Each of these domains was expressed alone for glycosylation analysis. **(B)** HEK293T cells were simultaneously transfected with FLAG-EPEA-tagged Zap-70 domain overexpression constructs and metabolically labeled with 100  $\mu$ M Ac<sub>4</sub>GalNAz for 48 h prior to lysis. Cell lysates were alkylated, then reacted with DBCO-PEG-5kDa, which bound to the labeled azido sugars and allowed visualization of O-GlcNAc stoichiometry by Western blot.

The results from the PEG blot analysis of Zap-70 domains led us to attempt single-protein mass spectrometry analysis to identify the Zap-70 glycosite. Both full-length Zap-70-FLAG-EPEA, as well as identically tagged Zap-70 domains, were expressed in HEK293T cells alone, or co-transfected with a modified OGT to increase O-GlcNAc. The Zap-70 constructs were immunoprecipitated by the C-terminal EPEA tag using C-tag resin. Successful transfection and enrichment was confirmed by Western blot before reduction, alkylation, proteolysis with trypsin or chymotrypsin, desalting, and analysis on an Orbitrap Fusion Lumos Tribrid mass spectrometer. No replicable glycosites were assigned in analysis of the individually expressed Zap-70 domains; however, the full-length Zap-70 analysis had HexNAc modifications assigned to two peptides, one from each of the SH2 domains, which aligns with the data in Figure 2.2.2. The peptide from the N-SH2 domain contained two possible glycosites – T155 and T156 (Supplementary Figures 1 and 2). The peptide from the C-SH2 domain contained two possible glycosites – S257, S258 (Supplementary Figures 3 and 4). Nearby S260 was also tested.

Our next objective was to test these five residues for glycosylation on full-length Zap-70. For this and subsequent experiments, we modified our method for labeling O-GlcNAc sites with an azide handle. A recent publication reported background cysteine labeling induced by the metabolic labeling method.<sup>136</sup> To eliminate the possibility of background cysteine reactivity generating a false positive result, we adopted a chemoenzymatic labeling method utilizing a modified GalT1 enzyme to label existing O-GlcNAc sites with GalNAz.<sup>48</sup>

Zap-70 T155, T156, S257, S258, and S260 were mutated in different combinations on full-length Zap-70, overexpressed in HEK293T cells, enzymatically labeled with GalNAz using modified GalT1, and brought through the PEG blot workflow to examine O-GlcNAc stoichiometry (Figure 2.2.3). Loss of the mass-shifted band was not observed on any of the mutant constructs, implying none of these residues are the Zap-70 glycosite, and called into question whether or not Zap-70 was O-GlcNAcylated to a significant degree at all.

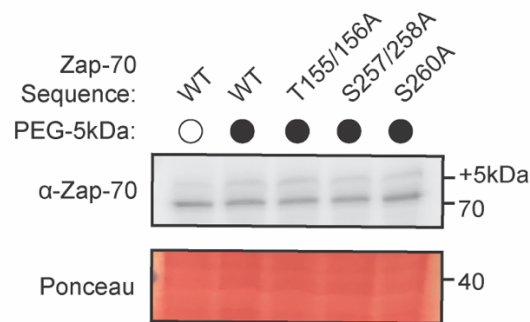


**Figure 2.2.3 PEG blot analysis of candidate glycosites from mass spectrometry analysis.** FLAG-EPEA-tagged Zap-70 domains were overexpressed in HEK293T cells. Cell lysates were quantified by BCA, and 500  $\mu$ g from each sample was GalT1 labeled, alkylated, and reacted with DBCO-PEG-5kDa. O-GlcNAc stoichiometry was visualized by Western blot.

Despite eliminating the possibility of background cysteine reactivity from the metabolic labeling approach by using the chemoenzymatic labeling approach, we were still concerned that background reactivity from other molecules, such as UDP-GalNAz in the metabolic labeling protocol, and DBCO-PEG-5kDa from the mass-shift assay protocol, was affecting our results. We designed a series of experiments to compare Zap-70 glycosylation in Jurkat cells to that of CREB, a well-characterized O-GlcNAcylated protein, using the mass-shift assay approach.<sup>137</sup> We sought to confirm whether the mass-shifted band originating from Zap-70 in Jurkat cells was responsive to treatment with chemical inhibitors of OGT and OGA comparably to CREB, and whether the band still appeared if GalT1 enzyme or UDP-GalNAz was withheld at the chemoenzymatic labeling step, or if DBCO-PEG-5kDa was withheld at the copper-free click reaction.

In the first experiment (Figure 2.2.4), no mass-shifted bands were observed for either protein in lanes 1–6, where DBCO-PEG-5kDa was excluded from the workflow. Faint mass-shifted bands were observed in lanes 7–9, where DBCO-PEG-5kDa was included in the click reaction, but GalT1 enzyme was excluded from the chemoenzymatic labeling reaction. This implies some level of background reactivity from the DBCO-PEG-5kDa molecule that is independent of enzymatically-attached GalNAz. The intensity of the mass-shifted bands from CREB in lanes 7–9 appears consistent, indicating that this background reactivity from DBCO-PEG-5kDa is not dependent on activity of OGT or OGA, and strongly implies that DBCO-PEG-

5kDa is not reacting with O-GlcNAc sites. Finally, the differences between the CREB and Zap-70 blots in lanes 10–12 deliver the most compelling data from this experiment. The mass-shifted band from CREB clearly increases in intensity with Thiamet G treatment, whereas the Zap-70 mass-shifted band does not change. This constitutes an additional piece of evidence that glycosylation of Zap-70, if real, cannot be distinguished from background levels.

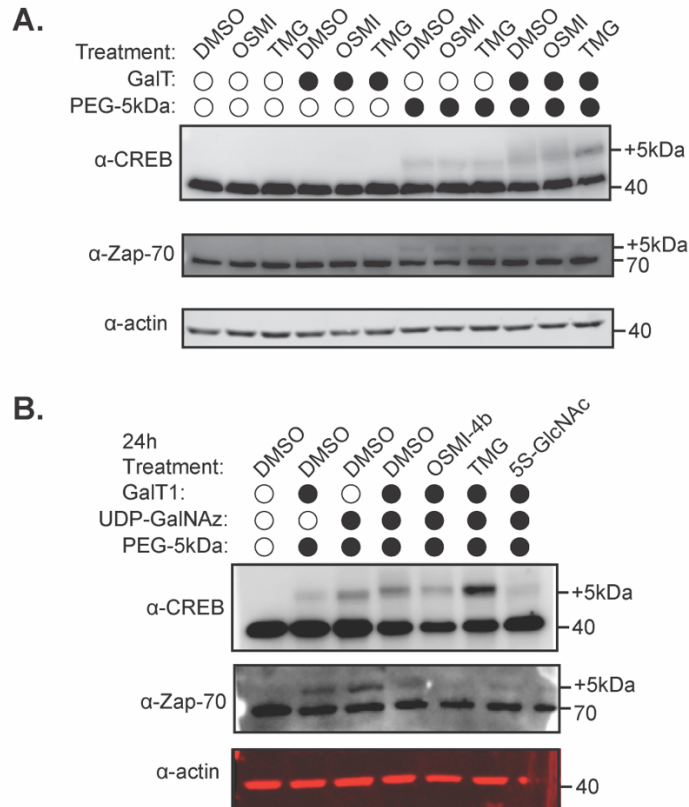


**Figure 2.2.4 Additional negative controls in GalT1 labeling and PEG blot workflow reveal glycosylation levels comparable to background, unaffected by TMG treatment. (A)** Jurkat cells were treated with 40  $\mu$ M OSMI-4b, 100  $\mu$ M Thiamet G (TMG), or an equivalent volume of DMSO for 24 hours before lysis, quantification, GalT1 labeling (+/– GalT enzyme), and DBCO-PEG-5kDa reaction (+/– DBCO-PEG) before visualization of O-GlcNAc stoichiometry by Western blot. Endogenous Zap-70, as well as established glycoprotein CREB, were both analyzed. **(B)** Similar workflow to A., with lanes included for –UDP-GalNAz at the GalT1 labeling step, 5S-GlcNAc-treated cells as an additional method for chemical inhibition of OGT.

In a follow-up experiment (Figure 2.2.4B), 5S-GlcNAc was included as an additional condition for OGT inhibition, and a –UDP-GalNAz condition was added to ascertain how excluding

GalT enzyme versus excluding UDP-GalNAz affects background DBCO-PEG-5kDa reactivity. Results from this experiment are largely consistent with those of the previous experiment. Mass-shifted Zap-70 bands are most intense in lanes 2 and 3, both of which are negative control conditions that exclude key components of the chemoenzymatic labeling protocol. By contrast, mass-shifted bands from CREB are clearly observable in lanes 4–7, and change in intensity as expected. Compared to the DMSO-treated condition in lane 4, the mass-shifted CREB band increases in intensity in lane 6 where OGA is inhibited. The same band decreases in intensity in lanes 5 and 7, where OGT is inhibited. These same conclusions cannot be drawn for the mass-shifted Zap-70 band, further implying that DBCO-PEG-5kDa is reacting with the Zap-70 in an O-GlcNAc-independent manner.

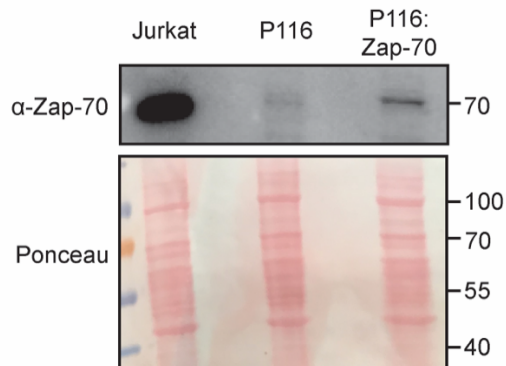


**Figure 2.2.5 Lentiviral transduction of Zap-70 in P116 cells results in lower Zap-70 expression compared to Jurkat cells.** Zap-70-deficient Jurkat cell line P116 was incubated with lentivirus containing transducible Zap-70-FLAG-EPEA and puromycin resistance expression elements for 72h. Cells were then incubated with 2 $\mu$ g/mL puromycin for two weeks to select for transduced cells. Zap-70 expression was confirmed by Western blot.

In conjunction with our work in HEK293T cells, we also sought avenues for transgenic Zap-70 expression in Jurkat cells to study Zap-70 glycosylation in a physiologically relevant cell line. We attempted lentiviral transduction as a method for expression of exogenous Zap-70 constructs. One obstacle to working in standard Jurkat cells would be to distinguish effects from our overexpressed Zap-70 constructs from endogenous Zap-70. Luckily, a Zap-70-deficient cell

line, P116, is commercially available. Lentivirus grown from transfection of HEK293T cells containing a transposable Zap-70 gene and a puromycin resistance gene was transduced into P116 cells for 72 hours. Incubation with 2 µg/mL puromycin was performed for negative selection. Zap-70 expression was confirmed by Western blot (Figure 2.2.5). Across multiple lentivirus production and transduction attempts, the level of Zap-70 expressed in HEK293T cells was never as high as that of Jurkat cells. The Zap-70 gene from the lentiviral construct is downstream of a cytomegalovirus (CMV) promoter. This promoter is standard for transgene expression in mammalian cells – however, it is known to be silenced over time in the genome by DNA methylation. This silencing likely occurs over the necessary two weeks of puromycin selection. Due to this obstacle, as well as the compelling data against glycosylation of Zap-70 in HEK293T cells, we decided to end our studies of Zap-70 glycosylation here.

### **2.3 Discussion**

Based on the data presented in the previous subchapter, we conclude that Zap-70 is a poor candidate for glycosylation analysis. The mass-shifted band observed in PEG blot experiments did not respond to chemical inhibition of OGT or OGA, implying a lack of dependence on either enzyme. While we agree that O-GlcNAc plays a regulatory role in early T cell activation, if this occurs through direct modification of one or multiple proteins involved in the activation cascade, it is highly unlikely Zap-70 is an important player in this process.

Our work indicates the Zap-70 glycosite at S497 identified in the Woo et al. study<sup>2</sup> is not a major glycosite in HEK293T cells or Jurkat cells. This is the only study in which the S497 glycosite is assigned to Zap-70 (the 2016 study from Lund et al. also identifies Zap-70 as a glycoprotein, but does not provide a glycosite).<sup>55</sup> This assignment was made from a singular peptide-spectrum match (PSM). The metabolic labeling method used for derivatization of O-GlcNAc sites in both studies may lead to background, non-enzymatic labeling of cysteine residues, generating false positive glycopeptides.<sup>136</sup> The chymotryptic peptide carrying the S497

glycosite does not have any cysteine residues, so it is unclear if this incorrect assignment was due to background from the metabolic labeling technique, or for another reason. While we initially used metabolic labeling for derivatization of O-GlcNAc sites in the work presented here, we eventually shifted to employing only chemoenzymatic labeling to eliminate the possibility of background cysteine labeling. One possibility is that the glycosite on Zap-70 occurs on cysteine naturally. Albeit very rare physiologically, OGT can glycosylate cysteine,<sup>62, 138</sup> and endogenous S-glycosites in mammalian cells have been reported in the literature.<sup>139</sup> An S-glycosite would explain the lack of the responsiveness of the mass-shifted band in the PEG blot experiments to OGA inhibition through TMG treatment; however, it would not explain the lack of responsiveness to OGT inhibition.

Regardless of background cysteine labeling, the primary source of background in this work is certainly from the mass-shift assays, also referred to as PEG blots, used as the primary method for detection of O-GlcNAc on Zap-70. Results from Figure 2.2.4B indicate both non-enzymatic attachment of UDP-GalNAz and background reactivity of the DBCO-PEG-5kDa contribute to mass-shifted bands in the resultant Western blot that are not representative of O-GlcNAcylation. In retrospect, integration of conditions lacking GalT1 enzyme and UDP-GalNAz as negative controls would have led us sooner to the conclusion that Zap-70 glycosylation cannot be distinguished from background in this assay. Quantification from mass-shift assay experiments utilizing GalT1 labeling followed by click reaction with DBCO-PEG-5kDa can be made more reliable if the mass-shifted band in the experimental condition is normalized to the mass-shifted band in a –GalT1 enzyme condition. Complementary methods for visualizing O-GlcNAc, such as immunoprecipitation followed by Western blotting with an  $\alpha$ -O-GlcNAc primary antibody, would have also been appreciated for this work. Multiple methods for O-GlcNAc visualization will be employed for glycoprotein analysis in the next chapter.

There is clear evidence that proper T cell activation requires OGT activity, whether through modification of a protein directly involved in T cell activation, or on a different substrate that is indirectly involved. When choosing candidates from glycoproteomics metadata, a glycoprotein with multiple PSMs, ideally across multiple glycoproteomic studies, would be a better candidate for biochemical characterization than Zap-70. Other candidate glycoproteins involved in T cell activation with assigned glycosites from the Woo et al. study<sup>2</sup> include LAT and NFATC2. Both glycopeptides correspond to multiple PSMs – 8 from LAT, and 15 for the predominant peptide from NFATC2. The LAT peptide (LVVLPDSTPATATAAPSAPALSTPGIRDSAF) contains multiple possible glycosites, while the predominant NFATC2 peptide (PGPPPVSQGQR) contains one possible glycosite at S850 downstream of proline and valine, making it a strong candidate glycosite.<sup>12</sup> O-GlcNAcylation of NFATC2 was also reported in a separate study.<sup>140</sup>

## **2.4 Materials and Methods**

### **Cell culture and transfection**

Jurkat cells (ATCC) were cultured in Roswell Park Memorial Institute (RPMI-1640) media (VWR 45000-396) supplemented with Penicillin-Streptomycin (VWR 12001-692, 50 µg mL<sup>-1</sup> each) and fetal bovine serum (Peak Serum PS-FB2, 10% vol/vol). HEK293T cells (ATCC) were cultured in Dulbecco's Modified Eagle's Medium with 4.5 g L<sup>-1</sup> glucose and L-glutamine (VWR 95042-498) supplemented with Penicillin-Streptomycin (VWR 12001-692, 50 µg mL<sup>-1</sup> each) and fetal bovine serum (Peak Serum PS-FB2, 10% vol/vol) and were passaged 1:10 at 100% confluence (roughly every three days). Jurkat cells (ATCC) were cultured in Roswell Park Memorial Institute Medium with L-glutamine (VWR 45000-396) supplemented Penicillin-Streptomycin (50 µg mL<sup>-1</sup> each) and fetal bovine serum (10% vol/vol) and were passaged 1:10 every three days. Cultures were maintained at 37°C in a humidified incubator with 5% CO<sub>2</sub> at a passage number no higher than 30.



HEK293T cells grown for transfection were seeded in 6-well plates (VWR 10062-892, 5 x 10<sup>5</sup> cells/well) 24 hours before transfection. All transfections were performed using TransIT-PRO (Mirus Bio MIR-5740) according to the manufacturer's instructions for 24 h.

Cells were collected in cold PBS and detached using a cell scraper. Detached cells were moved to microcentrifuge tubes and centrifuged 500xg for 3 minutes. Cells were lysed in either PBS + 1% SDS via sonication, or in Mammalian Protein Extraction Reagent (MPER, ThermoFisher 78501) supplemented with protease/phosphatase inhibitor cocktail (CST #5872) and 100 µM Thiamet G (Selleck Chem S7213).

### **Western blotting**

SDS-PAGE was performed using 6%–12% Tris-Glycine gels in a Mini-PROTEAN® BioRad gel system. Following PAGE at 200V for 40-45 minutes, proteins were transferred to a nitrocellulose membrane using an iBlot2 system (Thermo Scientific). Membranes were sometimes incubated in Ponceau staining solution (Thermo Scientific A40000279) for 5 min, then rinsed with deionized water for total protein visualization. Membranes were blocked with TBS containing 0.1% Tween-20 (TBST) plus 5% bovine serum albumin (BSA) (Sigma-Aldrich, A9647) for 60 minutes at room temperature, then incubated with the indicated primary antibodies in TBST + 1% BSA at 4°C overnight. Primary antibody staining solution was removed, and blots were washed once with TBST for 5 minutes at room temperature before addition of secondary antibodies (diluted 1:10,000) in TBST + 1% BSA and incubation at room temperature for 1 hour. Blots were washed thrice for 5 minutes in TBST before imaging. Immunoblot images were acquired using an Azure Imager C600 (Azure Biosystems) and analyzed with Fiji ImageJ. All infrared fluorescence Western blot images were converted to grayscale in Fiji ImageJ. Unsaturated exposure images were used for quantification, with the appropriate loading controls used as standards.

Primary antibodies used:  $\alpha$ -FLAG (CST #14793),  $\alpha$ -Zap-70 (CST #2705),  $\alpha$ -Zap-70 pY352 (CST #2717),  $\alpha$ -CREB (CST #9104),  $\alpha$ -Lck (abcam ab227975),  $\alpha$ -Lck pY393 (abcam ab138442),  $\alpha$ - $\beta$ -actin (CST #4970S),  $\alpha$ -tubulin (CST #2148),  $\alpha$ -LAT (CST #9166),  $\alpha$ -LAT pY191 (abcam ab59197),  $\alpha$ -OGT (CST #24083). All primary antibodies were used at a 1:1,000 dilution.

Horseradish peroxidase (HRP)-conjugated secondary antibodies were purchased from Rockland Immunochemicals. IRDye secondary antibodies were purchased from LI-COR Biosciences.

### **GalT1 labeling**

Following lysis, protein concentrations were determined by BCA assay. Cell lysates were reduced with 25 mM DTT (Thermo Scientific, 20290) at 95 °C for 5 min and alkylated with 50 mM iodoacetamide (Sigma-Aldrich, I1149) at room temperature for 1 h. Lysates were precipitated by addition of excess methanol and were resuspended in 20mM HEPES pH 7.9 + 1% SDS at a protein concentration of 5 mg mL<sup>-1</sup>. Purification of GalT1 (Y289L) enzyme and labeling of O-GlcNAcylated proteins with GalNAz were performed according to the procedure of Hsieh-Wilson and co-workers.<sup>141</sup> For 150  $\mu$ g of protein, the following components were added to cell lysates in order: water (49  $\mu$ l), 2.5X GalT labeling buffer (80  $\mu$ l; final concentrations, 50 mM NaCl, 20 mM HEPES, 2% NP-40, pH 7.9), 100 mM MnCl<sub>2</sub> (11  $\mu$ l), 500  $\mu$ M UDP-GalNAz (10  $\mu$ l) and 2 mg mL<sup>-1</sup> GalT1 (Y289L) (10  $\mu$ l). The reaction was gently rotated at 4 °C for at least 24 hours, and proteins were precipitated as described above.

### **C-Tag Immunoprecipitation and Mass Spectrometry Sample Preparation**

For immunoprecipitation of expressed Zap-70-FLAG-EPEA by the C-terminal EPEA tag, cell lysates in PBS + 1% SDS with equal amounts of protein were diluted fivefold with PBS and incubated with C-tag affinity matrix (Thermo Scientific, 191307005) overnight at 4 °C with rotation.

After washing the resin thrice with excess PBS, 5% of the resin was resuspended in 1X SDS sample buffer and incubated at 95 °C for 5 minutes. The supernatant was subjected to SDS-PAGE to validate immunoprecipitation. The remaining resin was incubated in 25mM DTT for 30 minutes at room temperature for reduction, followed by 50mM iodoacetamide for 30 minutes at room temperature in the dark for alkylation. Resin was washed thrice with excess PBS before resuspension trypsinization in 500mM urea at 37 °C overnight. Tryptic peptides were collected, desalted by C18 ZipTip (Millipore ZTC18S096), and submitted for LC-MS analysis on the Orbitrap Fusion Lumos Tribrid mass spectrometer in the Bauer Core. The raw data was processed using Proteome Discoverer 2.4 (Thermo Fisher Scientific). Data was searched against either the UniProt/SwissProt human (*Homo sapiens*) protein database (19 August 2016; 20,156 total entries) or the sequences of Zap-70-FLAG-EPEA or the sequences of the individually expressed and tagged Zap-70 domains. Both searches included contaminant proteins and used both Byonic and Sequest HT algorithms.

### **Lentiviral Production and Transduction**

For production of lentivirus, HEK293T cells were seeded into 10 cm or 15 cm dishes and grown to at least 70% confluence before transfection. The lentiviral system consists of three plasmids transfected together. The VSVG envelope plasmid and GagPol packaging plasmid (provided by the Liao lab) each contain necessary viral components, while the pLJM1 transfer plasmid (Addgene #19319) harbors the genetic material to be transduced into the genome of the target cell line. Our pLJM1 vector contains the Zap-70 gene as well as a puromycin resistance gene for selection. The amount of reagents used for 10 cm and 15 cm plates is shown in Table 2.4.1. Cells were transfected for 5-8 hours, then media was refreshed with antibiotic-free DMEM supplemented with 10% vol/vol FBS. After 24-48 hours, the media was collected and centrifuged at 500xg for 3 minutes to pellet suspended cells, passed through a sterile 0.2-0.45  $\mu\text{m}$  filter to

remove other small particles. This filtered media containing the desired lentivirus was flash frozen and stored at  $-80^{\circ}\text{C}$  for later use.

<b>Reagent</b>	<b>Amount for 10 cm dish</b>	<b>Amount for 15 cm dish</b>
OptiMEM	2 mL	3.1 mL
TransIT-PRO	20 $\mu\text{L}$	31.25 $\mu\text{L}$
VSVG plasmid	4 $\mu\text{g}$	6.25 $\mu\text{g}$
GagPol plasmid	6 $\mu\text{g}$	9.4 $\mu\text{g}$
pLJM1-Zap70-Puro plasmid	10 $\mu\text{g}$	15.6 $\mu\text{g}$

**Table 2.4.1 Transfection reagents used for lentiviral production in HEK293T cells.**

For lentiviral transduction, 1M P116 cells were seeded into a 6-well plate, with each well containing 1.6 mL antibiotic-free RPMI supplemented with 10% vol/vol FBS, 400  $\mu\text{L}$  lentiviral media, and 2  $\mu\text{L}$  polybrene (Santa Cruz Biotechnology sc-134220). After 48-72 hours, 4  $\mu\text{g}$  puromycin (Thermo Fisher A1113803) was added for selection, and cells were incubated for one week before being moved into T75 cell culture flasks for outgrowth. Successful transduction of Zap-70 was confirmed by Western blot.

## Chapter 3: O-GlcNAc on CK2 $\alpha$

## Adaptation

Parts of this chapter are adapted from Schwein, P. A.; Ge, Y.; Yang, B.; D'Souza, A.; Mody, A.; Shen, D.; Woo, C. M., Writing and Erasing O-GlcNAc on Casein Kinase 2 Alpha Alters the Phosphoproteome. *ACS Chemical Biology* **2022**. doi:10.1021/acscchembio.1c0098

## Contributions

Dr. Yun Ge, Dr. Bo Yang, Alexandria D'Souza, Alison Mody, Dr. Dacheng Shen, and Dr. Christina Woo all provided important contributions to both this chapter and the cited research paper. Dr. Yun Ge performed the cloning of the initial GFP-FLAG-CK2 $\alpha$ -EPEA construct, and provided valuable support with the nanobody-splitOGA system and general experimental protocols. Dr. Bo Yang performed the phosphoproteomics sample preparation and data acquisition. Alexandria D'Souza performed the phosphoproteomics computational analysis. Alison Mody assisted with generating the data shown in Figure 3.2.3 and Figure 3.3.2. Dr. Dacheng Shen performed synthesis of chemical probes used in this study. Dr. Christina Woo conceived of the study, provided valuable experimental feedback, and co-wrote the manuscript. The final manuscript was read and approved by all authors.

## Introduction

Despite the inconclusive outcome of the Zap-70 work, my fascination with the intersection of O-GlcNAc and phosphorylation remained. Rather than attempt to characterize an example of PTM cross-talk, we wanted to build off of our *ACS Chem. Biol* literature review<sup>71</sup> and characterize the function of O-GlcNAc on a phosphorylation writer. In selecting the next candidate kinase for O-GlcNAc functional analysis, we looked beyond the paradigm of T cell activation and sought kinases with multiple literature reports of O-GlcNAcylation. This brought us to casein kinase 2 (CK2) alpha, the catalytic subunit of protein kinase CK2. This chapter presents our findings from

selectivity manipulating glycosylation of CK2 $\alpha$ , confirming the glycosite in human cells, and how this targeted manipulation of O-GlcNAc affects the phosphoproteome.<sup>142</sup>

### 3.1 Introduction to CK2

Protein kinase CK2 is a dual-specific kinase that is constitutively active and ubiquitously expressed in human cells.<sup>143</sup> The kinase is most commonly observed as a tetramer consisting of two  $\alpha$  or  $\alpha'$  catalytic subunits, and two non-catalytic  $\beta$  subunits, but the  $\alpha$  monomer is also active.<sup>144</sup> CK2 has a large range of substrates,<sup>145</sup> some of which are modified predominantly by the holoenzyme, and others by the  $\alpha$  monomer.<sup>146</sup> Through its broad substrate scope, CK2 plays a central role in cell growth through modification of DNA replication machinery, and cell survival through inhibition of caspase activity. In development, CK2 has been reported to regulate neuronal, adipogenic, and osteogenic differentiation, and is involved in oncogenic pathways in certain cancers.

The minimum consensus sequence for phosphorylation by CK2 is S/T-X-X-D/E/pS/pY, wherein a negatively charged residue (other than phosphothreonine) at the n+3 position is sufficient to permit phosphorylation of S/T at the n position at the peptide level.<sup>147, 148</sup> The presence of additional acidic residues, ranging from n-2 to n+5, further enhances phosphorylation. This preference to phosphorylate S/T in clusters of negatively charged residues can be attributed to several basic residues on CK2 $\alpha$  involved in substrate binding. These include K74–K77, K79, R80, K83, R191, R195, and K198.<sup>149</sup> Mutation of any of these basic clusters to alanine results in reduced phosphorylation efficiency of a peptide substrate. Rare exceptions to this consensus sequence exist, including the S392 phosphosite of human p53,<sup>150</sup> implying additional determinants beyond an acidic microenvironment exist for CK2 phosphorylation. The ability for phosphoserine and phosphotyrosine to act as determinants for CK2 phosphorylation

indicates that CK2 acts in a hierarchical fashion on substrates shared with other protein kinases.<sup>151</sup>

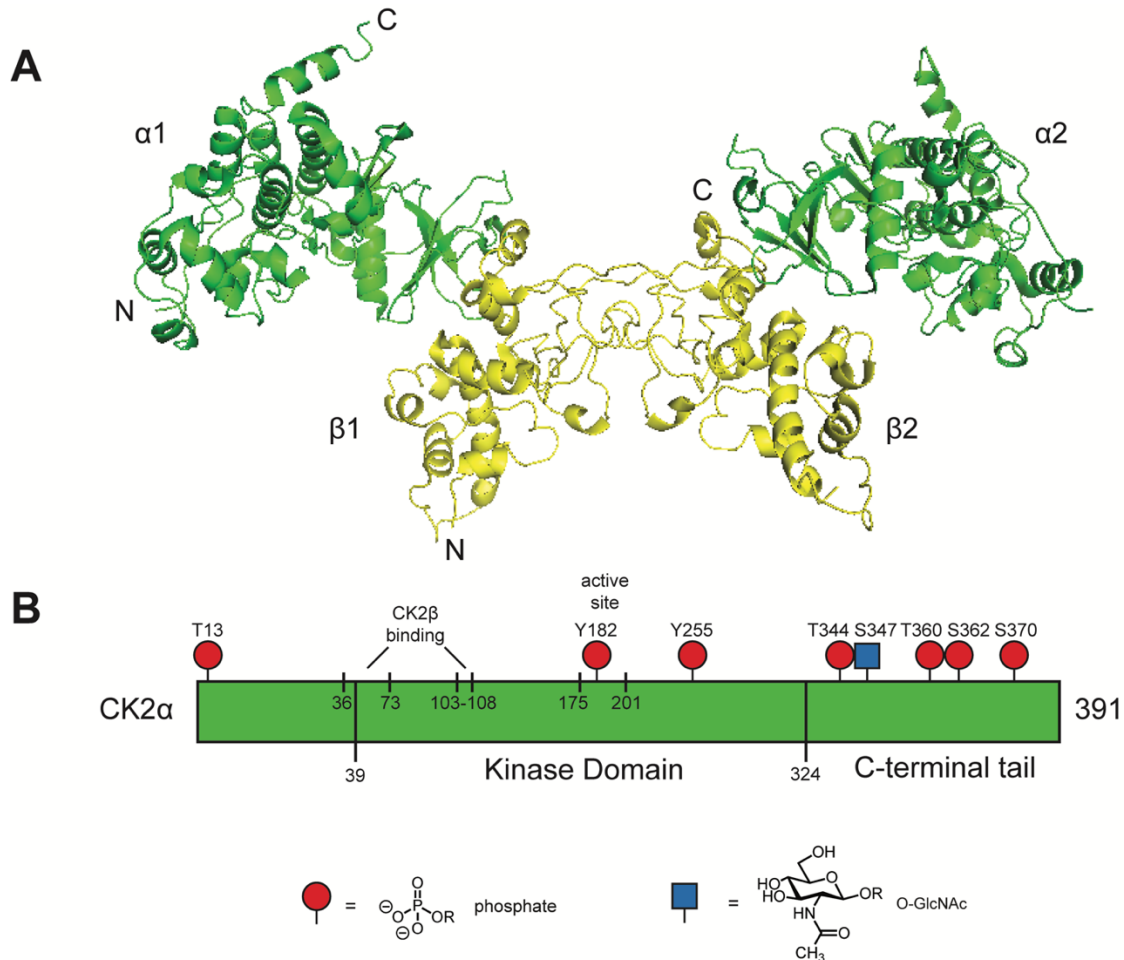


**Figure 3.1.1 Graphical representations of (A) CK2 holoenzyme crystal structure and (B) CK2 $\alpha$  monomer primary sequence**

The crystal structure of the CK2 holoenzyme was solved by Issinger and colleagues in 2001 (Figure 3.1.1A).<sup>152</sup> It corroborates previous evidence that the structural  $\beta$  subunits bind one another in the center, and the two catalytic  $\alpha$  subunits face outward and do not contact one another. Each  $\alpha$  subunit forms contacts with both  $\beta$  subunits – to elaborate, the crystal structure illustrates how subunit  $\alpha 2$  interacts with residues between secondary structure elements in the body of  $\beta 2$ , as well as the C-terminal tail of  $\beta 1$ . These  $\alpha/\beta$  interactions are predominantly



hydrophobic, and allow for more intersubunit flexibility compared to the  $\beta/\beta$  contacts, which occur through salt bridges and hydrogen bonds. It is possible that this intersubunit flexibility allows for a broad range of active conformational states, contributing to the high promiscuity of CK2. More structural data demonstrating how CK2 $\beta$  interacts with holoenzyme-reliant CK2 substrates during catalysis is needed to confirm this hypothesis.

The catalytic  $\alpha$  subunit of CK2 is phosphorylated at several sites. The T13 phosphosite at the N-terminus is installed by Akt1, and appears to increase the affinity of CK2 $\alpha$  for phosphorylation of transcription initiation factor I (TIF-IA) at S170 and S172, resulting in increased rRNA synthesis.<sup>153</sup> The Y182 phosphosite within the active site arises from a rare example of tyrosine phosphorylation by CK2 $\alpha$  itself. This intermolecular autophosphorylation is not necessary for catalytic activity. It is inhibited by either CK2 $\beta$  or excess peptide substrate, and is reversed by addition of ADP or GDP. Further investigation is needed to determine the physiological relevance of Y182 autophosphorylation. The Y255 phosphosite is installed by Src and correlates with increased catalytic activity, implying a role for CK2 activity in B cell activation.<sup>154</sup> Finally, the C-terminal tail of CK2 $\alpha$  is phosphorylated by the Cdk1/Cyclin B complex at T344, T360, S362, and S370.<sup>155, 156</sup> These phosphosites are modified in prophase and metaphase, and dephosphorylated during anaphase. While modification at these sites does not affect CK2 catalytic activity, there is evidence that they are involved in protein-protein interactions and subcellular localization.

In 2012, bovine CK2 $\alpha$  was reported to be O-GlcNAcylated at a conserved C-terminal serine, S347 (Figure 3.1.1B).<sup>75</sup> This mapped glycosite is proximal to the previously discussed C-terminal phosphosites. On the synthetic peptide level, S-GlcNAc at S347 was found to inhibit phosphorylation at T344 by Cdk1/Cyclin B. Phosphorylation at this position is necessary for a protein-protein interaction (PPI) – that of CK2 $\alpha$  and Pin1, a peptidyl-prolyl cis/trans isomerase. The authors argue that O-GlcNAcylation induces a net destabilization of CK2 $\alpha$  by downregulating

the CK2 $\alpha$ /Pin1 PPI, and show that endogenous CK2 $\alpha$  protein levels decrease in HeLa cells following treatment with global OGA inhibitor Thiamet G.

This publication from the Cole lab represents the only biological characterization of O-GlcNAc on CK2 $\alpha$  thus far. The study draws its conclusions through *in vitro* kinase assays on peptide substrates. These kinase assays were performed using semisynthetic CK2 $\alpha$  with or without O-GlcNAc installed, and in the presence or absence of CK2 $\beta$  or Pin1. How glycosylation affects CK2 $\alpha$  kinase activity has yet to be examined *in cellulo*, where the enzyme interacts with a multitude of other protein complexes that influence its subcellular localization and substrate specificity. Additionally, how phosphosites downstream of CK2 substrates are affected by CK2 $\alpha$  glycosylation has yet to be explored. In the following subchapters, we employ a protein-selective method to regulate O-GlcNAc on overexpressed CK2 $\alpha$ , and demonstrate the resultant effects on the phosphoproteome of HEK293T cells.

### **3.2 Manipulating glycosylation on CK2 $\alpha$**

We first evaluated whether O-GlcNAc alters CK2 $\alpha$  stability in HEK293T cells using a cycloheximide chase experiment and found a minor destabilization of CK2 $\alpha$  on Thiamet G treatment, but not OSMI-4b treatment, in line with prior work in HeLa cells (Figure 3.2.1).<sup>75</sup> This confirmation encouraged us to attempt protein-selective manipulation of O-GlcNAc on tagged CK2 $\alpha$ . Recently, Dr. Daniel Ramirez and Dr. Yun Ge respectively reported methods to write and erase O-GlcNAc from a desired target protein in cells using an engineered nanobody-OGT or -splitOGA system.<sup>59, 60</sup> The nanobody is a small, single-domain protein binder that recruits the fused O-GlcNAc editor to a target protein for selective modulation of O-GlcNAc in a cellular environment, without significantly affecting other glycoproteins. These targeted methods complement methods for global perturbation of O-GlcNAc (e.g., chemical inhibitors of OGT or

OGA, or genetic knockout)<sup>56, 58, 157</sup> and the study of specific glycosites by site-directed mutagenesis.<sup>158</sup>

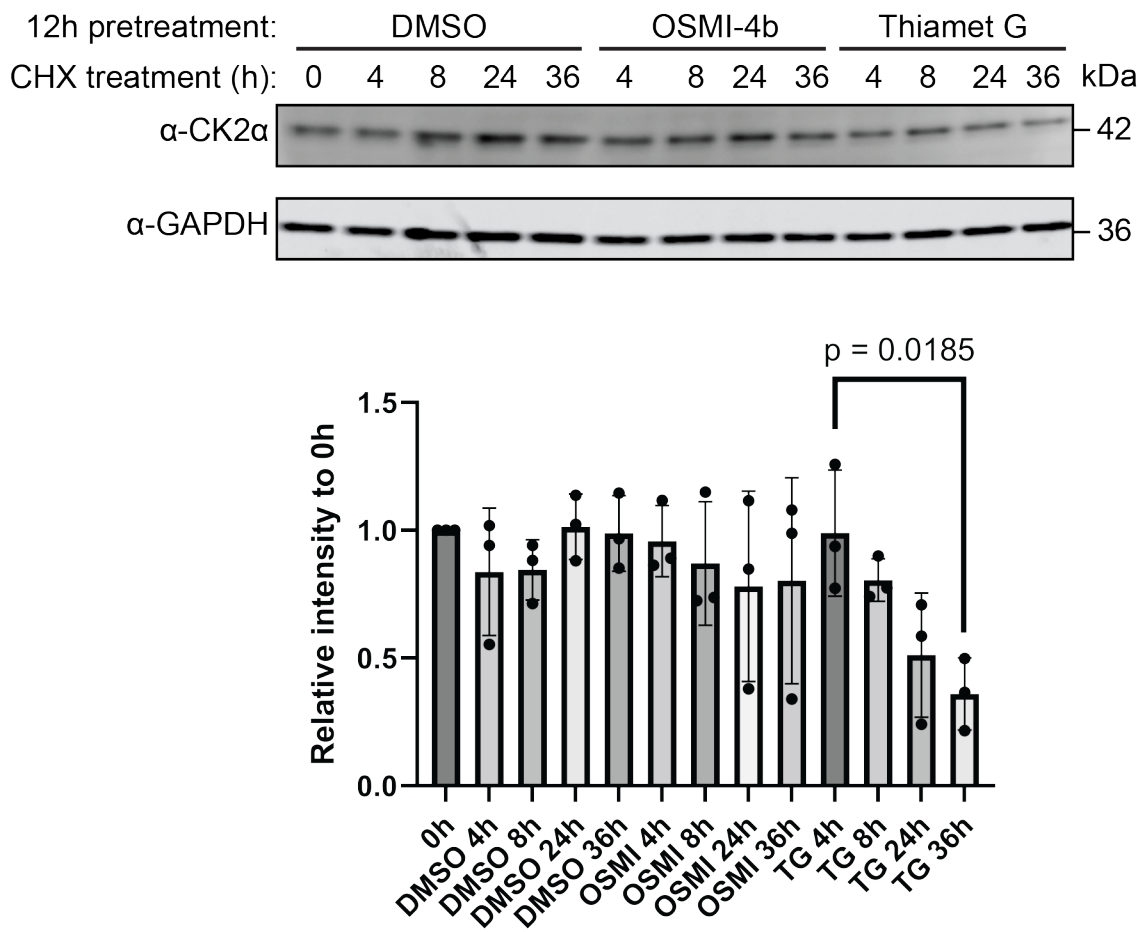


**Figure 3.2.1 – Endogenous CK2 $\alpha$  levels decrease following OGA Inhibition.** HEK293T cells in 6-well plates were treated with 50  $\mu$ M OSMI-4b, 100  $\mu$ M Thiamet G, or an equivalent volume of DMSO for 12 h before addition of 1X cycloheximide. Cell lysates were then collected at the notated timepoints and were separated by SDS-PAGE. CK2 $\alpha$  and GAPDH protein levels were measured by Western blot, and CK2 $\alpha$  intensity was normalized to the corresponding GAPDH intensity in ImageJ for quantification. Error bars are representative of three independent replicates. A two-tailed Student's *t*-test was used for statistical analysis.

We evaluated whether the nanobody-OGT and -splitOGA system were readily amenable to writing and erasing O-GlcNAc from GFP-FLAG-CK2 $\alpha$ -EPEA (Figure 3.2.2). To enhance selectivity for the target protein through the nanobody, we used an engineered OGT(4) bearing a truncated tetratricopeptide repeat (TPR) domain for introduction of O-GlcNAc<sup>59</sup> and an

engineered splitOGA system for removal of O-GlcNAc.<sup>60</sup> We additionally used the GFP-binding nanobody nLaG6 for recruitment of the engineered OGT and splitOGA to the target protein through GFP due to its superior efficiency in writing and erasing O-GlcNAc from a desired target protein.<sup>59, 159</sup>

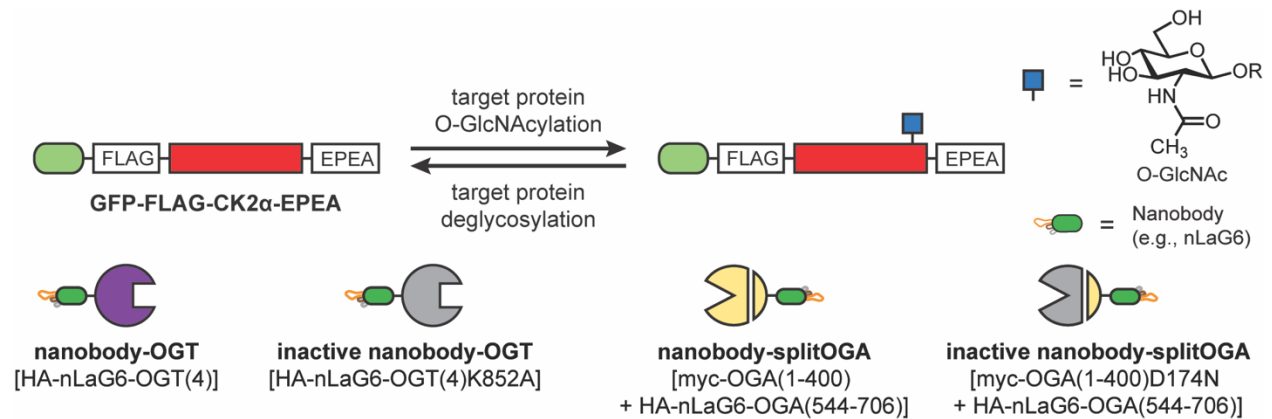


**Figure 3.2.2 – Approach for selectively manipulating glycosylation on tagged CK2 $\alpha$ .** GFP at the N-terminus of overexpressed CK2 $\alpha$  is recognized by a GFP-binding nanobody (nLaG6). O-GlcNAc is selectively written on CK2 $\alpha$  by co-transfected nanobody-OGT, or selectively erased by co-transfected nanobody-splitOGA. Catalytically inactive versions of nanobody-OGT and nanobody-splitOGA are used as negative controls.

To evaluate selective introduction of O-GlcNAc to CK2 $\alpha$ , GFP-FLAG-CK2 $\alpha$ -EPEA was co-expressed with nanobody-OGT [HA-nLaG6-OGT(4)] or a catalytically inactive nanobody-OGT [HA-nLaG6-OGT(4)K852A]. We additionally compared the target protein O-GlcNAcylation to global OGA inhibition by transfection of GFP-FLAG-CK2 $\alpha$ -EPEA to cells with or without Thiamet G treatment. After 24 h, O-GlcNAc levels of immunoprecipitated CK2 $\alpha$  and the broader proteome were examined by Western blot with the  $\alpha$ -O-GlcNAc antibody RL2 (Figure 3.2.3A). Interestingly, GFP-FLAG-CK2 $\alpha$ -EPEA was moderately O-GlcNAcylated and these levels were not perturbed by Thiamet G treatment, although global elevation of O-GlcNAc on the broader proteome was observed. By contrast, co-expression of nanobody-OGT, but not the inactive nanobody-OGT, selectively and significantly increased glycosylation of GFP-FLAG-CK2 $\alpha$ -EPEA (Figure 3.2.3B).

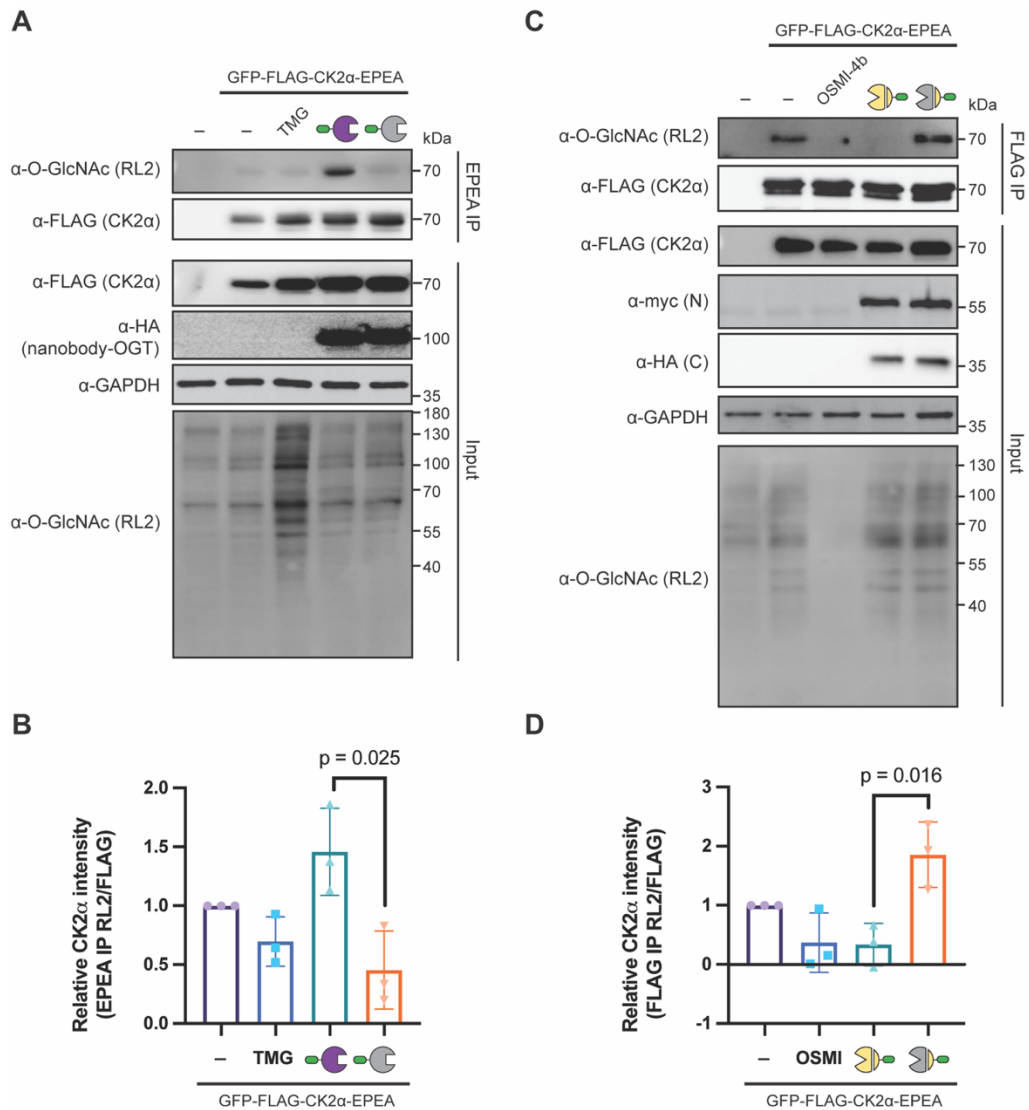


**Figure 3.2.3 Nanobody system selectively alters glycosylation of CK2 $\alpha$ .** (A) Nanobody-OGT selectively increases O-GlcNAc on GFP-FLAG-CK2 $\alpha$ -EPEA. HEK293T cells were transfected with GFP-FLAG-CK2 $\alpha$ -EPEA with active or inactive nanobody-OGT or treated with Thiamet G (TMG) (100 $\mu$ M), prior to immunoprecipitation with C-tag resin. (B) Relative O-GlcNAc levels on GFP-FLAG-CK2 $\alpha$ -EPEA from part B. (C) Nanobody-splitOGA selectively decreases O-GlcNAc on GFP-FLAG-CK2 $\alpha$ -EPEA. HEK293T cells were transfected with GFP-FLAG-CK2 $\alpha$ -EPEA with active or inactive nanobody-splitOGA, or treated with OSMI-4b (25 $\mu$ M), prior to immunoprecipitation with anti-FLAG resin. (D) Relative O-GlcNAc levels on GFP-FLAG-CK2 $\alpha$ -EPEA from part D. In C and E, error bars represent  $\pm$  one standard deviation from three independent replicates, and a two-tailed Student's *t*-test was used for statistical analysis.

We next evaluated if the proximity-directed nanobody-splitOGA system<sup>60</sup> would effectively deglycosylate CK2 $\alpha$  in a similar manner (Figure 3.2.3C and Figure 3.2.3D). The nanobody-

splitOGA was expressed as a myc-tagged N-terminal fragment containing residues 1–400 [myc-OGA(1–400)] with nLaG6-fused to a HA-tagged C-terminal fragment containing residues 544–706 [HA-nLaG6-OGA(544-706)]. The catalytically inactive version of splitOGA contains a D174N mutation in the N-terminal fragment [myc-OGA(1–400)D174N]. The targeted nanobody-splitOGA system was additionally compared to global inhibition of OGT by OSMI-4b treatment. To enhance detection of the basal levels of O-GlcNAc on GFP-FLAG-CK2 $\alpha$ -EPEA, we increased the cellular input for immunoprecipitation. We observed a decrease in glycosylation of GFP-FLAG-CK2 $\alpha$ -EPEA co-transfected with the nanobody-splitOGA comparable to OSMI-4b treatment that occurred selectively on the target protein without affecting global O-GlcNAc levels (Figure 3.2.3C). These observations were reproducible and statistically significant across replicates (Figure 3.2.3D). Taken together, the nanobody-OGT and nanobody-splitOGA can write and erase O-GlcNAc from GFP-FLAG-CK2 $\alpha$ -EPEA, without broad perturbations to the global glycoproteome.

### 3.3 CK2 $\alpha$ is glycosylated at S347 in human cells

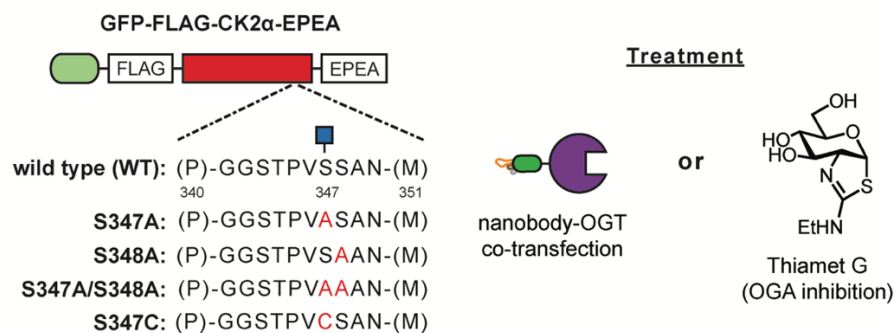


**Figure 3.3.1 Experimental design to map the glycosite(s) of GFP-FLAG-CK2 $\alpha$ -EPEA.** GFP-FLAG-CK2 $\alpha$ -EPEA was point mutated at positions Ser347 and Ser348 to Ala or Cys and evaluated in the presence or absence of nanobody-OGT or Thiamet G treatment.

After confirming the function of the nanobody-OGT and -splitOGA system on CK2 $\alpha$ , we sought to confirm that the O-GlcNAc modification on GFP-FLAG-CK2 $\alpha$ -EPEA aligned with the

previously reported Ser347 glycosite from bovine brain,<sup>75</sup> and that this glycosite was installed by nanobody-OGT. We used a site-directed mutagenesis approach, in conjunction with additional strategies beyond nanobody-OGT co-transfection to increase O-GlcNAc on CK2 $\alpha$ , to test these hypotheses (Figure 3.3.1). These additional strategies include treatment with OGA inhibitor Thiamet G and cysteine mutagenesis.<sup>62</sup>

We first examined Ser347 and the neighboring Ser348 as potential glycosites by mutating one or both to alanine and blotting the immunoprecipitated CK2 $\alpha$  for O-GlcNAc. Nanobody-OGT specifically installed O-GlcNAc to Ser347 and O-GlcNAc levels were readily reduced in mutants carrying S347A (Figure 3.3.2A). These data show that Ser347 is the location of the glycosite on CK2 $\alpha$  and it is installed by both endogenous OGT and nanobody-OGT [HA-nLaG6-OGT(4)].

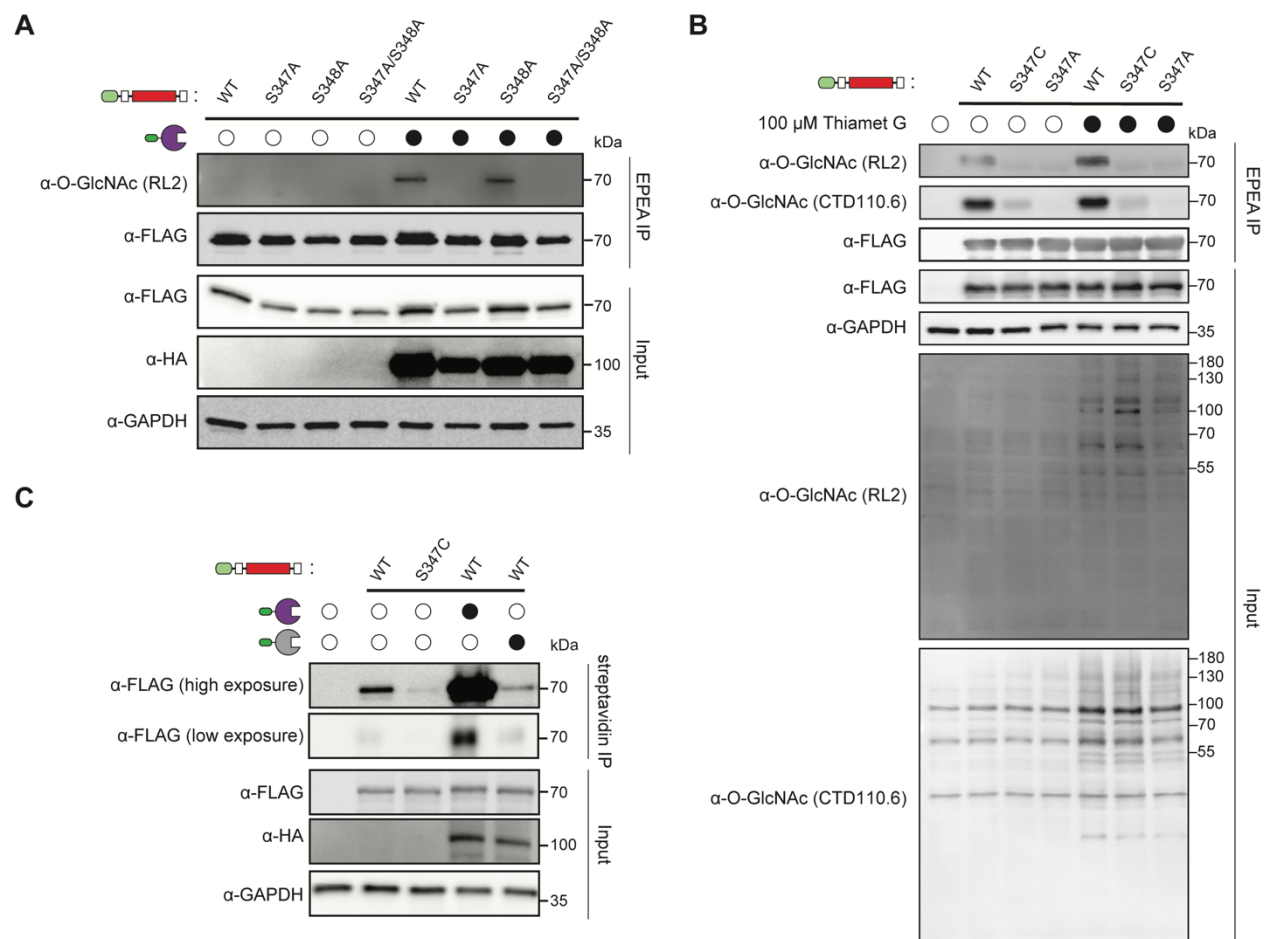


**Figure 3.3.2 GFP-FLAG-CK2 $\alpha$ -EPEA is O-GlcNAcylated at Ser347. (A)** GFP-FLAG-CK2 $\alpha$ -EPEA is glycosylated at Ser347 by nanobody-OGT. HEK293T cells were transfected with the

**Figure 3.3.2 (continued)** indicated CK2 $\alpha$  construct with or without nanobody-OGT, prior to immunoprecipitation with C-tag resin. **(B)** Endogenous OGT glycosylates GFP-FLAG-CK2 $\alpha$ -EPEA at Ser347. HEK293T cells were transfected with the indicated CK2 $\alpha$  construct with or without Thiamet G (100 $\mu$ M) treatment, prior to immunoprecipitation with C-tag resin. **(C)** Visualization of the GFP-FLAG-CK2 $\alpha$ -EPEA glycosite Ser347 by chemoenzymatic labeling. HEK293T cells were transfected with the indicated CK2 $\alpha$  construct with or without nanobody-OGT, prior to chemoenzymatic labeling of O-GlcNAc with GalNAz by GalT1(Y289L). Labeled glycosites were tagged with biotin-PEG(4)-alkyne prior to immunoprecipitation with streptavidin resin. All Western blot data are representative of three independent replicates.

As Ser347 is the primary glycosite on the tagged CK2 $\alpha$  construct, we investigated whether stable introduction of O-GlcNAc to the target protein could also be achieved by point mutagenesis, where mutation to Cys would potentially generate a S-GlcNAc site that is not hydrolyzed by OGA.<sup>62</sup> We evaluated these point mutants for responsiveness to Thiamet G treatment with two O-GlcNAc antibodies, RL2 and CTD110.6 (Figure 3.3.2B). Curiously, the RL2 antibody appeared more sensitive to O-GlcNAc levels on CK2 $\alpha$  in response to Thiamet G treatment than the CTD110.6 antibody. However, both the RL2 or CTD110.6 antibody showed poor glycosylation of the CK2 $\alpha$  S347C mutant.

We sought to confirm the responsiveness of the O-GlcNAc site on CK2 $\alpha$  to nanobody-OGT using chemoenzymatic labeling as an orthogonal O-GlcNAc detection method. In brief, HEK293T cell lysates after transfection were chemoenzymatically labeled with GalNAz using GalT1 (Y289L).<sup>48</sup> The azide on GalNAz is subsequently tagged to a biotin-PEG(4)-alkyne by copper-catalyzed azide-alkyne cycloaddition (CuAAC) to enable enrichment of O-GlcNAcylated proteins with streptavidin resin. Signal detected by  $\alpha$ -FLAG should be proportional to the amount of glycosylated GFP-FLAG-CK2 $\alpha$ -EPEA. Using this chemoenzymatic enrichment method, significantly more CK2 $\alpha$  was pulled down when GFP-FLAG-CK2 $\alpha$ -EPEA is co-transfected with active nanobody-OGT as compared to the inactive nanobody-OGT (Figure 3.3.2C). In addition, enrichment of the S347C mutant was poor compared to the wild-type CK2 $\alpha$ , despite equivalent



expression of both proteins. Therefore, the S347C mutant is not readily glycosylated by endogenous OGT and the modification does not build up as a result.

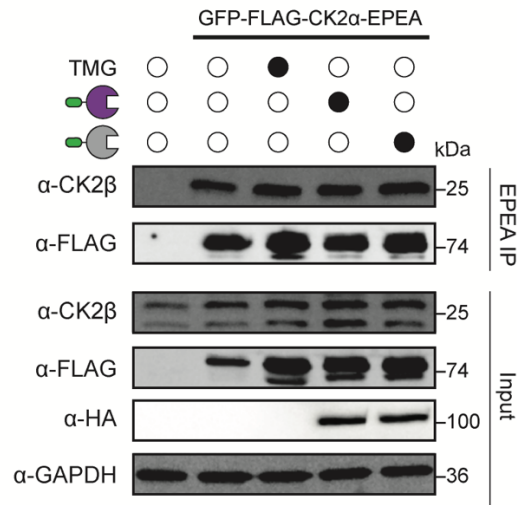


**Figure 3.3.3 GFP-FLAG-CK2α-EPEA binds to endogenous CK2β.** HEK293T cells were transfected with the indicated CK2α construct with or without 100 μM Thiamet G (TMG) treatment, prior to non-denaturing lysis, and co-immunoprecipitation with C-tag resin. Data are representative of three independent replicates.

While CK2α alone is catalytically active, many of the protein targets of the CK2 complex are dependent on association of CK2α with CK2β.<sup>160, 161</sup> We therefore verified that GFP-FLAG-CK2α-EPEA forms a complex with this important component of the CK2 holoenzyme (Figure 3.3.3). We observed that endogenous CK2β is co-immunoprecipitated when GFP-FLAG-CK2α-EPEA is overexpressed, and the amount of co-immunoprecipitated CK2β is not affected by Thiamet G treatment or nanobody-OGT co-transfection. This implies that O-GlcNAcylation of the C-terminal domain of CK2α does not affect CK2β binding, which aligns with prior reports as the CK2α residues involved in CK2β binding are between residues 36–108,<sup>152</sup> whereas the Ser347 glycosite is distal to these residues. With confirmation that nanobody-OGT modifies GFP-FLAG-CK2α-EPEA at its previously reported glycosite and does not affect association with CK2β, we were prepared to move forward with phosphoproteomic analysis.

### 3.4 CK2 $\alpha$ glycosylation affects the phosphoproteome

As CK2 is a horizontal regulator of multiple cellular processes, and has hundreds of reported substrates,<sup>75, 145, 162, 163</sup> if O-GlcNAc on CK2 $\alpha$  modulates the phosphoproteome, we would expect to observe changes to phosphosites that are directly and indirectly regulated by CK2 within central pathways, such as cell cycle progression, chromatin structure, and apoptosis. We turned to quantitative phosphoproteomics to investigate these expected phosphorylation changes. HEK293T cells were co-transfected with GFP-FLAG-CK2 $\alpha$ -EPEA and catalytically active or inactive forms of nanobody-OGT or nanobody-splitOGA for 24 h in triplicate (Figure 3.4.1). The cells were lysed, the lysates were trypsinized, and phosphopeptides were enriched by TiO<sub>2</sub> affinity chromatography. The enriched phosphopeptides were reacted with tandem mass tag (TMT)-10plex tags for quantitative analysis by mass spectrometry using Higher-energy C-trap Dissociation (HCD) fragmentation. Phosphopeptides were assigned by database searching using Sequest HT in Proteome Discoverer software.

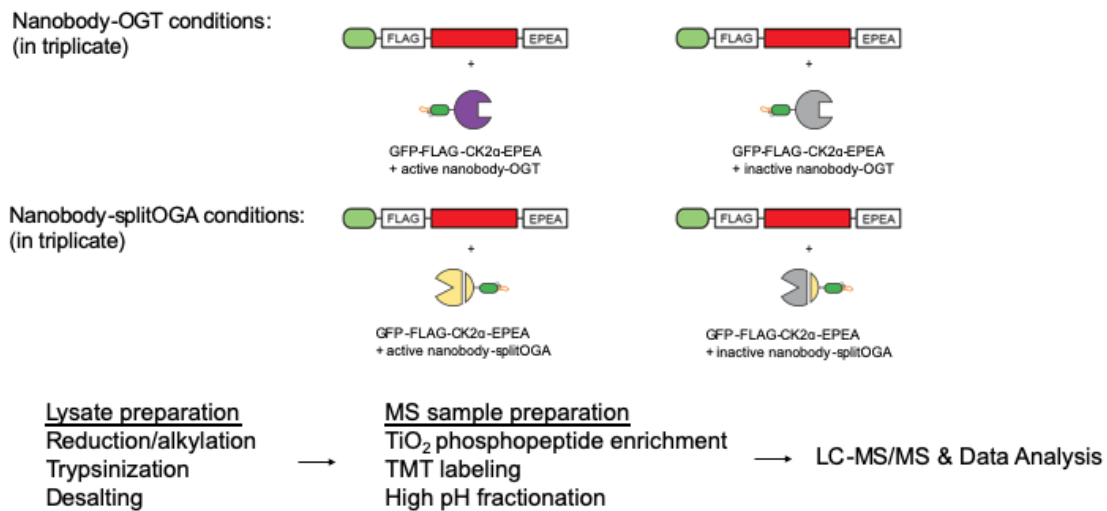


**Figure 3.4.1 – Phosphoproteomics Workflow.** Phosphoproteomic analysis took place over two separate experiments. In each, tagged CK2 $\alpha$  was overexpressed in conjunction with either active or inactive forms of nanobody-OGT or nanobody-splitOGA in triplicate. Following cell lysis, protein concentrations were quantified, and samples were reduced, alkylated, trypsinized, and desalted. The enrichment of phosphopeptides was performed by TiO<sub>2</sub> phosphopeptide

**Figure 3.4.1 (continued)** enrichment. Tandem mass tag (TMT)-10plex labeling was then performed to allow for sample pooling and quantification. Finally, high pH fractionation before LC-MS/MS analysis was employed to increase total phosphopeptide resolution.

The phosphoproteomics data was initially analyzed at the protein level (Figure 3.4.2A, Figure 3.4.2B, Supplementary Table 1). High confidence (1% False Discovery Rate (FDR)) phosphoproteins were evaluated based on their fold change (FC) in enrichment between the active and inactive nanobody-OGT and -splitOGA conditions, and their associated p-value. Specifically, a  $|\log_2(\text{FC})|$  of at least 0.5, a p value less than or equal to 0.05, and at least two peptide spectral matches (PSMs) were required for inclusion at the protein level. We considered a  $|\log_2(\text{FC})|$  between 0.5 and 1 a moderate enrichment and  $|\log_2(\text{FC})| \geq 1$  a major enrichment. Principal component analyses and normalization box plots for each level of analysis are included (Supplementary Figures 5–12). This statistical analysis indicates stronger independent clustering between the control and treatment samples in the nanobody-OGT condition compared to the nanobody-splitOGA condition.

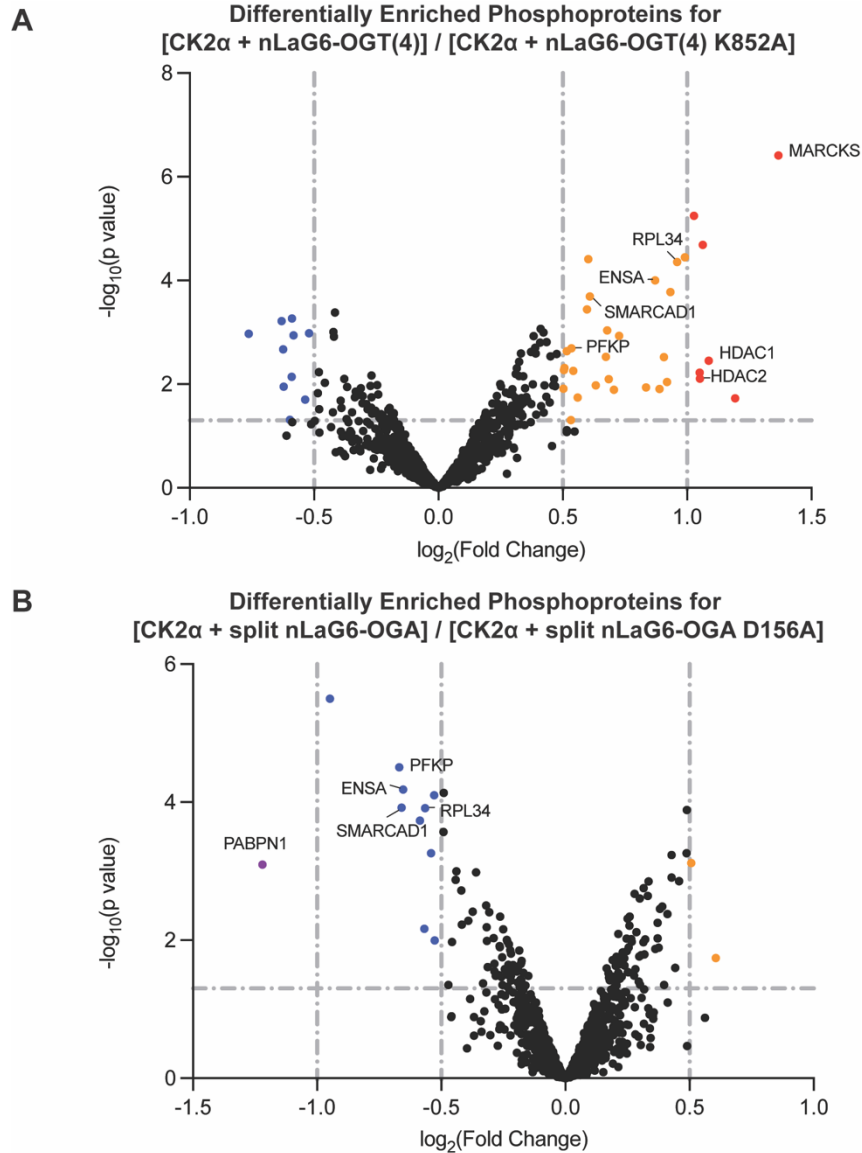


**Figure 3.4.2 O-GlcNAc on GFP-FLAG-CK2 $\alpha$ -EPEA affects the phosphoproteome. (A)** Volcano plot of the fold change in phosphoproteins enriched from cell lysates transfected with GFP-FLAG-CK2 $\alpha$ -EPEA and the active or inactive nanobody-OGT. **(B)** Volcano plot of the fold change in phosphoproteins enriched from cell lysates transfected with GFP-FLAG-CK2 $\alpha$ -EPEA and the active or inactive nanobody-splitOGA. In **A** and **B**, data points were colored purple, blue, orange, or red corresponding to their  $\log_2(\text{FC})$  ( $\leq -1$ ,  $-1$  to  $-0.5$ ,  $0.5$  to  $1$ , and  $\geq 1$  respectively) if they met the p-value threshold ( $p \leq 0.05$ ).

In the nanobody-OGT condition, increased O-GlcNAc on CK2 $\alpha$  may promote phosphorylation of some substrates while reducing phosphorylation of others, such as substrates that are dependent on interaction with unmodified Ser347 or phosphorylated Thr344 on the C-

terminus of CK2 $\alpha$ . Seven phosphoproteins were majorly enriched in a nanobody-OGT activity-dependent manner ( $|\log_2(\text{FC})| \geq 1$ , p-value  $\leq 0.05$ , Figure 3.4.2A). Of these phosphoproteins, HDAC1 and HDAC2 are previously reported substrates of CK2.<sup>164</sup> An additional 25 phosphoproteins show a moderate increase in enrichment, and ten phosphoproteins show a moderate decrease in enrichment ( $0.5 \leq |\log_2(\text{FC})| < 1$ , p-value  $\leq 0.05$ ). The majority of other phosphoproteins detected do not change phosphorylation significantly, suggesting that they are unaffected by increased O-GlcNAc on CK2 $\alpha$ .

Conversely, phosphoproteins that are dependent on O-GlcNAc on CK2 $\alpha$  should decrease in enrichment after treatment with nanobody-splitOGA, while those that are inhibited by O-GlcNAc on CK2 $\alpha$  should increase. Only one protein, PABPN1, was majorly down-regulated based on nanobody-splitOGA activity ( $|\log_2(\text{FC})| \geq 1$ , Figure 3.4.2B). PABPN1 is a phosphorylated RNA-binding protein that is a substrate of ATM1, a known CK2 substrate.<sup>165</sup> PABPN1 also appears in the OGT dataset, but its FC is insignificant based on p-value. In the moderate FC threshold ( $0.5 \leq |\log_2(\text{FC})| < 1$ , p-value  $\leq 0.05$ ), two proteins increase, and ten proteins decrease in enrichment. The more limited changes in the phosphoproteome due to nanobody-splitOGA treatment may be a result of the low level of basal O-GlcNAc on CK2 $\alpha$  observed by Western blot (Figure 3.2.3C). Reducing O-GlcNAc on CK2 $\alpha$  with nanobody-splitOGA even further may not produce as large an effect on the phosphoproteome as we observed with increasing O-GlcNAc with nanobody-OGT.

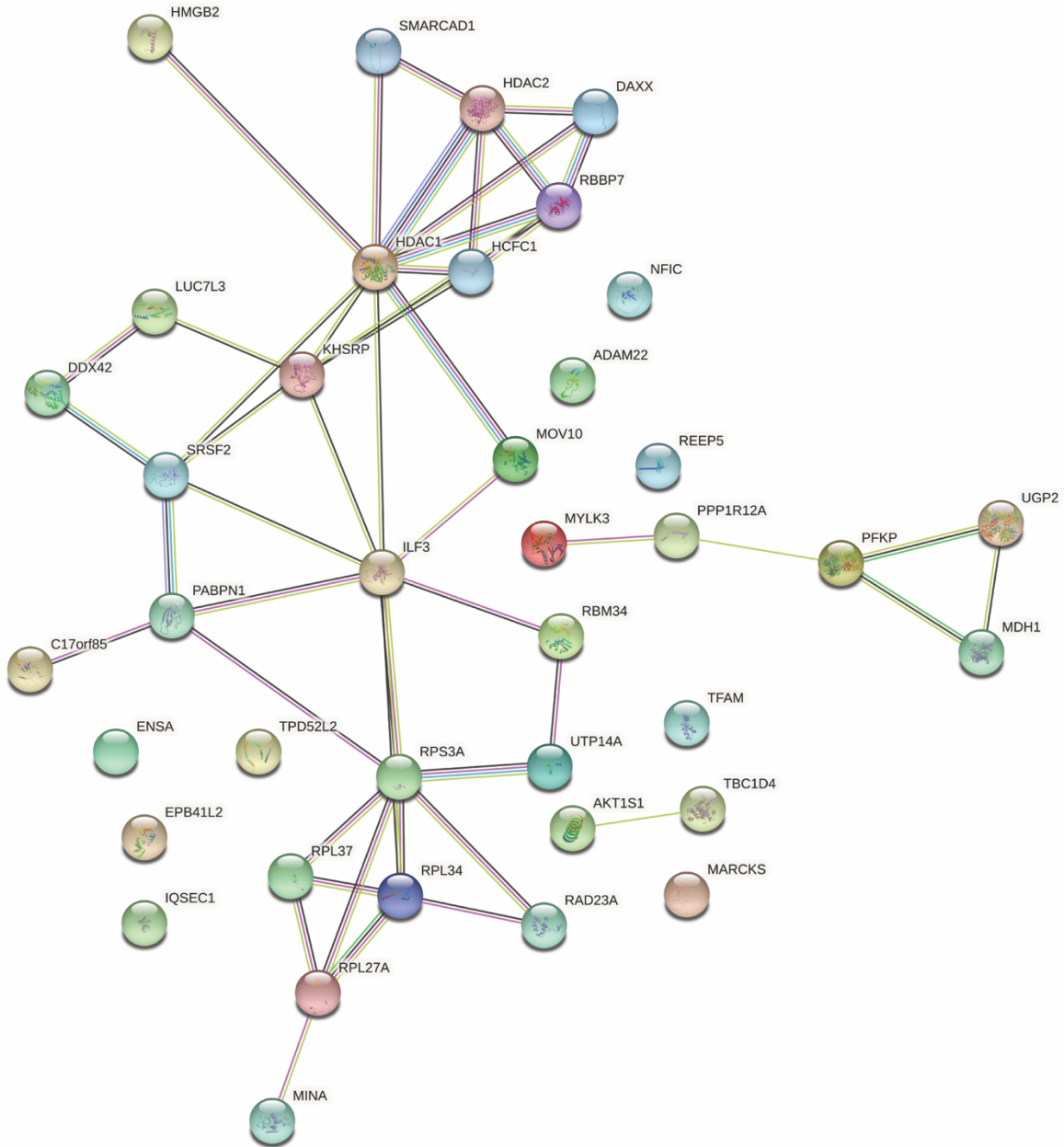


**Figure 3.4.3 STRING<sup>166</sup> network of phosphoproteins with a moderate/major increase in the nanobody-OGT condition, or moderate/major decrease in the nanobody-splitOGA condition.**

Based on the protein-level analysis, we obtained a list of 51 statistically significant phosphoproteins that change by the activity of nanobody-OGT or nanobody-splitOGA [ $|\log_2(\text{FC})| \geq 0.5$ ,  $p\text{-value} \leq 0.05$ ]. Of these 51 proteins, 39 increased in enrichment in the nanobody-OGT

condition and/or decreased in enrichment in the nanobody-splitOGA condition. This list of phosphoproteins whose regulation correlated with O-GlcNAc on CK2 $\alpha$  was imported into STRING, an online database of protein functional interactions (Figure 3.4.3).<sup>166</sup> Interactome analysis of these 39 phosphoproteins reveals a nexus of proteins involved in chromatin regulation, including histone deacetylases HDAC1 and HDAC2, and the heavily O-GlcNAcylated cell cycle regulator HCFC1. HDAC1, HDAC2, HMGB2, and DAXX are all reported CK2 substrates (Figure 3.4.4A), which may provide the point of entry for CK2 to affect phosphorylation of other connected proteins in a glycosylation-dependent manner. We also observe clusters of phosphoproteins involved in metabolism (PFKP, MDH1, UGP2) and the ribosome (RPS3A, RPL27A, RPL34, RPL36).

A small subset of phosphoproteins (ENSA/ARPP-19, SMARCAD1, PFKP, and RPL34) met the moderate threshold for enrichment in both conditions. Enrichment of phosphopeptides from these proteins increased with active nanobody-OGT co-transfection and decreased with active nanobody-splitOGA co-transfection (Figure 3.4.4B). Although these are not reported CK2 substrates, and none of the identified phosphosites possess the consensus sequence typically recognized by CK2,<sup>167</sup> these phosphoproteins appear to be dependent on O-GlcNAc on CK2 $\alpha$ .

Integration of these indirect phosphorylation changes with direct CK2 substrates points to possible connections for how cellular pathways may be regulated by O-GlcNAc on CK2 $\alpha$  (Figure 3.4.3). ENSA/ARPP-19 is a 19kDa regulator of PP2A. The Ser67 phosphosite detected in our data is installed by the kinase Gwl.<sup>168</sup> Phosphorylation of ENSA at Ser67 results in inhibition of PP2A and an increase in Cdk1/Cyclin B activity, a kinase complex known to modify CK2 $\alpha$  near its glycosite. This interaction network represents a possible mechanism for glycosylated CK2 $\alpha$  to upregulate Cdk1/Cyclin B activity and regulate M phase progression.

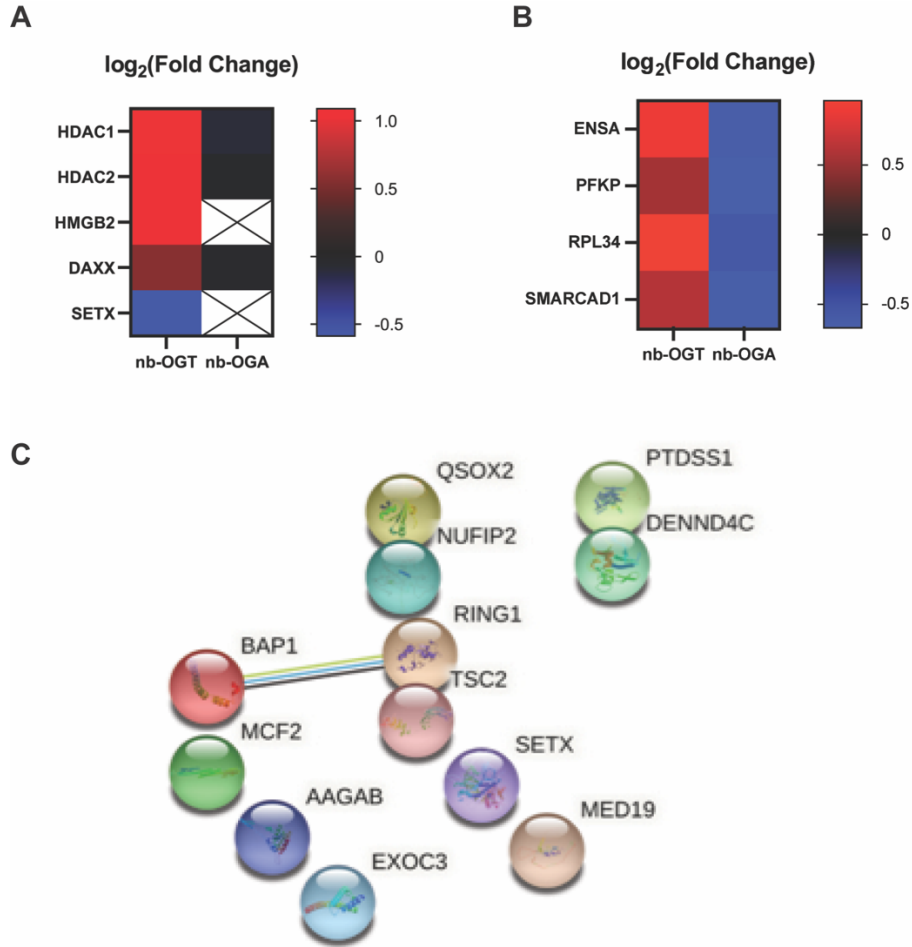


**Figure 3.4.4 Further phosphoprotein analysis** (A) Heatmap demonstrating the log<sub>2</sub>(FC) of reported CK2 substrates HDAC1, HDAC2, HMGB2, DAXX, and SETX. (B) Heatmap demonstrating the similar trend in log<sub>2</sub>(FC) of ENSA, SMARCAD1, PFKP, and RPL34 in both phosphoproteomics datasets. (C) STRING<sup>166</sup> network of phosphoproteins negatively correlated with CK2 $\alpha$  glycosylation. Phosphoproteins that significantly increased in enrichment in the nanobody-splitOGA condition or decreased in the nanobody-OGT condition were compiled and imported into STRING for interactome analysis. Only BAP1 and RING1 are functionally associated (with ubiquitination of histones).

Once in M phase, the cell simultaneously replicates the genome and maintains the epigenetic markers associated with each gene. SMARCAD1 plays a central role in this process by directing deacetylation of H3 and H4, promoting H3 Lys9 methylation, and establishing heterochromatin during the cell cycle.<sup>169</sup> SMARCAD1 also interacts with HDAC1 and HDAC2, two CK2 target proteins that similarly deacetylate histones and have phosphosites whose



occupancy increases with CK2 $\alpha$  glycosylation. Together, these results indicate that these chromatin regulating complexes may be regulated by O-GlcNAc on CK2 $\alpha$ .

Phosphorylation of PFKP and RPL34 were also moderately altered in a manner dependent on CK2 $\alpha$  glycosylation. PFKP is one of three phosphofructokinase isoforms, all of which catalyze the first step of glycolysis. While PFKP is not directly regulated by CK2, the observed PFKP phosphosite at Ser386 is installed by Akt1, a CK2 target protein.<sup>170</sup> This phosphorylation event stabilizes PFKP by blocking its interaction with an E3 ubiquitin ligase.<sup>170</sup> It is also upregulated under amino acid deprivation, and leads to ATG4B phosphorylation at Ser34 and initiation of autophagic processes in HEK293T cells.<sup>171</sup> RPL34 is a protein component of the 60S ribosome. The observed phosphosite at Ser12 has been assigned in other phosphoproteomics studies,<sup>172, 173</sup> but the specific function of phosphorylation at Ser12 is not known. If the nearby Thr15 on RPL34 is phosphorylated by another kinase, this negative charge three residues downstream of Ser12 creates a favorable environment for CK2 to phosphorylate Ser12; however, no phosphorylated Ser12/Thr15 peptides from RPL34 were assigned in our analysis.

The remaining 12 proteins phosphoproteins with  $|\log_2(\text{FC})| \geq 0.5$  and  $p\text{-value} \leq 0.05$  either increased in the nanobody-splitOGA condition or decreased in the nanobody-OGT condition. STRING network analysis indicates only two of them are functionally associated (Figure 3.4.4C). BAP1 and RING1 are both involved with ubiquitination of histones, representing another potential connection between O-GlcNAc on CK2 $\alpha$  and chromatin modification.

To gain higher resolution to the changes in phosphorylation at specific sites, the phosphoproteomics data was also analyzed at the phosphopeptide level, where the fold change of individual phosphopeptides was examined (Figure 3.4.5, Supplementary Table 2). We identified one CK2 $\alpha$  phosphosite at S294 in the nanobody-splitOGA condition, although the site occupancy did not change significantly with nanobody-splitOGA activity. To allow for analysis of

only the strongest shifts, only the major threshold for phosphopeptide enrichment ( $|\log_2(\text{FC})| \geq 1$ ,  $p\text{-value} \leq 0.05$ ) was analyzed. Twelve distinct phosphosites from 13 phosphopeptides met these criteria. Three of the 12 phosphosites, HDAC1 Ser393, HDAC2 Ser394, and MDC1 Ser329 are reported sites installed by CK2.<sup>164</sup> A peptide derived from HMGB2, another CK2 substrate, also appears in this dataset, but the Thr179 phosphosite identified is unlikely to be installed by CK2 based on the consensus sequence.

Ten of the 12 majorly changing phosphosites were derived from the nanobody-OGT condition (Figure 3.4.5A). The highest  $\log_2(\text{FC})$  hit, MARCKS, is a substrate of PKC and plays a role in crosslinking of filamentous actin.<sup>174</sup> Inactive MARCKS is normally sequestered to the cytoplasmic side of the plasma membrane. Phosphorylation at multiple sites by PKC, including Ser170, induces its release into the cytoplasm. In mouse melanoma cells, increased phosphorylated MARCKS correlates with increased cell motility,<sup>175</sup> which may correspond to increased metastatic potential in cancer. PKC and CK2 function in an antagonistic manner on p53,<sup>176</sup> and multiple examples of PKC regulating CK2 have been reported.<sup>177, 178</sup> Currently, no evidence of direct PKC regulation by CK2 exists.

Enrichment of HDAC1 Ser393 and HDAC2 Ser394 were both increased in the nanobody-OGT condition. HDAC1 and HDAC2 are each catalytic components of protein complexes involved in modulating gene expression and cell cycle progression through chromatin regulation. The role of phosphorylation at these two CK2-regulated sites is to promote dissociation of HDAC1 and HDAC2 heterodimers, leading to formation of other regulatory complexes, including homodimers, during mitosis.<sup>164</sup> This likely promotes differential substrate targeting, as HDAC1 and HDAC2 possess both distinct and overlapping substrates (Figure 3.4.5B).<sup>179</sup>

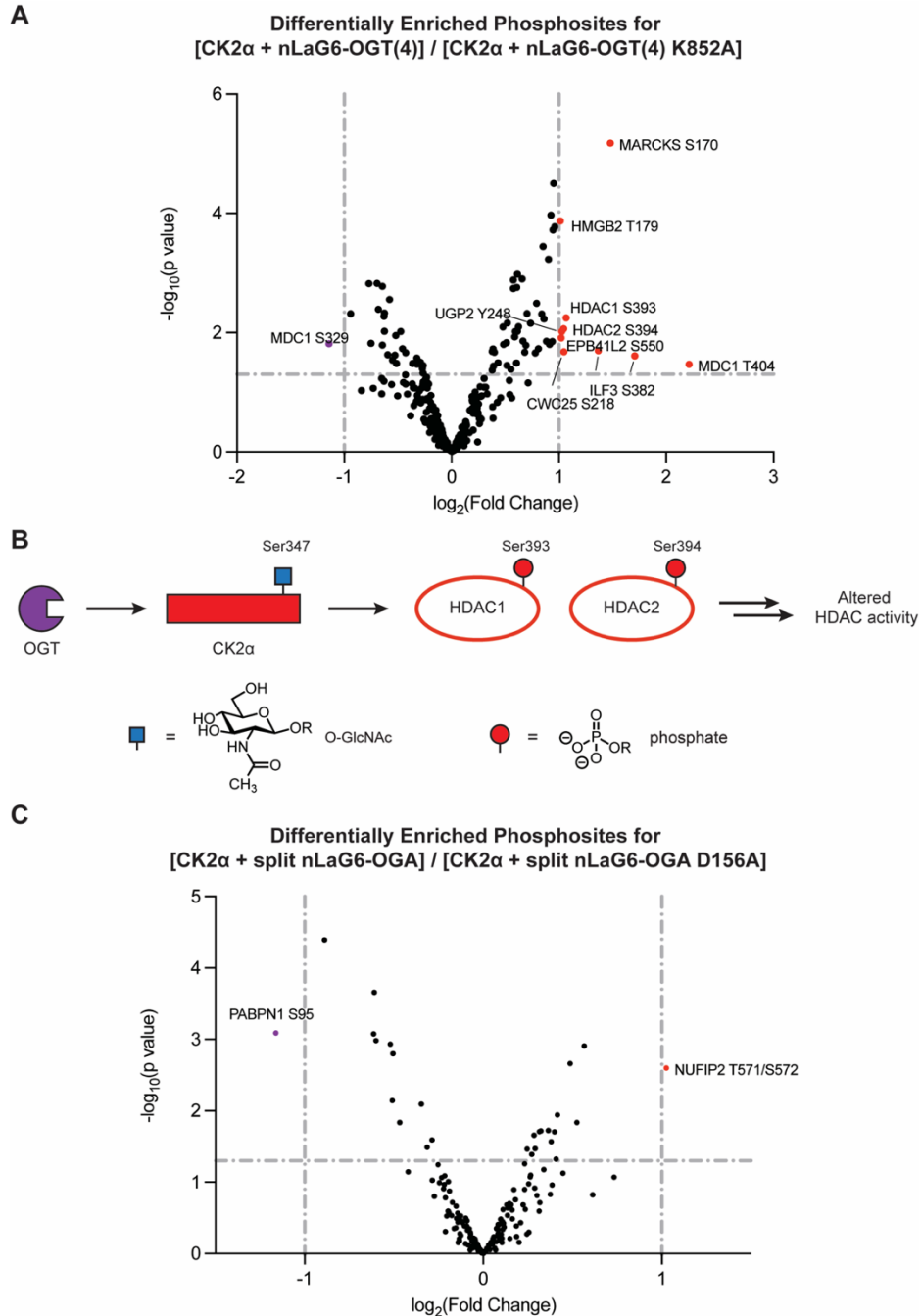


**Figure 3.4.5 O-GlcNAc on GFP-FLAG-CK2 $\alpha$ -EPEA affects specific phosphosites. (A)** Volcano plot of the fold change in phosphopeptides enriched from cell lysates transfected with GFP-FLAG-CK2 $\alpha$ -EPEA and the active or inactive nanobody-OGT. **(B)** Proposed pathway representation of the connection between O-GlcNAcylation of CK2 $\alpha$  and phosphorylation of HDAC1 at Ser393 and HDAC2 at Ser394. **(C)** Volcano plot of the fold change in phosphopeptides enriched from cell lysates transfected with GFP-FLAG-CK2 $\alpha$ -EPEA and the active or inactive nanobody-splitOGA. Each annotated data point represents a specific phosphopeptide that is majorly increased or decreased ( $|\log FC| \geq 1$ ,  $p\text{-value} \leq 0.5$ ) after enrichment.

HMGB2 is also a reported CK2 substrate. CK2 is known to phosphorylate HMGB2 at the C-terminus, but the specific location of this phosphosite is not known.<sup>180</sup> While Thr179 does not resemble a canonical CK2 phosphosite, especially compared to nearby site Ser168, this finding still warrants further investigation.

MDC1 possesses differentially regulated phosphosites. Two phosphosites on this protein show major changes, but in opposite directions – Thr404 increases, while Ser329 decreases. MDC1 is phosphorylated by CK2 at multiple sites, including these two,<sup>181</sup> all of which facilitate its interaction with NBS1. This is a necessary step in the DNA damage response, and these two MDC1 phosphosites serve redundant functions. Further investigation will reveal why MDC1 Thr404 was increased and Ser329 was decreased compared to other CK2 phosphorylation sites on MDC1.

Two of the 12 significantly differentiated phosphosites, NUFIP2 Thr571/Ser572 and PABPN1 Ser95, arose from the nanobody-splitOGA condition (Figure 3.4.5C). Both proteins are relatively understudied. NUFIP2 is a 76kDa RNA-binding protein with important roles in post-transcriptional regulation in nerve and immune cells.<sup>182, 183</sup> PABPN1 is a heavily phosphorylated RNA-binding protein that facilitates polyA tail elongation.<sup>165</sup> Neither are reported CK2 substrates, but PABPN1 Ser95 may be installed by CK2, as Glu98 can facilitate CK2 association.

### **3.5 Limitations\***

Although the approach adopted here enabled characterization of the phosphoproteome as a function of O-GlcNAc on CK2 $\alpha$  specifically, there were some limitations. Direct measurement of the C-terminal tail of CK2 $\alpha$  is challenging with the proteomics methods used here, as this region of CK2 $\alpha$  is generally intractable to trypsin or chymotrypsin digestion. Therefore, we could not draw conclusions about how O-GlcNAc affected the occupancy of the T344 phosphosite previously

---

\* A complete discussion of Chapter 3 is provided in the next chapter.

reported to engage in reverse crosstalk with S347 O-GlcNAc. Continued expression of endogenous CK2 $\alpha$  may reduce the signal to noise measured from glycosylation-dependent phosphosites. Because basal protein levels were not quantified, differences in enriched phosphopeptides among samples could arise from changes in phosphosite occupancy or protein expression. The nanobody-OGT and -splitOGA system is also dependent on the fidelity of nLaG6, which may produce off-target effects through the association to tagged CK2 $\alpha$  or modification of off-target substrates, which could be better understood through glycoproteomic analysis. Lastly, our phosphoproteomics dataset was obtained after TiO<sub>2</sub> enrichment, which could be further expanded using other phosphopeptide enrichment methods, such as Fe-NTA enrichment or Ca<sup>2+</sup> precipitation. Despite these limitations, this work both provides connections between O-GlcNAc signaling and new cellular pathways through modification of CK2 $\alpha$  and demonstrates the power of targeted writers and erasers of O-GlcNAc for the study of glycoproteins.

### **3.6 Materials and Methods**

#### **Cloning**

The vectors encoding GFP-FLAG-CK2 $\alpha$ -EPEA, HA-nLaG6-OGT(4), HA-nLaG6-OGT(4)K852A, myc-OGA(1-400), myc-OGA(1-400)D174N, and HA-nLaG6-OGA(544-706) were all generated in a pcDNA3.1 backbone by Daniel Ramirez and Yun Ge in the Woo lab, and are cited in previously published studies.<sup>59-61</sup> Subcloning of GFP-FLAG-CK2 $\alpha$ -EPEA to generate S347A, S348A, S347A/S348A, and S347C point mutants was achieved using whole-plasmid PCR. Subcloning results were validated via Sanger sequencing.

#### **Cell culture and transfection**

HEK293T cells (ATCC) were cultured in Dulbecco's Modified Eagle's Medium with 4.5 g L<sup>-1</sup> glucose and L-glutamine (VWR 95042-498) supplemented with Penicillin-Streptomycin (VWR 12001-692, 50 µg mL<sup>-1</sup> each) and fetal bovine serum (Peak Serum PS-FB2, 10% vol/vol). Cultures were maintained at 37°C in a humidified incubator with 5% CO<sub>2</sub> at a passage number no higher than 30.

Cells grown for transfection were seeded in 6-well plates (VWR 10062-892, 5 x 10<sup>5</sup> cells/well), 10cm dish (VWR 25382-166, 3.5 x 10<sup>6</sup> cells/well) or 15cm dish (VWR 25383-103, 9 x 10<sup>6</sup> cells/well) 24 hours before transfection. All transfections were performed using TransIT-PRO (Mirus Bio MIR-5740) according to the manufacturer's instructions for 24 h.

Cells were collected in cold PBS and detached using a cell scraper. Detached cells were moved to microcentrifuge tubes and centrifuged 500xg for 3 minutes. For experiments that required chemoenzymatic labeling of O-GlcNAc with modified GalT1, cells were lysed in PBS + 1% SDS via sonication. For all other experiments, cells were lysed on ice in Cell Signaling Technology lysis buffer (CST #9803) supplemented with protease/phosphatase inhibitor cocktail (CST #5872) and 100µM Thiamet G (Selleck Chem S7213).

#### **EPEA/FLAG Immunoprecipitation (CST lysis buffer)**

For immunoprecipitation of mutant CK2αs by their C-terminal EPEA tag, cell lysates with equal amounts of protein were diluted fivefold with PBS and incubated with C-tag affinity matrix (Thermo Scientific, 191307005) overnight at 4 °C with rotation. After washing the resin thrice with excess PBS, the resin was resuspended in 1X SDS sample buffer and incubated at 95 °C for 5 minutes. The supernatant was subjected to SDS-PAGE.

For immunoprecipitation of mutant CK2α by the FLAG tag, cell lysates with equal amounts of protein were diluted fivefold with TBS and incubated with anti-FLAG M2 magnetic beads (Sigma-Aldrich, M8823) overnight at 4 °C with rotation. Beads were washed with TBS buffer

(50 mM Tris-HCl pH 7.4 and 150 mM NaCl) three times. Enriched proteins were eluted by incubation with 100 ng  $\mu\text{L}^{-1}$  FLAG peptide in 100  $\mu\text{L}$  TBS for 1 hour at room temperature with rotation. Eluates were combined with 5X SDS sample buffer (1X final concentration) and subjected to SDS-PAGE.

### **GalT labeling (1% SDS lysis buffer)**

Following lysis, protein concentrations were determined by BCA assay. Cell lysates were reduced with 25 mM DTT (Thermo Scientific, 20290) at 95 °C for 5 min and alkylated with 50 mM iodoacetamide (Sigma-Aldrich, I1149) at room temperature for 1 h. Lysates were precipitated by addition of excess methanol and were resuspended in 20 mM HEPES pH 7.9 + 1% SDS at a protein concentration of 5 mg  $\text{mL}^{-1}$ . Purification of GalT1 (Y289L) enzyme and labeling of O-GlcNAcylated proteins with GalNAz were performed according to the procedure of Hsieh-Wilson and co-workers.<sup>141</sup> For 150  $\mu\text{g}$  of protein, the following components were added to cell lysates in order: water (49  $\mu\text{l}$ ), 2.5X GalT labeling buffer (80  $\mu\text{l}$ ; final concentrations, 50 mM NaCl, 20 mM HEPES, 2% NP-40, pH 7.9), 100 mM  $\text{MnCl}_2$  (11  $\mu\text{l}$ ), 500  $\mu\text{M}$  UDP-GalNAz (10  $\mu\text{l}$ ) and 2 mg  $\text{mL}^{-1}$  GalT1 (Y289L) (10  $\mu\text{l}$ ). The reaction was gently rotated at 4 °C for at least 24 hours, and proteins were precipitated as described above.

### **Click chemistry**

As an alternative method for detection of O-GlcNAcylated proteins, copper-catalyzed azide-alkyne cycloaddition (CuAAC) was performed based on the procedure of Woo and co-workers<sup>184</sup> following GalT labeling. Lysates were resolubilized in PBS + 1% SDS and were incubated at room temperature for 1 hour with 100  $\mu\text{M}$  THPTA (Sigma-Aldrich, 762342), 0.5 mM  $\text{CuSO}_4$ , 2.5 mM fresh sodium ascorbate and 100  $\mu\text{M}$  of biotin-PEG4-alkyne (Click Chemistry

Tools, TA105) for immunoblotting/enrichment. Reactions were quenched by addition of excess methanol, and protein pellets were resolubilized in PBS + 1% SDS for downstream applications.

### **Western blotting**

SDS-PAGE was performed using 6%–12% Tris-Glycine gels in a Mini-PROTEAN® BioRad gel system. Following PAGE at 200V for 40-45 minutes, proteins were transferred to a nitrocellulose membrane using an iBlot2 system (Thermo Scientific). Membranes were blocked with TBS containing 0.1% Tween-20 (TBST) plus 5% BSA (Sigma-Aldrich, A9647) for 90 minutes at room temperature, then incubated with the indicated primary antibodies in TBST + 1% BSA at 4°C overnight. Primary antibody staining solution was removed, and blots were washed once with TBST for 5 minutes at room temperature before addition of secondary antibodies (diluted 1:10,000) in TBST + 1% BSA and incubation at room temperature for 1 hour. Blots were washed thrice for 5 minutes in TBST before imaging. Immunoblot images were acquired using an Azure Imager C600 (Azure Biosystems) and analyzed with Fiji ImageJ. All infrared fluorescence Western blot images were converted to grayscale in Fiji ImageJ. Unsaturated exposure images were used for quantification, with the appropriate loading controls used as standards.

Primary antibodies used:  $\alpha$ -FLAG (CST #14793),  $\alpha$ -GAPDH (CST #97166),  $\alpha$ -myc (CST #2276),  $\alpha$ -HA (CST #3724),  $\alpha$ -CK2 $\alpha$  (CST #2656),  $\alpha$ -CK2 $\beta$  (abcam ab76025), RL2 (abcam ab2739), CTD110.6 (CST #9875). All primary antibodies except  $\alpha$ -GAPDH were used at a 1:1,000 dilution.  $\alpha$ -GAPDH was used at a 1:3,000 dilution.

Horseradish peroxidase (HRP)-conjugated secondary antibodies were purchased from Rockland Immunochemicals. IRDye secondary antibodies were purchased from LI-COR Biosciences.

### **Phosphoproteomics & MS Method**



Cells were lysed by adding 1 mL of lysis buffer (20 mM HEPES pH 7.9, 1% SDS, 1 × protease inhibitors). Protein concentrations were determined by BCA assay. Reduction and alkylation were performed as previously described.<sup>185</sup> S-trap digestion was done according to the manufacturer's instructions resulting in 0.8 mg tryptic peptides. Samples were desalted on C18 spin columns and evaporated to near dryness in a vacuum concentrator. The enrichment of phosphopeptides was performed by TiO<sub>2</sub> Phosphopeptide Enrichment Kit (cat.no. A32993, ThermoFisher Scientific). Briefly, approximately 0.8 mg of tryptic peptides were resuspended in 150 µL of Binding/Equilibration buffer. The suspended peptide sample was added to a pre-equilibrated TiO<sub>2</sub> spin tip and centrifuged at 1000 × g for 5 minutes. The spin tip was then washed with 20 µL of Binding/Equilibration/Wash Buffer for three times and eluted by 50 µL of Elution buffer for two times. The eluates were evaporated to near dryness and subjected to the TMT-labeling.

For each sample, 10 µL the corresponding amine-based TMT 10-plex reagents (10 µg µL<sup>-1</sup>) was added and reacted for 1 h at room temperature. The reactions were quenched with 2 µL 5% hydroxylamine solution and combined. The combined mixture was concentrated to dryness. High-pH fractionation (ThermoFisher Scientific) was done according to the manufacturer's instructions resulting in 6 fractions.

A Thermo Scientific EASY-nLC 1000 system was coupled to a Thermo Scientific Orbitrap Fusion Tribrid with a nano-electrospray ion source. Mobile phases A and B were water with 0.1% formic acid (v/v) and acetonitrile with 0.1% formic acid (v/v), respectively. For each fraction, peptides were separated with a linear gradient from 4 to 32% B within 45 min, followed by an increase to 50% B within 10 min and further to 98% B within 10 min, and re-equilibration. peptides were separated using a linear gradient from 4% to 32% B within 50 min, followed by an increase to 50% B within 10 min and further to 98% B within 10 min and re-equilibration. The following instrument parameters were used as previously described.<sup>60</sup>

## Phosphoproteomics data analysis

The raw data was processed using Proteome Discoverer 2.4 (Thermo Fisher Scientific). Data was searched against the UniProt/SwissProt human (*Homo sapiens*) protein database (19 August 2016; 20,156 total entries) and contaminant proteins using the Sequest HT algorithm. The database was adjusted by adding the sequences of GFP-FLAG-CK2 $\alpha$ -EPEA and either HA-nLaG6-OGT(4) or myc-OGA(1-400) + Ha-nLaG6-OGA(544-706). Searches were performed with the following guidelines: spectra with a signal-to-noise ratio greater than 1.5; trypsin as enzyme, 2 missed cleavages; variable oxidation on methionine residues (15.995 Da), deamidation on asparagine and glutamine (0.984 Da) and phosphorylation on serine, threonine and tyrosine (79.966 Da); static carbamidomethylation of cysteine residues (57.021 Da), static TMT labeling (229.163 Da) at lysine residues and peptide N-termini; total variable modification max to 3 per peptide; 10 ppm mass error tolerance on precursor ions, and 0.02 Da mass error on fragment ions. Data were filtered with a peptide-to-spectrum match (PSM) of 1% FDR using Percolator. The TMT reporter ions were quantified using the Reporter Ions Quantifier with total peptide normalization. For the obtained PSMs, the data was further filtered with the following guidelines: confidence is high; PSM ambiguity is unambiguous; modifications contain phosphorylation; exclude all contaminant proteins. Data was processed using in-house script. After methods are applied for calculating and adjusting missing data in TMT Proteomics data, the file is further filtered with protein FDR confidence is high, unique peptides greater than 2, master proteins only, and no contaminants. Some of the graphs and tables produced include PCA plots, Volcano plots, and tables including all the statistics presented in the graphs. Applied here is a VSN normalization computed on the imputed matrix using a robust variant of the maximum-likelihood estimator for an additive-multiplicative error model and affine calibration. The model incorporates dependence of the variance on the mean intensity and a variance stabilizing data transformation. A linear model is fitted to the expression data for control and treatment, then *t*-statistics are computed by empirical Bayes moderation of standard errors towards a common value.

## Chapter 4: Discussion

In Chapter 3, we discuss the first use of nanobody-OGT and -splitOGA to edit O-GlcNAcylation of a kinase, CK2 $\alpha$ , and resultant effects on the phosphoproteome in HEK293T cells. After demonstrating the selective regulation of O-GlcNAc on GFP-FLAG-CK2 $\alpha$ -EPEA in cells, we confirmed the glycosite at Ser347 using point mutagenesis. Although point mutagenesis showed that S347A was an effective method to remove O-GlcNAc from CK2 $\alpha$ , mutagenesis to S347C, as an approach to stably introduce S-GlcNAc,<sup>62, 138</sup> revealed limited introduction of S-GlcNAc to the construct by RL2, CTD110.6, or chemoenzymatic labeling methods for detecting O-GlcNAc. These data imply that while O-GlcNAc may be readily reduced with point mutagenesis to remove the Ser/Thr site, not all O-GlcNAc sites can be turned into S-GlcNAc sites. Additionally, we observed a significant increase in O-GlcNAc on CK2 $\alpha$  that was above levels observed by inhibition of OGA, indicating that a trigger to stimulate glycosylation of CK2 $\alpha$  may exist. Overall, these data demonstrate methods for regulating O-GlcNAc at the global, protein, and site levels are useful and needed.

By modulating O-GlcNAc with nanobody-OGT and -splitOGA on a tagged CK2 $\alpha$ , we observed a small number of phosphosites over hundreds of PSMs whose enrichment and detection changed in a CK2 $\alpha$  glycosylation-dependent manner. By contrast, large changes to the phosphoproteome are observed from global inhibitors of OGT or OGA.<sup>3, 86, 131, 186</sup> We observed that basal O-GlcNAcylation of overexpressed GFP-FLAG-CK2 $\alpha$ -EPEA is relatively low, which can be increased by nanobody-OGT or decreased by nanobody-splitOGA. As the qualitative increase of O-GlcNAc on CK2 $\alpha$  appears to result in a greater differential than reducing O-GlcNAc on CK2 $\alpha$ , this explains the greater differences in the phosphoproteome when modulating O-GlcNAc on CK2 $\alpha$  with nanobody-OGT as compared to nanobody-splitOGA. CK2 is different from other kinases in that it is ubiquitously expressed and constitutively active. Because the activity of CK2 $\alpha$  is not regulated by a PTM-mediated on or off switch, other mechanisms must lead to differential

substrate and phosphosite targeting, including changes in subcellular localization, association with protein complexes, and rate of CK2 holoenzyme assembly.<sup>187</sup> We establish here that CK2 $\alpha$  glycosylation did not affect the amount of co-immunoprecipitated CK2 $\beta$ , but does alter the phosphoproteome, presumably through altered selectivity or another aforementioned mechanism.

At the protein and phosphosite level we observed connections between CK2 $\alpha$  and three significantly changing phosphoproteins involved in histone deacetylation – SMARCAD1, HDAC1, and HDAC2. With the histone deacetylases, we found that HDAC1 and 2 may relate to the metabolic state of the cell through tuning their association in a CK2 $\alpha$  O-GlcNAc-dependent manner, since they are reported CK2 substrates. We found two phosphosites, HDAC1 Ser393 and HDAC2 Ser394, which increased significantly in the nanobody-OGT condition and decreased insignificantly in the nanobody-splitOGA condition. Phosphorylation at these sites is responsible for initiating the dissociation of HDAC1 and HDAC2 from one another, promoting their association with other protein complexes and differential protein targeting.<sup>164</sup> Khan and colleagues also report that HDAC2 is more readily phosphorylated by CK2 than HDAC1. Our data suggests that elevated O-GlcNAc on CK2 $\alpha$  may facilitate cell cycle progression by promoting HDAC1/2 dissociation (Figure 3.4.5B), where effects on histone acetylation, cell cycle progression, and other processes may be evaluated in the future.

In addition, these data point to new opportunities in the study of the interplay of O-GlcNAc and phosphorylation on the C-terminal tail of CK2 $\alpha$ . The main regulator of phosphosites on CK2 $\alpha$  proximal to the Ser347 glycosite on its C-terminal tail is Cdk1/Cyclin B.<sup>156</sup> The T344, T360, S362, and S370 phosphosites are modified in prophase and metaphase, and dephosphorylated during anaphase.<sup>155, 156</sup> Cdk1 is a well-studied mitotic regulator, and prior work established that Thr344 phosphorylation influences CK2 $\alpha$  substrate specificity *in vitro*.<sup>75</sup> Therefore, this implies that active Cdk1 redirects CK2 during initiation of mitosis to phosphorylate key substrates. To ascertain what

these substrates are and their dependence on CK2 $\alpha$  glycosylation, a similar phosphoproteomics experiment with synchronized cells may provide more sensitive quantification of phosphosite differences. In addition, the GFP tag on the CK2 $\alpha$  used in this study would facilitate examination of its subcellular localization by microscopy. This would provide insight into how glycosylation and the nanobody system affect CK2 $\alpha$  localization.

The O-GlcNAc modification is associated with nutrient sensing and signaling.<sup>188</sup> If the glycosite on CK2 $\alpha$  is tuned to the nutrient availability of the cell, then this study implies that pathways like chromatin regulation and cell cycle progression can be tuned by the metabolic state of the cell with OGT as the reporter and CK2 $\alpha$  as the messenger. Use of the targeted writer and eraser for O-GlcNAc on overexpressed CK2 $\alpha$  enabled this work and will enable study of additional glycoproteins, including other kinases, in the future. Based on the glycoproteomic datasets cited in Chapter 1,<sup>2, 4, 52, 90-96</sup> additional O-GlcNAcylated kinases that could be studied in a similar manner with the nanobody-OGT and -splitOGA system include RIPK1, RIPK3, WNK1, and WNK3.

Receptor-interacting serine/threonine-protein kinase 1 (RIPK1) is a 76 kDa Ser/Thr kinase that functions in tandem with related 57 kDa kinase RIPK3 to control inflammatory and necroptotic pathways in immune cells. The Thr467 O-GlcNAc site of RIPK3 was characterized in *Cell* in 2019.<sup>189</sup> Thr467 is localized within the RIP homotypic interaction motif (RHIM) of RIPK3, through which it interacts with other RIP kinases. Glycosylation at this site inhibits the formation of both RIPK3-RIPK3 homodimers and RIPK3-RIPK1 heterodimers, thereby inhibiting pro-inflammatory/necroptotic signaling in macrophages. Contrary to the necessity for OGT activity in T cell activation, deletion of OGT in macrophages enhances the innate immune response, implying distinct outcomes for O-GlcNAc signaling across different cell types of the immune system. Employing nanobody-OGT to attenuate cytokine production through direct glycosylation

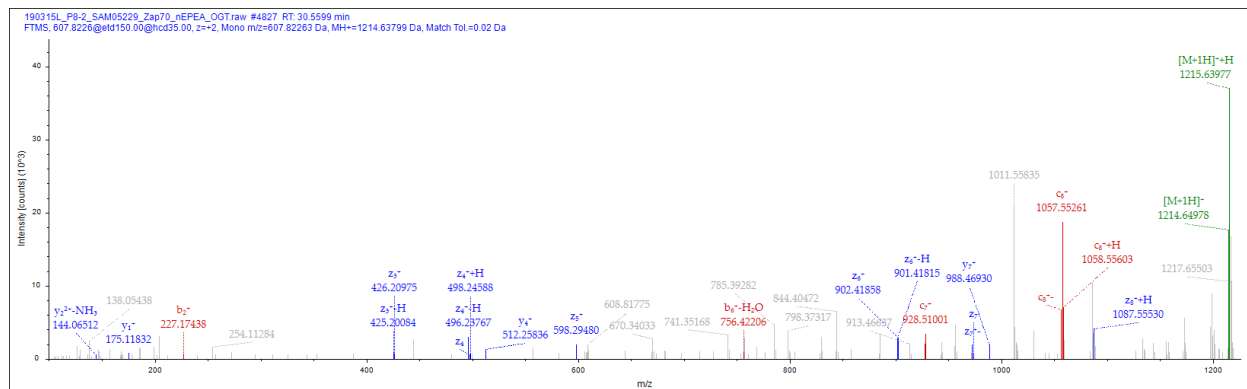
of RIPK3 would emphasize the key role RIPK3 plays in integrating O-GlcNAc signaling with macrophage activation.

The Ser330 glycosite of RIPK1 has yet to be characterized. In the same study,<sup>189</sup> Li and colleagues determined that kinase activity of RIPK3, but not RIPK1, was necessary for increased cytokine production in OGT-deficient macrophages, and that OGT activity attenuated stimulatory phosphorylation of RIPK3, but not RIPK1; additionally, Ser330 is distal to the RHIM domain of RIPK1, implying the glycosite may not regulate RIPK1-RIPK3 heterodimer formation. These data indicate a separate role for the RIPK1 glycosite compared to the RIPK3 glycosite, one that may be more prevalent in a different RIPK1-expressing cell line. RIPK1 is involved in NF- $\kappa$ B and Akt signaling in a variety of cell types.<sup>190</sup> How O-GlcNAc on RIPK1 affects RIPK1 stability, PPIs, or NF- $\kappa$ B/Akt signaling all represent possible points of entry for study of this kinase.

Lysine deficient protein kinases 1 and 3 (WNK1/WNK3) are both involved in the regulation of sodium- and potassium-coupled chloride channels. Both kinases are large (250 kDa and 200 kDa respectively) and regulate the activity of SPAK and OSR1, both of which phosphorylate the aforementioned chloride channels to affect intracellular electrolyte homeostasis.<sup>191</sup> Both WNK1 and WNK3 have multiple potential O-GlcNAc sites. Notably, 190 PSMs were assigned to the six potential glycosites (Ser1235, Thr1244, Ser1562, Thr1848, Ser1849, and Ser1850) of WNK1 across the aggregated glycoproteomics data.<sup>2, 4, 52, 90-96</sup> Chloride channels, and therefore WNK1 and WNK3, play central roles in the function kidney cells. The ability to regulate multiple glycosites, regardless of orthogonal methods to confirm glycosite localization, without altering the primary sequence of WNK1 or WNK3 represent a key advantage of the nanobody system for study of these proteins.

# Appendix

## Supplementary Figures



### Supplementary Figure 1 – ETHcD spectrum assigned to Zap70-FLAG-EPEA T155 glycosite from HEK293T cells

Sequence: LIATTAHER, T4-HexNAc(1) (203.07937 Da)

Charge: +2, Monoisotopic m/z: 607.82263 Da (+0.22 mmu/+0.37 ppm), MH+: 1214.63799

Da, RT: 30.5599 min,

Identified with: PMI-Byonic (v1.0); |Log Prob|:4.47, Byonic Score:357.5, Delta Byonic

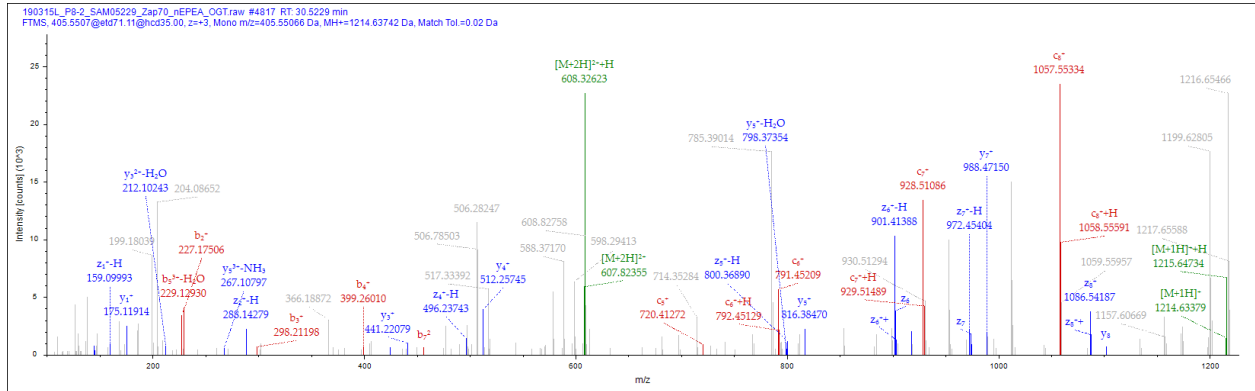
Score:143.0, Delta Mod Score:20.5, PEP 2D:3.42E-05, q-Value 2D:4.36E-05, FDR 2D:4.12E-

05, Peptide Group FDR 2D:0, PEP 1D:0.000757, q-Value 1D:9.21E-05, FDR 1D:9.01E-05,

Peptide Group FDR 1D:0,

Fragment match tolerance used for search: 20 ppm

Fragments used for search: b; c; y; z



**Supplementary Figure 2 – EThcD spectrum assigned to Zap70-FLAG-EPEA T156 glycosite from HEK293T cells**

Sequence: LIATTAHER, T5-HexNAc(1) (203.07937 Da)

Charge: +3, Monoisotopic m/z: 405.55066 Da (-0.04 mmu/-0.1 ppm), MH+: 1214.63742 Da,

RT: 30.5229 min,

Identified with: PMI-Byonic (v1.0); |Log Prob|:7.43, Byonic Score:543.5, Delta Byonic

Score:249.3, Delta Mod Score:15.8, PEP 2D:3.72E-08, q-Value 2D:2.79E-09, FDR 2D:0,

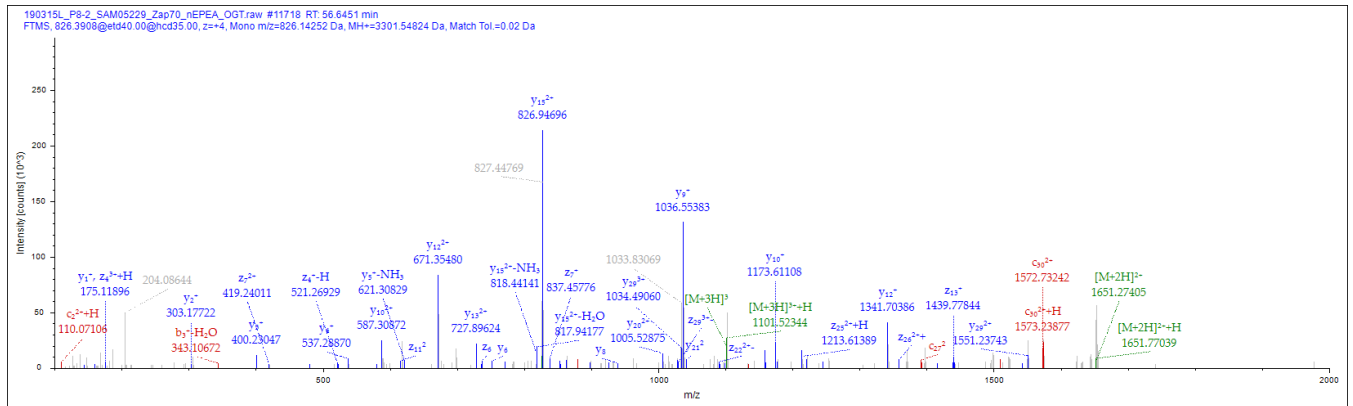
Peptide Group FDR 2D:0, PEP 1D:8.25E-07, q-Value 1D:6.34E-08, FDR 1D:0, Peptide Group

FDR 1D:0,

Fragment match tolerance used for search: 20 ppm

Fragments used for search: b; c; y; z





**Supplementary Figure 3 – EThcD spectrum assigned to Zap70-FLAG-EPEA S257 glycosite from HEK293T cells**

Sequence: EACPNSSASNASGAAAPTLPHPSTLTHPQR, C3-Carbamidomethyl (57.02146

Da), S6-HexNAc(1) (203.07937 Da)

Charge: +4, Monoisotopic m/z: 826.14252 Da (-0.49 mmu/-0.6 ppm), MH+: 3301.54824 Da,

RT: 56.6451 min,

Identified with: PMI-Byonic (v1.0); |Log Prob|:12.63, Byonic Score:580.7, Delta Byonic

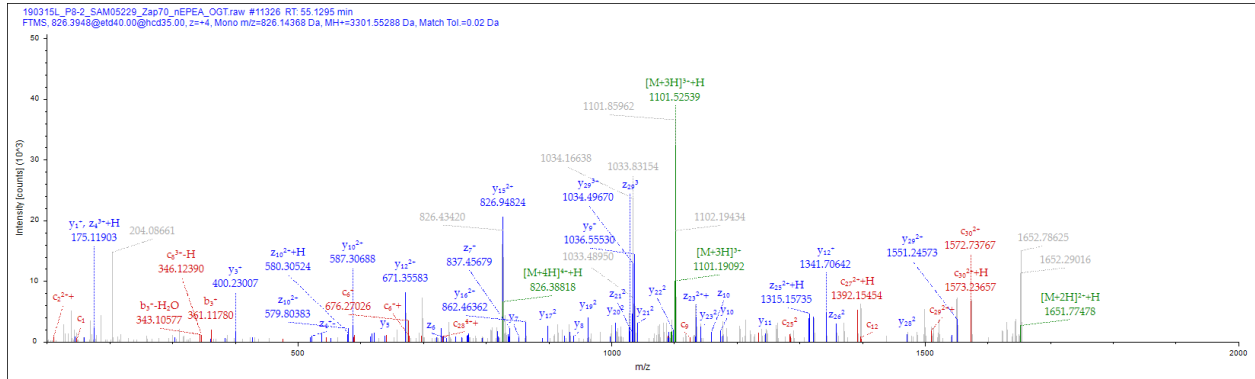
Score:580.7, Delta Mod Score:27.4, PEP 2D:2.36E-13, q-Value 2D:2.5E-14, FDR 2D:0, Peptide

Group FDR 2D:0, PEP 1D:5.22E-12, q-Value 1D:5.34E-13, FDR 1D:0, Peptide Group FDR

1D:0,

Fragment match tolerance used for search: 20 ppm

Fragments used for search: b; c; y; z



**Supplementary Figure 4 – EThcD spectrum assigned to Zap70-FLAG-EPEA S258 glycosite from HEK293T cells**

Sequence: EACPNSNASGAAAPTLPHPSTLTHPQR, C3-Carbamidomethyl (57.02146

Da), S7-HexNAc(1) (203.07937 Da)

Charge: +4, Monoisotopic m/z: 826.14368 Da (+0.67 mmu/+0.81 ppm), MH+: 3301.55288

Da, RT: 55.1295 min,

Identified with: PMI-Byonic (v1.0); |Log Prob|:16.68, Byonic Score:761.6, Delta Byonic

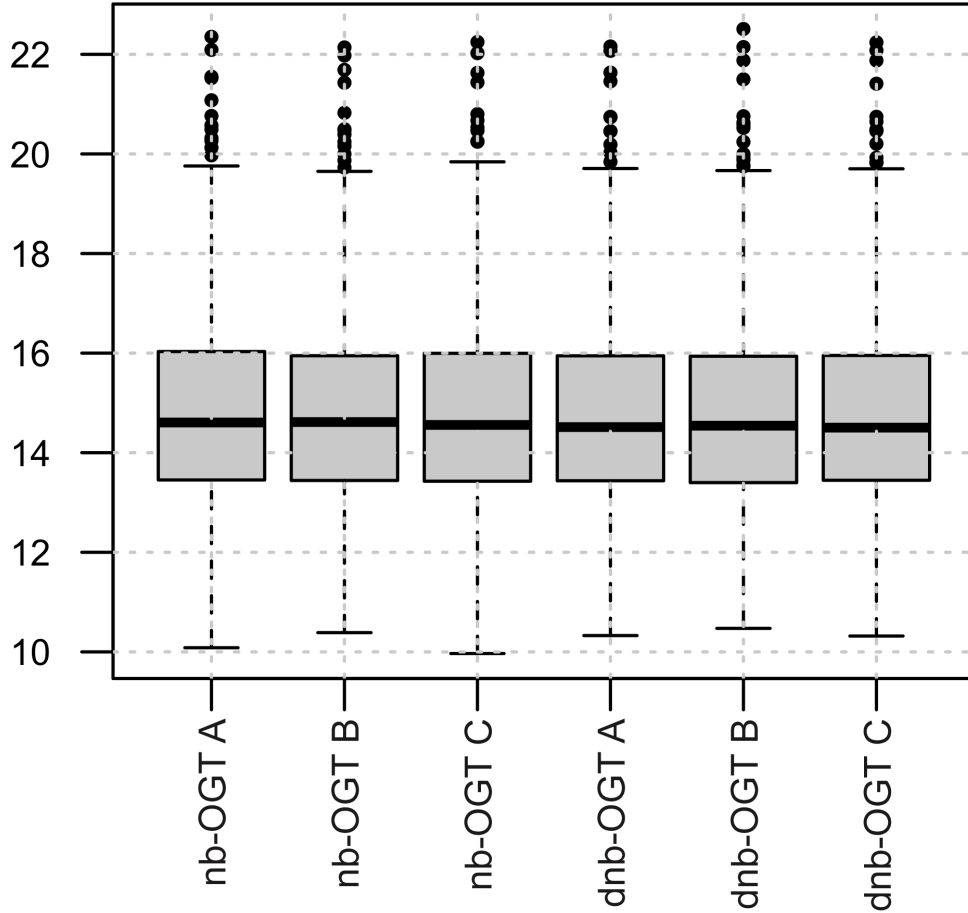
Score:735.6, Delta Mod Score:21.4, PEP 2D:2.11E-17, q-Value 2D:4.11E-18, FDR 2D:0,

Peptide Group FDR 2D:0, PEP 1D:4.67E-16, q-Value 1D:8.91E-17, FDR 1D:0, Peptide Group

FDR 1D:0,

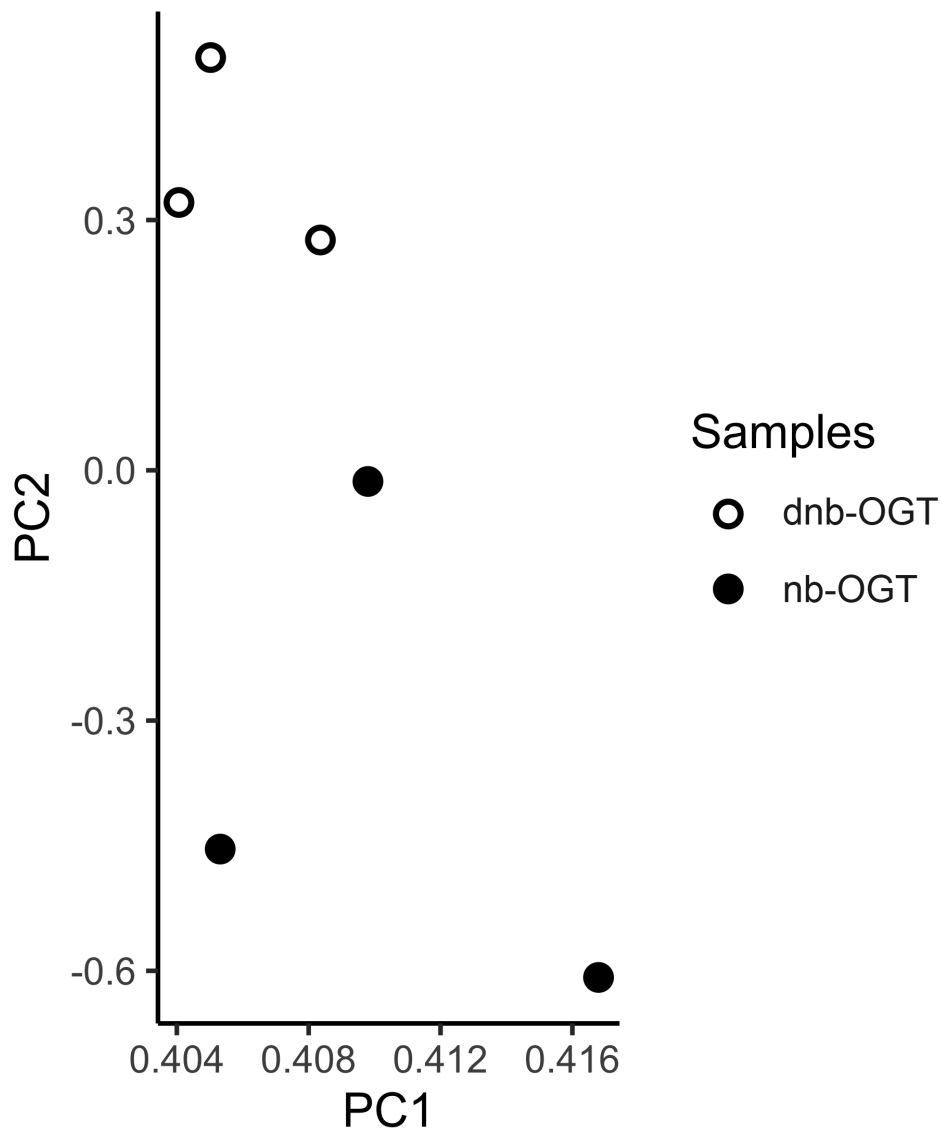
Fragment match tolerance used for search: 20 ppm

Fragments used for search: b; c; y; z



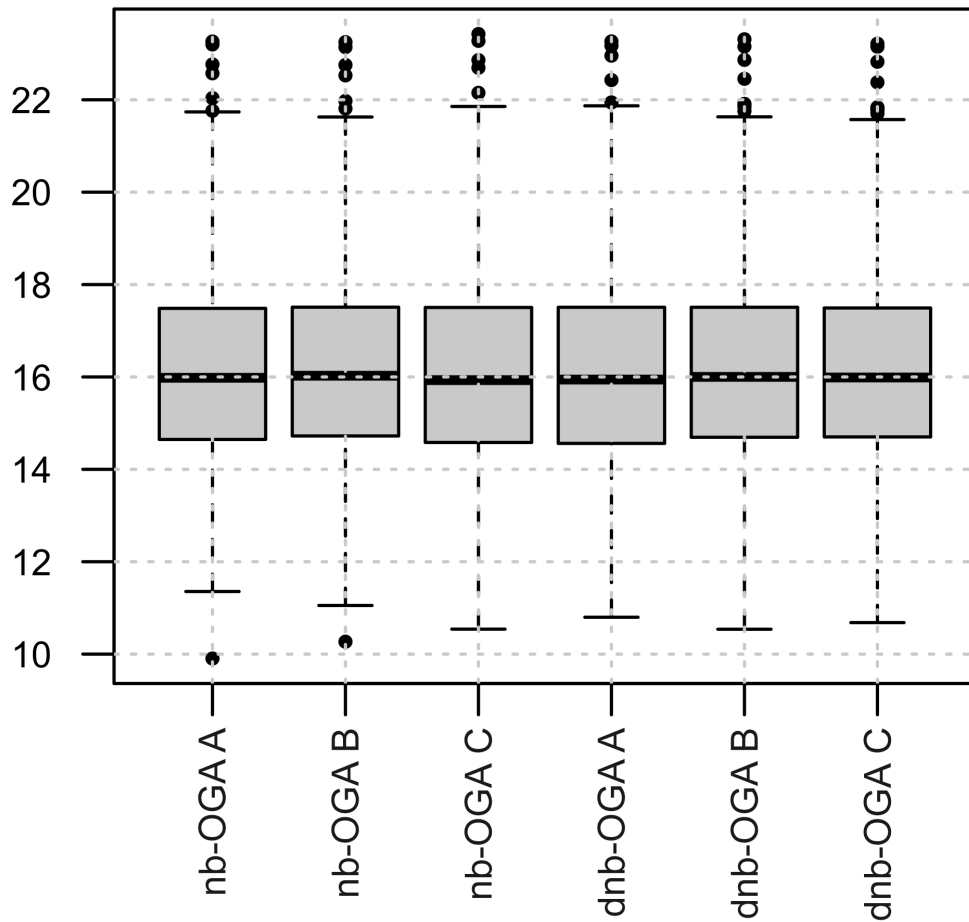
**Supplementary Figure 5 – Nanobody-OGT Phosphoprotein Level Normalization Box Plot**

Normalization of TMT channels during protein-level analysis of nanobody-OGT phosphoproteomics experiment. Each channel represents GFP-FLAG-CK2 $\alpha$ -EPEA co-transfected with active or inactive nanobody-OGT. nb-OGT = active nanobody-OGT, dnb-OGT = inactive nanobody-OGT.



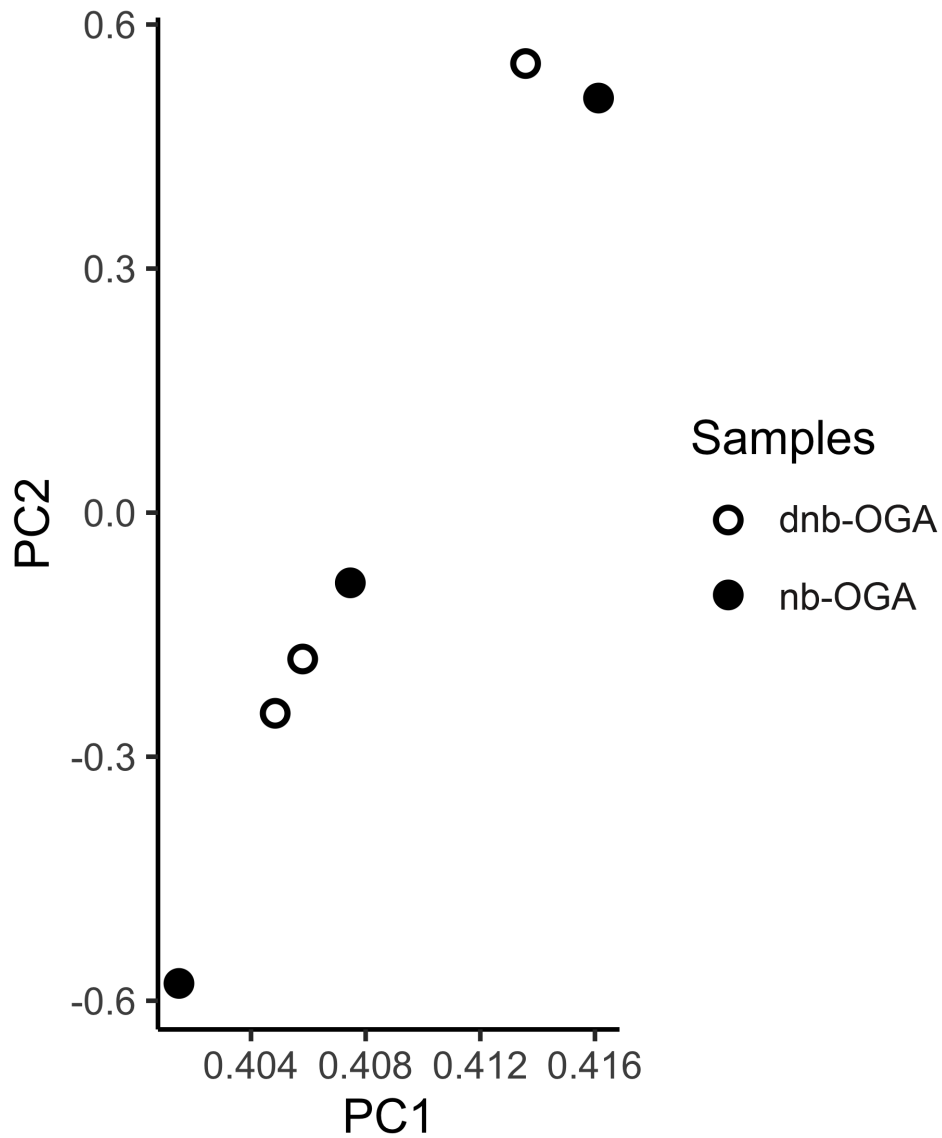
**Supplementary Figure 6 – Nanobody-OGT Phosphoprotein Level Principal Component Analysis**

Principal component analysis of nanobody-OGT protein level data indicating independent clustering between the control (inactive nanobody-OGT co-transfection) and treatment (active nanobody-OGT co-transfection). ■ nb-OGT = active nanobody-OGT, ○ dnb-OGT = inactive nanobody-OGT.



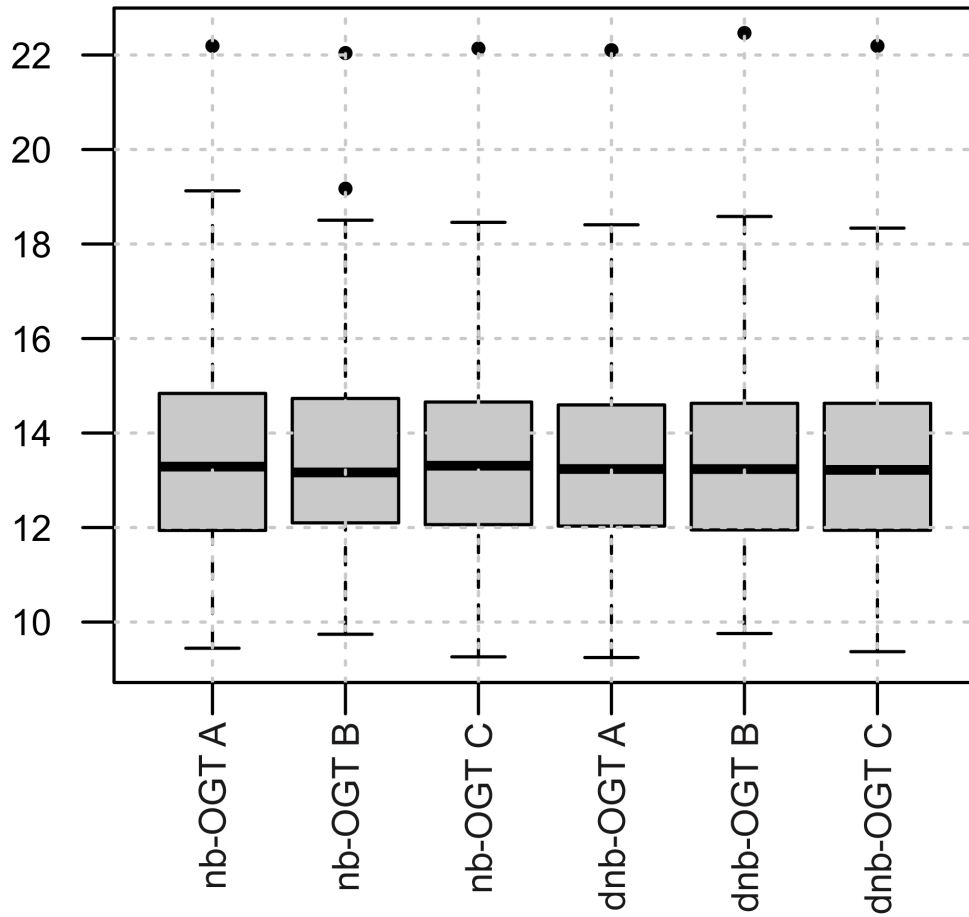
**Supplementary Figure 7 – Nanobody-splitOGA Phosphoprotein Level Normalization Box Plot**

Normalization of TMT channels during protein-level analysis of nanobody-splitOGA phosphoproteomics experiment. Each channel represents GFP-FLAG-CK2 $\alpha$ -EPEA co-transfected with active or inactive nanobody-splitOGA. nb-OGA = active nanobody-splitOGA, dnb-OGA = inactive nanobody-splitOGA.



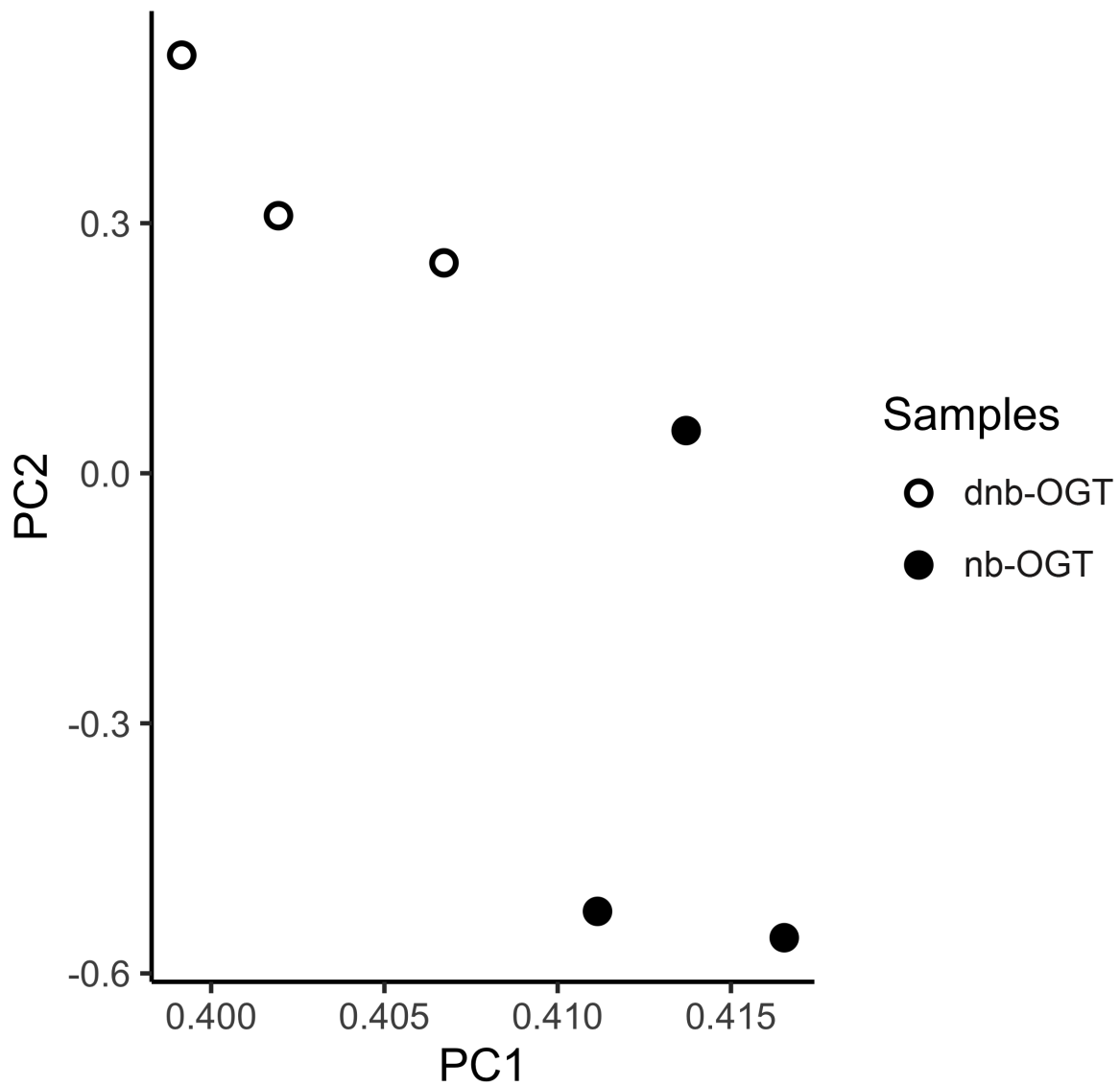
**Supplementary Figure 8 – Nanobody-splitOGA Phosphoprotein Level Principal Component Analysis**

Principal component analysis of nanobody-splitOGA protein level data indicating clustering between the control (inactive nanobody-splitOGA co-transfection) and treatment (active nanobody-splitOGA co-transfection). nb-OGA = active nanobody-splitOGA, dnb-OGA = inactive nanobody-splitOGA.



**Supplementary Figure 9 – Nanobody-OGT Phosphosite Level Normalization Box Plot**

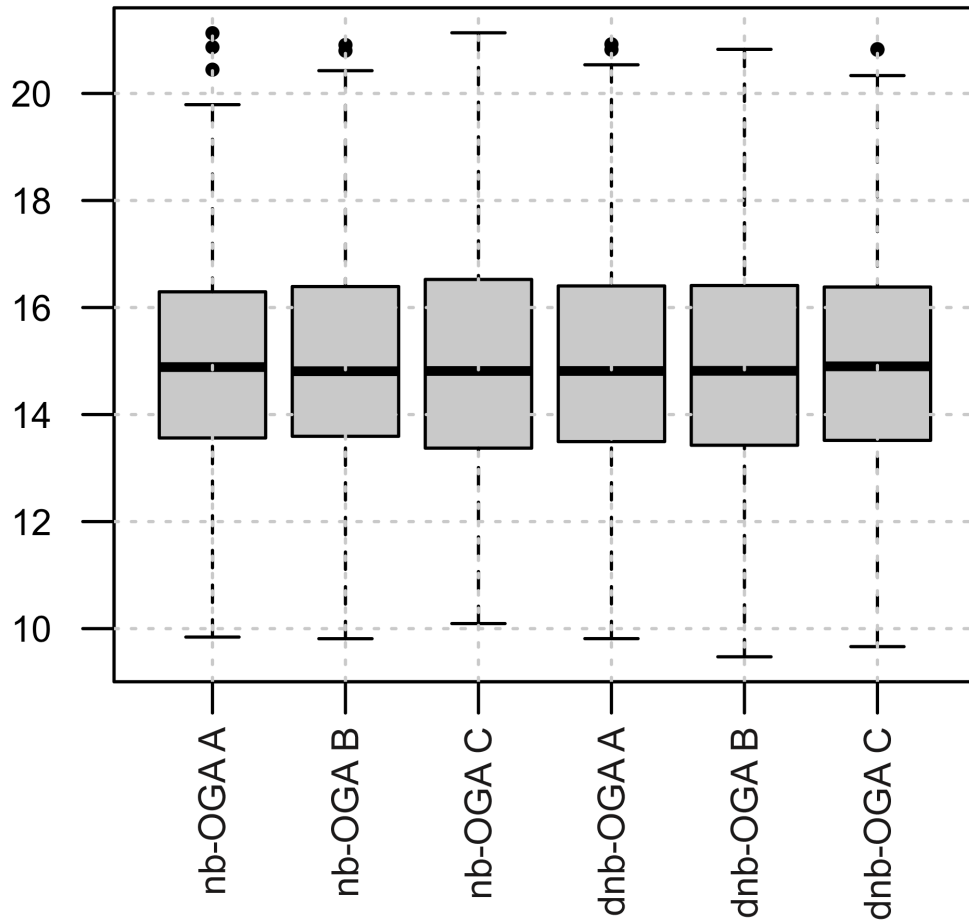
Normalization of TMT channels during site-level analysis of nanobody-OGT phosphoproteomics experiment. Each channel represents GFP-FLAG-CK2 $\alpha$ -EPEA co-transfected with active or inactive nanobody-OGT. nb-OGT = active nanobody-OGT, dnb-OGT = inactive nanobody-OGT.



**Supplementary Figure 10 – Nanobody-OGT Phosphosite Level Principal Component Analysis**

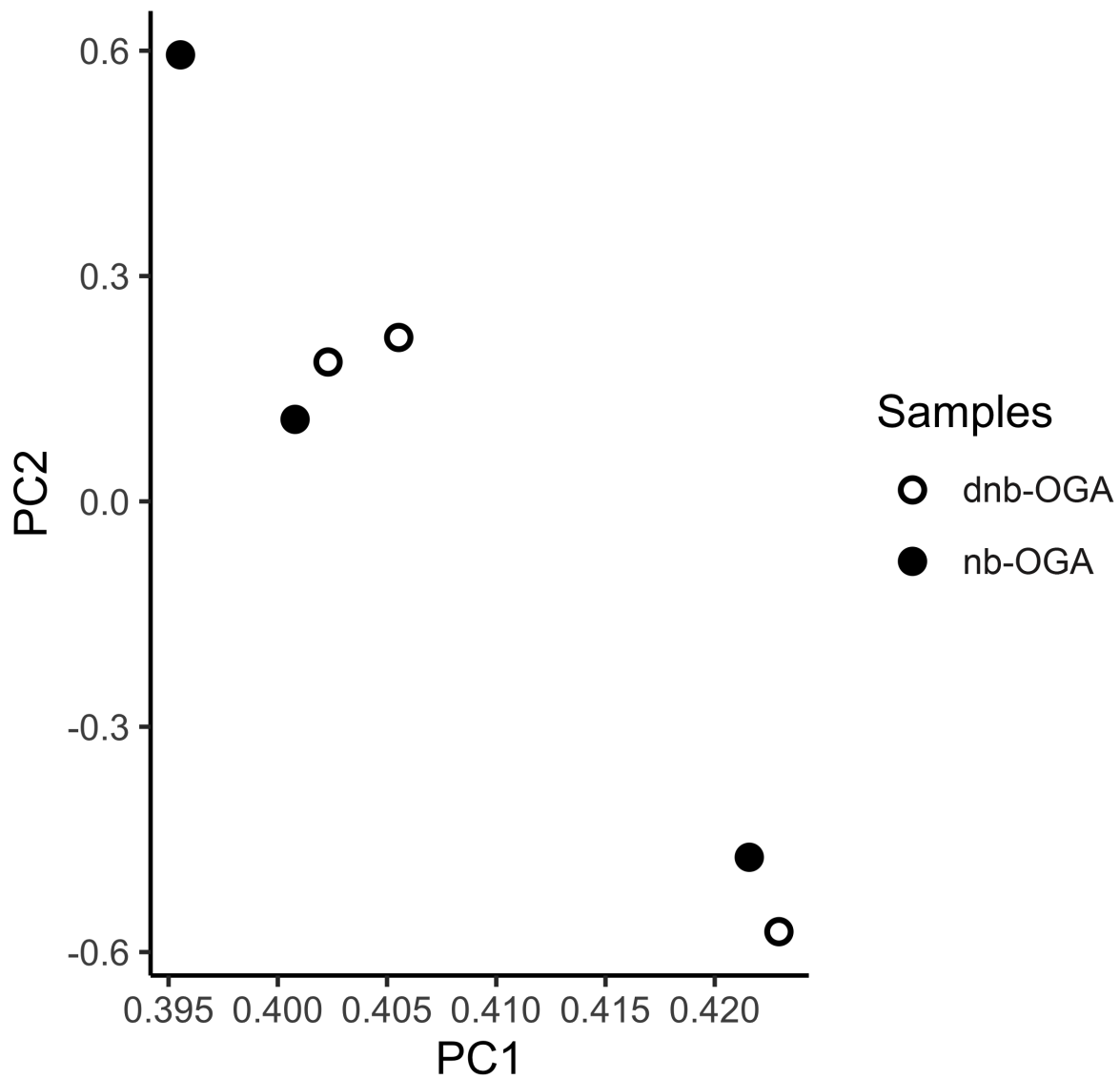
Principal component analysis of nanobody-OGT phosphosite level data indicating independent clustering between the control (inactive nanobody-OGT co-transfection) and treatment (active nanobody-OGT co-transfection). nb-OGT = active nanobody-OGT, dnb-OGT = inactive nanobody-OGT.





**Supplementary Figure 11 – Nanobody-splitOGA Phosphosite Level Normalization Box Plot**

Normalization of TMT channels during site-level analysis of nanobody-splitOGA phosphoproteomics experiment. Each channel represents GFP-FLAG-CK2 $\alpha$ -EPEA co-transfected with active or inactive nanobody-splitOGA. nb-OGA = active nanobody-splitOGA, dnb-OGA = inactive nanobody-splitOGA.



**Supplementary Figure 12 – Nanobody-splitOGA Phosphosite Level Principal Component Analysis**

Principal component analysis of nanobody-splitOGA phosphosite level data indicating clustering between the control (inactive nanobody-splitOGA co-transfection) and treatment (active nanobody-splitOGA co-transfection). nb-OGA = active nanobody-splitOGA, dnb-OGA = inactive nanobody-splitOGA.

## Supplementary Tables

Supplementary Table 1 – MS Data (protein level hits)

Gene Name	PDB ID	Log <sub>2</sub> (FC) OGT	P value OGT	Log <sub>2</sub> (FC) OGA	P value OGA	Reported CK2 sub.?
MARCKS	P29966	1.36750281	3.8657E-07	-0.009162	0.89814825	No
ILF3	Q12906	1.19323052	0.01876606	-0.0733866	0.30002011	No
HDAC1	Q13547	1.08712459	0.00351943	-0.0990389	0.43198513	Yes <sup>162</sup>
HMGB2	P26583	1.06279556	2.0455E-05	N/A	N/A	Yes <sup>145</sup>
HDAC2	Q92769	1.05118692	0.00777629	-0.0332643	0.6414608	Yes <sup>162</sup>
UGP2	Q16851	1.05007777	0.00600021	N/A	N/A	No
EPB41L2	O43491	1.02714016	5.6632E-06	-0.0670828	0.32753689	No
RPL27A	P46776	0.99070725	3.5807E-05	N/A	N/A	No
RPL34	P49207	0.95956758	4.3797E-05	-0.5646497	0.00012171	No
TPD52L2	O43399	0.93300518	0.00016678	0.42744399	0.00058086	No
HCFC1	P51610	0.91898783	0.00905294	-0.0628119	0.53619673	No
RPS3A	P61247	0.90641691	0.00299694	N/A	N/A	No
DDX42	Q86XP3	0.8890198	0.01237976	N/A	N/A	No
ENSA	O43768	0.87119279	9.9768E-05	-0.6537205	6.5355E-05	No
MYLK3	Q32MK0	0.83529321	0.01151515	N/A	N/A	No
MED19	A0JLT2	-0.7632699	0.00107056	0.12685194	0.53994595	No
AKT1S1	Q96B36	0.7265354	0.00116863	-0.0565795	0.60974879	No
UTP14A	Q9BVJ6	0.70578475	0.01287049	N/A	N/A	No
IQSEC1	Q6DN90	0.68529865	0.00801551	-0.1387021	0.11543139	No
NFIC	P08651	0.6787496	0.00091429	N/A	N/A	No

TBC1D4	O60343	0.67332465	0.00297638	-0.0780943	0.48076431	No
MDH1	P40925	0.63299339	0.01058569	-0.0878243	0.18815606	No
PTDSS1	P48651	-0.6310514	0.00060673	0.03246701	0.85838788	No
QSOX2	Q6ZRP7	-0.6246512	0.00211926	N/A	N/A	No
BAP1	Q92560	-0.6224754	0.01120594	N/A	N/A	No
SMARCAD1	Q9H4L7	0.60898284	0.00020408	-0.6594163	0.00011993	No
KHSRP	Q92945	0.60236907	3.8665E-05	-0.1613364	0.29451128	No
EXOC3	O60645	-0.5971443	0.0486203	N/A	N/A	No
RBM34	P42696	0.59702178	0.00036202	-0.37369	0.00385585	No
DENND4C	Q5VZ89	-0.5898665	0.00721184	-0.0054706	0.93685289	No
SETX	Q7Z333	-0.5887437	0.00054032	N/A	N/A	Yes <sup>163</sup>
MCF2	P10911	-0.5832619	0.00114332	N/A	N/A	No
DAXX	Q9UER7	0.55998809	0.01803783	-0.0409057	0.53149013	Yes <sup>162</sup>
LUC7L3	O95232	0.54222196	0.00549679	N/A	N/A	No
RING1	Q06587	-0.5355431	0.01986045	-0.1315409	0.81440089	No
PFKP	Q01813	0.53464855	0.00202774	-0.6693487	3.1213E-05	No
NCBP3	Q53F19	0.53253321	0.04912922	0.08806703	0.25442596	No
AAGAB	Q6PD74	-0.5202489	0.00104418	N/A	N/A	No
RIOX2	Q8IUF8	0.51598347	0.00231079	N/A	N/A	No
ADAM22	Q9P0K1	0.50719107	0.00485886	N/A	N/A	No
RPL37	P61927	0.50432442	0.0053132	N/A	N/A	No
TFAM	Q00059	0.50214963	0.0122408	0.03561791	0.57239368	No
PABPN1	Q86U42	0.02174837	0.8726238	-1.2207843	0.00080145	No
SRSF2	Q01130	-0.1694018	0.07328998	-0.9482095	3.1687E-06	No
NUFIP2	Q7Z417	0.07818113	0.51571786	0.6055824	0.01815937	No

MOV10	Q9HCE1	N/A	N/A	-0.5864239	0.00018435	No
RBBP7	Q16576	N/A	N/A	-0.568389	0.00683292	No
PPP1R12A	O14974	0.31895842	0.03708686	-0.5415793	0.00054957	No
REEP5	Q00765	N/A	N/A	-0.5286674	7.9512E-05	No
PABPN1	Q86U42	0.02174837	0.8726238	-1.2207843	0.00080145	No
SRSF2	Q01130	-0.1694018	0.07328998	-0.9482095	3.1687E-06	No

**Supplementary Table 2 – MS Data (site level hits)**

<b>Gene Name</b>	<b>PDB ID</b>	<b>Phospho-site</b>	<b>Condition</b>	<b>Log<sub>2</sub>(FC)</b>	<b>P value</b>	<b>Reported CK2 sub.?</b>
MARCKS	P29966	S170	OGT	1.47934	6.6677E-06	No
HMGB2	P26583	T179	OGT	1.01355	0.00013414	Yes <sup>145</sup>
HDAC1	Q13547	S343	OGT	1.06832832	0.00567005	Yes <sup>164</sup>
HDAC2	Q92769	S394	OGT	1.04528135	0.00861108	Yes <sup>164</sup>
UGP2	Q16851	Y248	OGT	1.02774156	0.00953618	No
CWC25	Q9NXE8	S218	OGT	1.04628939	0.0209202	No
ILF3	Q12906	S382	OGT	1.36850275	0.0200335	No
EPB41L2	O43491	S550	OGT	1.02099418	0.01224519	No
MDC1	Q14676	T404	OGT	2.21424469	0.03398253	Yes <sup>181</sup>
MDC1	Q14676	S329	OGT	-1.1436185	0.01538304	Yes <sup>181</sup>
NUFIP2	Q7Z417	T571/S572	OGA	1.02597445	0.00252018	No
PABPN1	Q86U42	S95	OGA	-1.1619051	0.00081583	No

## References

1. Sacco, F.; Perfetto, L.; Castagnoli, L.; Cesareni, G., The human phosphatase interactome: An intricate family portrait. *FEBS Lett* **2012**, *586* (17), 2732-9.
2. Woo, C. M.; Lund, P. J.; Huang, A. C.; Davis, M. M.; Bertozzi, C. R.; Pitteri, S. J., Mapping and Quantification of Over 2000 O-linked Glycopeptides in Activated Human T Cells with Isotope-Targeted Glycoproteomics (Isotag). *Mol Cell Proteomics* **2018**, *17* (4), 764-775.
3. Hart, G. W.; Slawson, C.; Ramirez-Correa, G.; Lagerlof, O., Cross talk between O-GlcNAcylation and phosphorylation: roles in signaling, transcription, and chronic disease. *Annu Rev Biochem* **2011**, *80*, 825-58.
4. Wang, Z.; Udeshi, N. D.; Slawson, C.; Compton, P. D.; Sakabe, K.; Cheung, W. D.; Shabanowitz, J.; Hunt, D. F.; Hart, G. W., Extensive crosstalk between O-GlcNAcylation and phosphorylation regulates cytokinesis. *Sci Signal* **2010**, *3* (104), ra2.
5. Wulff-Fuentes, E.; Berendt, R. R.; Massman, L.; Danner, L.; Malard, F.; Vora, J.; Kahsay, R.; Olivier-Van Stichelen, S., The human O-GlcNAcome database and meta-analysis. *Sci Data* **2021**, *8* (1), 25.
6. Torres, C. R.; Hart, G. W., Topography and polypeptide distribution of terminal N-acetylglucosamine residues on the surfaces of intact lymphocytes. Evidence for O-linked GlcNAc. *J Biol Chem* **1984**, *259* (5), 3308-17.
7. Kreppel, L. K.; Blomberg, M. A.; Hart, G. W., Dynamic glycosylation of nuclear and cytosolic proteins. Cloning and characterization of a unique O-GlcNAc transferase with multiple tetratricopeptide repeats. *J Biol Chem* **1997**, *272* (14), 9308-15.
8. Thornton, T.; Kreppel, L.; Hart, G.; Olszewski, N., Genetic and biochemical analysis of arabidopsis SPY. *Plant Biotechnology and in Vitro Biology in the 21st Century* **1999**, *36*, 445-448.
9. Shafi, R.; Iyer, S. P.; Ellies, L. G.; O'Donnell, N.; Marek, K. W.; Chui, D.; Hart, G. W.; Marth, J. D., The O-GlcNAc transferase gene resides on the X chromosome and is essential for embryonic stem cell viability and mouse ontogeny. *Proc Natl Acad Sci* **2000**, *97* (11), 5735-9.
10. Yang, Y. R.; Song, M.; Lee, H.; Jeon, Y.; Choi, E. J.; Jang, H. J.; Moon, H. Y.; Byun, H. Y.; Kim, E. K.; Kim, D. H.; Lee, M. N.; Koh, A.; Ghim, J.; Choi, J. H.; Lee-Kwon, W.; Kim, K. T.; Ryu, S. H.; Suh, P. G., O-GlcNAcase is essential for embryonic development and maintenance of genomic stability. *Aging Cell* **2012**, *11* (3), 439-48.
11. Ma, J.; Wu, C.; Hart, G. W., Analytical and Biochemical Perspectives of Protein O-GlcNAcylation. *Chem Rev* **2021**, *121* (3), 1513-1581.
12. Leney, A. C.; El Atmioui, D.; Wu, W.; Ovaa, H.; Heck, A. J. R., Elucidating crosstalk mechanisms between phosphorylation and O-GlcNAcylation. *Proc Natl Acad Sci U S A* **2017**, *114* (35), E7255-E7261.
13. Iyer, S. P. N.; Hart, G. W., Roles of the Tetratricopeptide Repeat Domain in O-GlcNAc Transferase Targeting and Protein Substrate Specificity. *J Biol Chem* **2003**, *278* (27), 24608-24616.
14. Lazarus, M. B.; Nam, Y.; Jiang, J.; Sliz, P.; Walker, S., Structure of human O-GlcNAc transferase and its complex with a peptide substrate. *Nature* **2011**, *469* (7331), 564-7.
15. Levine, Z. G.; Walker, S., The Biochemistry of O-GlcNAc Transferase: Which Functions Make It Essential in Mammalian Cells? *Ann Rev Biochem* **2016**, *85* (1), 631-657.
16. Joiner, C. M.; Levine, Z. G.; Aonbangkhen, C.; Woo, C. M.; Walker, S., Aspartate Residues Far from the Active Site Drive O-GlcNAc Transferase Substrate Selection. *J Am Chem Soc* **2019**, *141* (33), 12974-12978.
17. Levine, Z. G.; Fan, C.; Melicher, M. S.; Orman, M.; Benjamin, T.; Walker, S., O-GlcNAc Transferase Recognizes Protein Substrates Using an Asparagine Ladder in the Tetratricopeptide Repeat (TPR) Superhelix. *J Am Chem Soc* **2018**, *140* (10), 3510-3513.

18. Lubas, W. A.; Hanover, J. A., Functional Expression of O-linked GlcNAc Transferase: DOMAIN STRUCTURE AND SUBSTRATE SPECIFICITY. *J Biol Chem* **2000**, *275* (15), 10983-10988.
19. Maynard, J. C.; Burlingame, A. L.; Medzihradszky, K. F., Cysteine S-linked N-acetylglucosamine (S-GlcNAcylation), a new post-translational modification in mammals. *Mol Cell Proteomics* **2016**, mcp.M116.061549.
20. Darabedian, N.; Gao, J.; Chuh, K. N.; Woo, C. M.; Pratt, M. R., The Metabolic Chemical Reporter 6-Azido-6-deoxy-glucose Further Reveals the Substrate Promiscuity of O-GlcNAc Transferase and Catalyzes the Discovery of Intracellular Protein Modification by O-Glucose. *J Am Chem Soc* **2018**, *140* (23), 7092-7100.
21. Lazarus, M. B.; Jiang, J.; Kapuria, V.; Bhuiyan, T.; Janetzko, J.; Zandberg, W. F.; Vocadlo, D. J.; Herr, W.; Walker, S., HCF-1 is cleaved in the active site of O-GlcNAc transferase. *Science* **2013**, *342* (6163), 1235-9.
22. Janetzko, J.; Walker, S., Aspartate Glycosylation Triggers Isomerization to Isoaspartate. *J Am Chem Soc* **2017**, *139* (9), 3332-3335.
23. Kreppel, L. K.; Hart, G. W., Regulation of a Cytosolic and Nuclear O-GlcNAc Transferase: ROLE OF THE TETRATRICOPEPTIDE REPEATS. *J Biol Chem* **1999**, *274* (45), 32015-32022.
24. Wrabl, J. O.; Grishin, N. V., Homology between O-linked GlcNAc transferases and proteins of the glycogen phosphorylase superfamily. *J Mol Biol* **2001**, *314* (3), 365-74.
25. Meek, R. W.; Blaza, J. N.; Busmann, J. A.; Alteen, M. G.; Vocadlo, D. J.; Davies, G. J., Cryo-EM structure provides insights into the dimer arrangement of the O-linked beta-N-acetylglucosamine transferase OGT. *Nat Commun* **2021**, *12* (1), 6508.
26. Nagel, A. K.; Ball, L. E., O-GlcNAc transferase and O-GlcNAcase: achieving target substrate specificity. *Amino Acids* **2014**, *46* (10), 2305-2316.
27. Dong, D. L.; Hart, G. W., Purification and characterization of an O-GlcNAc selective N-acetyl-beta-D-glucosaminidase from rat spleen cytosol. *J Biol Chem* **1994**, *269* (30), 19321-30.
28. Whisenhunt, T. R.; Yang, X.; Bowe, D. B.; Paterson, A. J.; Van Tine, B. A.; Kudlow, J. E., Disrupting the enzyme complex regulating O-GlcNAcylation blocks signaling and development. *Glycobiology* **2006**, *16* (6), 551-63.
29. Alonso, J.; Schimpl, M.; van Aalten, D. M., O-GlcNAcase: promiscuous hexosaminidase or key regulator of O-GlcNAc signaling? *J Biol Chem* **2014**, *289* (50), 34433-9.
30. Keembiyehetty, C. N.; Krzeslak, A.; Love, D. C.; Hanover, J. A., A lipid-droplet-targeted O-GlcNAcase isoform is a key regulator of the proteasome. *J Cell Sci* **2011**, *124* (16), 2851-2860.
31. Elsen, N. L.; Patel, S. B.; Ford, R. E.; Hall, D. L.; Hess, F.; Kandula, H.; Kornienko, M.; Reid, J.; Selnick, H.; Shipman, J. M.; Sharma, S.; Lumb, K. J.; Soisson, S. M.; Klein, D. J., Insights into activity and inhibition from the crystal structure of human O-GlcNAcase. *Nat Chem Biol* **2017**, *13* (6), 613-615.
32. Li, B.; Li, H.; Lu, L.; Jiang, J., Structures of human O-GlcNAcase and its complexes reveal a new substrate recognition mode. *Nat Struct Mol Biol* **2017**, *24* (4), 362-369.
33. Roth, C.; Chan, S.; Offen, W. A.; Hemsworth, G. R.; Willems, L. I.; King, D. T.; Varghese, V.; Britton, R.; Vocadlo, D. J.; Davies, G. J., Structural and functional insight into human O-GlcNAcase. *Nat Chem Biol* **2017**, *13* (6), 610-612.
34. Zhang, Z.; Tan, E. P.; VandenHull, N. J.; Peterson, K. R.; Slawson, C., O-GlcNAcase expression is sensitive to changes in O-GlcNAc homeostasis. *Front Endocrinol* **2014**, *5*.
35. Khidekel, N.; Ficarro, S. B.; Clark, P. M.; Bryan, M. C.; Swaney, D. L.; Rexach, J. E.; Sun, Y. E.; Coon, J. J.; Peters, E. C.; Hsieh-Wilson, L. C., Probing the dynamics of O-GlcNAc glycosylation in the brain using quantitative proteomics. *Nat Chem Biol* **2007**, *3* (6), 339-48.
36. Zachara, N.; Akimoto, Y.; Hart, G. W., The O-GlcNAc Modification. In *Essentials of Glycobiology*, Varki, A.; Cummings, R. D.; Esko, J. D.; Stanley, P.; Hart, G. W.; Aebi, M.;

- Darvill, A. G.; Kinoshita, T.; Packer, N. H.; Prestegard, J. H.; Schnaar, R. L.; Seeberger, P. H., Eds. Cold Spring Harbor Laboratory Press: Cold Spring Harbor (NY), 2015; pp 239-251.
37. Woo, C. M.; Iavarone, A. T.; Spiciarich, D. R.; Palaniappan, K. K.; Bertozzi, C. R., Isotope-targeted glycoproteomics (IsoTaG): a mass-independent platform for intact N- and O-glycopeptide discovery and analysis. *Nat Meth* **2015**, *12* (6), 561-7.
38. Nilsson, J.; Halim, A.; Grahn, A.; Larson, G., Targeting the glycoproteome. *Glycoconj J* **2013**, *30*, 119-136.
39. Nilsson, J.; Ruetschi, U.; Halim, A.; Hesse, C.; Carlsohn, E.; Brinkmalm, G.; Larson, G., Enrichment of glycopeptides for glycan structure and attachment site identification. *Nat Meth* **2009**, *6* (11), 809-811.
40. Palaniappan, K. K.; Bertozzi, C. R., Chemical Glycoproteomics. *Chem Rev* **2016**, *116* (23), 14277-14306.
41. Boyce, M.; Carrico, I. S.; Ganguli, A. S.; Yu, S.; Hangauer, M. J.; Hubbard, S. C.; Kohler, J. J.; Bertozzi, C. R., Metabolic cross-talk allows labeling of O-linked  $\beta$ -N-acetylglucosamine-modified proteins via the N-acetylgalactosamine salvage pathway. *Proc Natl Acad Sci* **2011**, *108* (8), 3141-3146.
42. Zaro, B. W.; Yang, Y. Y.; Hang, H. C.; Pratt, M. R., Chemical reporters for fluorescent detection and identification of O-GlcNAc-modified proteins reveal glycosylation of the ubiquitin ligase NEDD4-1. *Proc Natl Acad Sci* **2011**, *108* (20), 8146-51.
43. Clark, P. M.; Dweck, J. F.; Mason, D. E.; Hart, C. R.; Buck, S. B.; Peters, E. C.; Agnew, B. J.; Hsieh-Wilson, L. C., Direct in-gel fluorescence detection and cellular imaging of O-GlcNAc-modified proteins. *J Am Chem Soc* **2008**, *130* (35), 11576-7.
44. Chuh, K. N.; Batt, A. R.; Zaro, B. W.; Darabedian, N.; Marotta, N. P.; Brennan, C. K.; Amirhekmat, A.; Pratt, M. R., The New Chemical Reporter 6-Alkynyl-6-deoxy-GlcNAc Reveals O-GlcNAc Modification of the Apoptotic Caspases That Can Block the Cleavage/Activation of Caspase-8. *J Am Chem Soc* **2017**, *139* (23), 7872-7885.
45. Chuh, K. N.; Zaro, B. W.; Piller, F.; Piller, V.; Pratt, M. R., Changes in metabolic chemical reporter structure yield a selective probe of O-GlcNAc modification. *J Am Chem Soc* **2014**, *136* (35), 12283-95.
46. Hao, Y.; Fan, X.; Shi, Y.; Zhang, C.; Sun, D.-e.; Qin, K.; Qin, W.; Zhou, W.; Chen, X., Next-generation unnatural monosaccharides reveal that ESRRB O-GlcNAcylation regulates pluripotency of mouse embryonic stem cells. *Nat Commun* **2019**, *10* (1), 4065.
47. Qin, W.; Qin, K.; Fan, X.; Peng, L.; Hong, W.; Zhu, Y.; Lv, P.; Du, Y.; Huang, R.; Han, M.; Cheng, B.; Liu, Y.; Zhou, W.; Wang, C.; Chen, X., Artificial Cysteine S-Glycosylation Induced by Per-O-Acetylated Unnatural Monosaccharides during Metabolic Glycan Labeling. *Angew Chem Int Ed* **2018**, *57* (7), 1817-1820.
48. Khidekel, N.; Arndt, S.; Lamarre-Vincent, N.; Lippert, A.; Poulin-Kerstien, K. G.; Ramakrishnan, B.; Qasba, P. K.; Hsieh-Wilson, L. C., A chemoenzymatic approach toward the rapid and sensitive detection of O-GlcNAc posttranslational modifications. *J Am Chem Soc* **2003**, *125* (52), 16162-3.
49. Thompson, J. W.; Griffin, M. E.; Hsieh-Wilson, L. C., Chapter Four - Methods for the Detection, Study, and Dynamic Profiling of O-GlcNAc Glycosylation. In *Methods in Enzymology*, Imperiali, B., Ed. Academic Press: 2018; Vol. 598, pp 101-135.
50. Darabedian, N.; Thompson, J. W.; Chuh, K. N.; Hsieh-Wilson, L. C.; Pratt, M. R., Optimization of Chemoenzymatic Mass Tagging by Strain-Promoted Cycloaddition (SPAAC) for the Determination of O-GlcNAc Stoichiometry by Western Blotting. *Biochemistry* **2018**, *57* (40), 5769-5774.
51. Greis, K. D.; Hayes, B. K.; Comer, F. I.; Kirk, M.; Barnes, S.; Lowary, T. L.; Hart, G. W., Selective detection and site-analysis of O-GlcNAc-modified glycopeptides by beta-elimination and tandem electrospray mass spectrometry. *Anal Biochem* **1996**, *234* (1), 38-49.



52. Woo, C. M.; Felix, A.; Byrd, W. E.; Zuegel, D. K.; Ishihara, M.; Azadi, P.; Iavarone, A. T.; Pitteri, S. J.; Bertozzi, C. R., Development of IsoTaG, a Chemical Glycoproteomics Technique for Profiling Intact N- and O-Glycopeptides from Whole Cell Proteomes. *J Proteome Res* **2017**, *16* (4), 1706-1718.
53. Hahne, H.; Sobotzki, N.; Nyberg, T.; Helm, D.; Borodkin, V. S.; van Aalten, D. M.; Agnew, B.; Kuster, B., Proteome wide purification and identification of O-GlcNAc-modified proteins using click chemistry and mass spectrometry. *J Proteome Res* **2013**, *12* (2), 927-36.
54. Rexach, J. E.; Rogers, C. J.; Yu, S.-H.; Tao, J.; Sun, Y. E.; Hsieh-Wilson, L. C., Quantification of O-glycosylation stoichiometry and dynamics using resolvable mass tags. *Nat Chem Biol* **2010**, *6* (9), 645-651.
55. Lund, P. J.; Elias, J. E.; Davis, M. M., Global Analysis of O-GlcNAc Glycoproteins in Activated Human T Cells. *J Immunol* **2016**, *197* (8), 3086-3098.
56. Yuzwa, S. A.; Macauley, M. S.; Heinonen, J. E.; Shan, X.; Dennis, R. J.; He, Y.; Whitworth, G. E.; Stubbs, K. A.; McEachern, E. J.; Davies, G. J.; Vocadlo, D. J., A potent mechanism-inspired O-GlcNAcase inhibitor that blocks phosphorylation of tau in vivo. *Nat Chem Biol* **2008**, *4* (8), 483-90.
57. Gloster, T. M.; Zandberg, W. F.; Heinonen, J. E.; Shen, D. L.; Deng, L.; Vocadlo, D. J., Hijacking a biosynthetic pathway yields a glycosyltransferase inhibitor within cells. *Nat Chem Biol* **2011**, *7* (3), 174-81.
58. Martin, S. E. S.; Tan, Z. W.; Itkonen, H. M.; Duveau, D. Y.; Paulo, J. A.; Janetzko, J.; Boutz, P. L.; Tork, L.; Moss, F. A.; Thomas, C. J.; Gygi, S. P.; Lazarus, M. B.; Walker, S., Structure-Based Evolution of Low Nanomolar O-GlcNAc Transferase Inhibitors. *J Am Chem Soc* **2018**, *140* (42), 13542-13545.
59. Ramirez, D. H.; Aonbangkhen, C.; Wu, H. Y.; Naftaly, J. A.; Tang, S.; O'Meara, T. R.; Woo, C. M., Engineering a Proximity-Directed O-GlcNAc Transferase for Selective Protein O-GlcNAcylation in Cells. *ACS Chem Biol* **2020**, *15* (4), 1059-1066.
60. Ge, Y.; Ramirez, D. H.; Yang, B.; D'Souza, A. K.; Aonbangkhen, C.; Wong, S.; Woo, C. M., Target protein deglycosylation in living cells by a nanobody-fused split O-GlcNAcase. *Nat Chem Biol* **2021**, *17* (5), 593-600.
61. Ramirez, D. H.; Ge, Y.; Woo, C. M., O-GlcNAc Engineering on a Target Protein in Cells with Nanobody-OGT and Nanobody-splitOGA. *Curr Protoc* **2021**, *1* (5), e117.
62. Gorelik, A.; Bartual, S. G.; Borodkin, V. S.; Varghese, J.; Ferenbach, A. T.; van Aalten, D. M. F., Genetic recoding to dissect the roles of site-specific protein O-GlcNAcylation. *Nat Struct Mol Biol* **2019**, *26* (11), 1071-1077.
63. Muyldermans, S.; Baral, T. N.; Retamozzo, V. C.; De Baetselier, P.; De Genst, E.; Kinne, J.; Leonhardt, H.; Magez, S.; Nguyen, V. K.; Revets, H.; Rothbauer, U.; Stijlemans, B.; Tillib, S.; Wernery, U.; Wyns, L.; Hassanzadeh-Ghassabeh, G.; Saerens, D., Camelid immunoglobulins and nanobody technology. *Vet Immunol Immunopathol* **2009**, *128* (1-3), 178-83.
64. Zhu, Y. Regulating O-GlcNacylation on Specific Proteins Using Rna Aptamers. 2019.
65. Vlastaridis, P.; Kyriakidou, P.; Chaliotis, A.; Van de Peer, Y.; Oliver, S. G.; Amoutzias, G. D., Estimating the total number of phosphoproteins and phosphorylation sites in eukaryotic proteomes. *Gigascience* **2017**, *6* (2), 1-11.
66. Fischer, E. H.; Krebs, E. G., Conversion of phosphorylase b to phosphorylase a in muscle extracts. *J Biol Chem* **1955**, *216* (1), 121-32.
67. Krebs, E. G.; Fischer, E. H., Phosphorylase activity of skeletal muscle extracts. *J Biol Chem* **1955**, *216* (1), 113-20.
68. Hayes, J. S.; Mayer, S. E., Regulation of guinea pig heart phosphorylase kinase by cAMP, protein kinase, and calcium. *Am J Physiol* **1981**, *240* (3), E340-9.

69. Olsen, J. V.; Blagoev, B.; Gnad, F.; Macek, B.; Kumar, C.; Mortensen, P.; Mann, M., Global, in vivo, and site-specific phosphorylation dynamics in signaling networks. *Cell* **2006**, *127* (3), 635-48.
70. Hardman, G.; Perkins, S.; Brownridge, P. J.; Clarke, C. J.; Byrne, D. P.; Campbell, A. E.; Kalyuzhnyy, A.; Myall, A.; Evers, P. A.; Jones, A. R.; Evers, C. E., Strong anion exchange-mediated phosphoproteomics reveals extensive human non-canonical phosphorylation. *EMBO J* **2019**, *38* (21), e100847.
71. Schwein, P. A.; Woo, C. M., The O-GlcNAc Modification on Kinases. *ACS Chem Biol* **2020**, *15* (3), 602-617.
72. Ubersax, J. A.; Ferrell, J. E., Jr., Mechanisms of specificity in protein phosphorylation. *Nat Rev Mol Cell Biol* **2007**, *8* (7), 530-41.
73. Ross, A. H.; Baltimore, D.; Eisen, H. N., Phosphotyrosine-containing proteins isolated by affinity chromatography with antibodies to a synthetic hapten. *Nature* **1981**, *294* (5842), 654-6.
74. Dias, W. B.; Cheung, W. D.; Wang, Z.; Hart, G. W., Regulation of calcium/calmodulin-dependent kinase IV by O-GlcNAc modification. *J Biol Chem* **2009**, *284* (32), 21327-37.
75. Tarrant, M. K.; Rho, H. S.; Xie, Z.; Jiang, Y. L.; Gross, C.; Culhane, J. C.; Yan, G.; Qian, J.; Ichikawa, Y.; Matsuoka, T.; Zachara, N.; Etzkorn, F. A.; Hart, G. W.; Jeong, J. S.; Blackshaw, S.; Zhu, H.; Cole, P. A., Regulation of CK2 by phosphorylation and O-GlcNAcylation revealed by semisynthesis. *Nat Chem Biol* **2012**, *8* (3), 262-9.
76. Yang, W. H.; Kim, J. E.; Nam, H. W.; Ju, J. W.; Kim, H. S.; Kim, Y. S.; Cho, J. W., Modification of p53 with O-linked N-acetylglucosamine regulates p53 activity and stability. *Nat Cell Biol* **2006**, *8* (10), 1074-83.
77. Chou, T. Y.; Hart, G. W.; Dang, C. V., c-Myc is glycosylated at threonine 58, a known phosphorylation site and a mutational hot spot in lymphomas. *J Biol Chem* **1995**, *270* (32), 18961-5.
78. Yuzwa, S. A.; Shan, X.; Macauley, M. S.; Clark, T.; Skorobogatko, Y.; Vosseller, K.; Vocadlo, D. J., Increasing O-GlcNAc slows neurodegeneration and stabilizes tau against aggregation. *Nat Chem Biol* **2012**, *8* (4), 393-9.
79. Brister, M. A.; Pandey, A. K.; Bielska, A. A.; Zondlo, N. J., OGlcNAcylation and phosphorylation have opposing structural effects in tau: phosphothreonine induces particular conformational order. *J Am Chem Soc* **2014**, *136* (10), 3803-16.
80. Chen, Y. X.; Du, J. T.; Zhou, L. X.; Liu, X. H.; Zhao, Y. F.; Nakanishi, H.; Li, Y. M., Alternative O-GlcNAcylation/O-phosphorylation of Ser16 induce different conformational disturbances to the N terminus of murine estrogen receptor beta. *Chem Biol* **2006**, *13* (9), 937-44.
81. Mao, X.; Zhang, D.; Tao, T.; Liu, X.; Sun, X.; Wang, Y.; Shen, A., O-GlcNAc glycosylation of p27(kip1) promotes astrocyte migration and functional recovery after spinal cord contusion. *Exp Cell Res* **2015**, *339* (2), 197-205.
82. Holt, G. D.; Haltiwanger, R. S.; Torres, C. R.; Hart, G. W., Erythrocytes contain cytoplasmic glycoproteins. O-linked GlcNAc on Band 4.1. *J Biol Chem* **1987**, *262* (31), 14847-50.
83. Wang, Z.; Gucek, M.; Hart, G. W., Cross-talk between GlcNAcylation and phosphorylation: site-specific phosphorylation dynamics in response to globally elevated O-GlcNAc. *Proc Natl Acad Sci U S A* **2008**, *105* (37), 13793-8.
84. Lefebvre, T.; Alonso, C.; Mahboub, S.; Dupire, M. J.; Zanetta, J. P.; Caillet-Boudin, M. L.; Michalski, J. C., Effect of okadaic acid on O-linked N-acetylglucosamine levels in a neuroblastoma cell line. *Biochim Biophys Acta* **1999**, *1472* (1-2), 71-81.
85. Griffith, L. S.; Schmitz, B., O-linked N-acetylglucosamine levels in cerebellar neurons respond reciprocally to perturbations of phosphorylation. *Eur J Biochem* **1999**, *262* (3), 824-31.

86. Leney, A. C.; Rafie, K.; van Aalten, D. M. F.; Heck, A. J. R., Direct Monitoring of Protein O-GlcNAcylation by High-Resolution Native Mass Spectrometry. *ACS Chem Biol* **2017**, *12* (8), 2078-2084.
87. Slawson, C.; Lakshmanan, T.; Knapp, S.; Hart, G. W., A mitotic GlcNAcylation/phosphorylation signaling complex alters the posttranslational state of the cytoskeletal protein vimentin. *Mol Biol Cell* **2008**, *19* (10), 4130-40.
88. Cheung, W. D.; Hart, G. W., AMP-activated protein kinase and p38 MAPK activate O-GlcNAcylation of neuronal proteins during glucose deprivation. *J Biol Chem* **2008**, *283* (19), 13009-20.
89. Dias, W. B.; Cheung, W. D.; Hart, G. W., O-GlcNAcylation of kinases. *Biochem Biophys Res Commun* **2012**, *422* (2), 224-8.
90. Trinidad, J. C.; Schoepfer, R.; Burlingame, A. L.; Medzihradsky, K. F., N- and O-glycosylation in the murine synaptosome. *Mol Cell Proteomics* **2013**, *12* (12), 3474-88.
91. Li, J.; Li, Z.; Duan, X.; Qin, K.; Dang, L.; Sun, S.; Cai, L.; Hsieh-Wilson, L. C.; Wu, L.; Yi, W., An Isotope-Coded Photocleavable Probe for Quantitative Profiling of Protein O-GlcNAcylation. *ACS Chem Biol* **2019**, *14* (1), 4-10.
92. Alfaro, J. F.; Gong, C. X.; Monroe, M. E.; Aldrich, J. T.; Clauss, T. R.; Purvine, S. O.; Wang, Z.; Camp, D. G., 2nd; Shabanowitz, J.; Stanley, P.; Hart, G. W.; Hunt, D. F.; Yang, F.; Smith, R. D., Tandem mass spectrometry identifies many mouse brain O-GlcNAcylated proteins including EGF domain-specific O-GlcNAc transferase targets. *Proc Natl Acad Sci U S A* **2012**, *109* (19), 7280-5.
93. Qin, W.; Lv, P.; Fan, X.; Quan, B.; Zhu, Y.; Qin, K.; Chen, Y.; Wang, C.; Chen, X., Quantitative time-resolved chemoproteomics reveals that stable O-GlcNAc regulates box C/D snoRNP biogenesis. *Proc Natl Acad Sci U S A* **2017**, *114* (33), E6749-E6758.
94. Ma, J.; Liu, T.; Wei, A. C.; Banerjee, P.; O'Rourke, B.; Hart, G. W., O-GlcNAc Profiling Identifies Widespread O-Linked beta-N-Acetylglucosamine Modification (O-GlcNAcylation) in Oxidative Phosphorylation System Regulating Cardiac Mitochondrial Function. *J Biol Chem* **2015**, *290* (49), 29141-53.
95. Wang, X.; Yuan, Z. F.; Fan, J.; Karch, K. R.; Ball, L. E.; Denu, J. M.; Garcia, B. A., A Novel Quantitative Mass Spectrometry Platform for Determining Protein O-GlcNAcylation Dynamics. *Mol Cell Proteomics* **2016**, *15* (7), 2462-75.
96. Xiao, H.; Chen, W.; Smeekens, J. M.; Wu, R., An enrichment method based on synergistic and reversible covalent interactions for large-scale analysis of glycoproteins. *Nat Commun* **2018**, *9* (1), 1692.
97. Xie, S.; Jin, N.; Gu, J.; Shi, J.; Sun, J.; Chu, D.; Zhang, L.; Dai, C. L.; Gu, J. H.; Gong, C. X.; Iqbal, K.; Liu, F., O-GlcNAcylation of protein kinase A catalytic subunits enhances its activity: a mechanism linked to learning and memory deficits in Alzheimer's disease. *Aging Cell* **2016**, *15* (3), 455-64.
98. Gandy, J. C.; Rountree, A. E.; Bijur, G. N., Akt1 is dynamically modified with O-GlcNAc following treatments with PUGNAc and insulin-like growth factor-1. *FEBS Lett* **2006**, *580* (13), 3051-8.
99. Whelan, S. A.; Dias, W. B.; Thiruneelakantapillai, L.; Lane, M. D.; Hart, G. W., Regulation of insulin receptor substrate 1 (IRS-1)/AKT kinase-mediated insulin signaling by O-Linked beta-N-acetylglucosamine in 3T3-L1 adipocytes. *J Biol Chem* **2010**, *285* (8), 5204-11.
100. Shi, J.; Gu, J. H.; Dai, C. L.; Gu, J.; Jin, X.; Sun, J.; Iqbal, K.; Liu, F.; Gong, C. X., O-GlcNAcylation regulates ischemia-induced neuronal apoptosis through AKT signaling. *Sci Rep* **2015**, *5*, 14500.
101. Hart, J. R.; Vogt, P. K., Phosphorylation of AKT: a mutational analysis. *Oncotarget* **2011**, *2* (6), 467-76.

102. Park, S. Y.; Ryu, J.; Lee, W., O-GlcNAc modification on IRS-1 and Akt2 by PUGNAc inhibits their phosphorylation and induces insulin resistance in rat primary adipocytes. *Exp Mol Med* **2005**, *37* (3), 220-9.
103. Niu, Y.; Xia, Y.; Wang, J.; Shi, X., O-GlcNAcylation promotes migration and invasion in human ovarian cancer cells via the RhoA/ROCK/MLC pathway. *Mol Med Rep* **2017**, *15* (4), 2083-2089.
104. Kaasik, K.; Kivimae, S.; Allen, J. J.; Chalkley, R. J.; Huang, Y.; Baer, K.; Kissel, H.; Burlingame, A. L.; Shokat, K. M.; Ptacek, L. J.; Fu, Y. H., Glucose sensor O-GlcNAcylation coordinates with phosphorylation to regulate circadian clock. *Cell Metab* **2013**, *17* (2), 291-302.
105. Wang, Z.; Pandey, A.; Hart, G. W., Dynamic interplay between O-linked N-acetylglucosaminylation and glycogen synthase kinase-3-dependent phosphorylation. *Mol Cell Proteomics* **2007**, *6* (8), 1365-79.
106. Kazemi, Z.; Chang, H.; Haserodt, S.; McKen, C.; Zachara, N. E., O-linked beta-N-acetylglucosamine (O-GlcNAc) regulates stress-induced heat shock protein expression in a GSK-3beta-dependent manner. *J Biol Chem* **2010**, *285* (50), 39096-107.
107. Qiu, H.; Liu, F.; Tao, T.; Zhang, D.; Liu, X.; Zhu, G.; Xu, Z.; Ni, R.; Shen, A., Modification of p27 with O-linked N-acetylglucosamine regulates cell proliferation in hepatocellular carcinoma. *Mol Carcinog* **2017**, *56* (1), 258-271.
108. Pyo, K. E.; Kim, C. R.; Lee, M.; Kim, J. S.; Kim, K. I.; Baek, S. H., ULK1 O-GlcNAcylation Is Crucial for Activating VPS34 via ATG14L during Autophagy Initiation. *Cell Rep* **2018**, *25* (10), 2878-2890 e4.
109. Bullen, J. W.; Balsbaugh, J. L.; Chanda, D.; Shabanowitz, J.; Hunt, D. F.; Neumann, D.; Hart, G. W., Cross-talk between two essential nutrient-sensitive enzymes: O-GlcNAc transferase (OGT) and AMP-activated protein kinase (AMPK). *J Biol Chem* **2014**, *289* (15), 10592-606.
110. Boutros, T.; Chevet, E.; Metrakos, P., Mitogen-activated protein (MAP) kinase/MAP kinase phosphatase regulation: roles in cell growth, death, and cancer. *Pharmacol Rev* **2008**, *60* (3), 261-310.
111. Cross, T. G.; Scheel-Toellner, D.; Henriquez, N. V.; Deacon, E.; Salmon, M.; Lord, J. M., Serine/threonine protein kinases and apoptosis. *Exp Cell Res* **2000**, *256* (1), 34-41.
112. Liu, F.; Shi, J.; Tanimukai, H.; Gu, J.; Gu, J.; Grundke-Iqbal, I.; Iqbal, K.; Gong, C. X., Reduced O-GlcNAcylation links lower brain glucose metabolism and tau pathology in Alzheimer's disease. *Brain* **2009**, *132* (Pt 7), 1820-32.
113. Bennmann, D.; Weidemann, W.; Thate, A.; Kreuzmann, D.; Horstkorte, R., Aberrant O-GlcNAcylation disrupts GNE enzyme activity in GNE myopathy. *FEBS J* **2016**, *283* (12), 2285-94.
114. Chaiyawat, P.; Chokchaichamnankit, D.; Lirdprapamongkol, K.; Srisomsap, C.; Svasti, J.; Champattanachai, V., Alteration of O-GlcNAcylation affects serine phosphorylation and regulates gene expression and activity of pyruvate kinase M2 in colorectal cancer cells. *Oncol Rep* **2015**, *34* (4), 1933-1942.
115. Yi, W.; Clark, P. M.; Mason, D. E.; Keenan, M. C.; Hill, C.; Goddard III, W. A.; Peters, E. C.; Driggers, E. M.; Hsieh-Wilson, L. C., Phosphofructokinase 1 Glycosylation Regulates Cell Growth and Metabolism *Science* **2012**, *337*, 975-980.
116. Wells, L.; Kreppel, L. K.; Comer, F. I.; Wadzinski, B. E.; Hart, G. W., O-GlcNAc transferase is in a functional complex with protein phosphatase 1 catalytic subunits. *J Biol Chem* **2004**, *279* (37), 38466-70.
117. Sager, R. A.; Woodford, M. R.; Backe, S. J.; Makedon, A. M.; Baker-Williams, A. J.; DiGregorio, B. T.; Loiselle, D. R.; Haystead, T. A.; Zachara, N. E.; Prodromou, C.; Bourboulia, D.; Schmidt, L. S.; Linehan, W. M.; Bratslavsky, G.; Mollapour, M., Post-translational Regulation of FNIP1 Creates a Rheostat for the Molecular Chaperone Hsp90. *Cell Rep* **2019**, *26* (5), 1344-1356 e5.

118. Vicart, A.; Lefebvre, T.; Imbert, J.; Fernandez, A.; Kahn-Perles, B., Increased chromatin association of Sp1 in interphase cells by PP2A-mediated dephosphorylations. *J Mol Biol* **2006**, *364* (5), 897-908.
119. Trinidad, J. C.; Barkan, D. T.; Gullledge, B. F.; Thalhammer, A.; Sali, A.; Schoepfer, R.; Burlingame, A. L., Global identification and characterization of both O-GlcNAcylation and phosphorylation at the murine synapse. *Mol Cell Proteomics* **2012**, *11* (8), 215-29.
120. Zhao, Y.; Tang, Z.; Shen, A.; Tao, T.; Wan, C.; Zhu, X.; Huang, J.; Zhang, W.; Xia, N.; Wang, S.; Cui, S.; Zhang, D., The Role of PTP1B O-GlcNAcylation in Hepatic Insulin Resistance. *Int J Mol Sci* **2015**, *16* (9), 22856-69.
121. Koo, J.; Bahk, Y. Y., In vivo putative O-GlcNAcylation of human SCP1 and evidence for possible role of its N-terminal disordered structure. *BMB Rep* **2014**, *47* (10), 593-8.
122. Roos, D.; Loos, J. A., Changes in the carbohydrate metabolism of mitogenically stimulated human peripheral lymphocytes. II. Relative importance of glycolysis and oxidative phosphorylation on phytohaemagglutinin stimulation. *Exp Cell Res* **1973**, *77* (1), 127-35.
123. Nakaya, M.; Xiao, Y.; Zhou, X.; Chang, J. H.; Chang, M.; Cheng, X.; Blonska, M.; Lin, X.; Sun, S. C., Inflammatory T cell responses rely on amino acid transporter ASCT2 facilitation of glutamine uptake and mTORC1 kinase activation. *Immunity* **2014**, *40* (5), 692-705.
124. Jones, R. G.; Thompson, C. B., Revving the engine: signal transduction fuels T cell activation. *Immunity* **2007**, *27* (2), 173-8.
125. DeBerardinis, R. J.; Cheng, T., Q's next: the diverse functions of glutamine in metabolism, cell biology and cancer. *Oncogene* **2010**, *29* (3), 313-24.
126. Shi, L.; Tu, B. P., Acetyl-CoA and the regulation of metabolism: mechanisms and consequences. *Curr Opin Cell Biol* **2015**, *33*, 125-31.
127. Chiaradonna, F.; Ricciardiello, F.; Palorini, R., The Nutrient-Sensing Hexosamine Biosynthetic Pathway as the Hub of Cancer Metabolic Rewiring. *Cells* **2018**, *7* (6).
128. Kearse, K. P.; Hart, G. W., Lymphocyte activation induces rapid changes in nuclear and cytoplasmic glycoproteins. *Proc Natl Acad Sci U S A* **1991**, *88* (5), 1701-5.
129. Golks, A.; Tran, T. T.; Goetschy, J. F.; Guerini, D., Requirement for O-linked N-acetylglucosaminyltransferase in lymphocytes activation. *EMBO J* **2007**, *26* (20), 4368-79.
130. Ai, W.; Li, H.; Song, N.; Li, L.; Chen, H., Optimal method to stimulate cytokine production and its use in immunotoxicity assessment. *Int J Environ Res Public Health* **2013**, *10* (9), 3834-42.
131. Tan, Z. W.; Fei, G.; Paulo, J. A.; Bellaousov, S.; Martin, S. E. S.; Dubeau, D. Y.; Thomas, C. J.; Gygi, S. P.; Boutz, P. L.; Walker, S., O-GlcNAc regulates gene expression by controlling detained intron splicing. *Nucleic Acids Res* **2020**, *48* (10), 5656-5669.
132. Chan, A. C.; Iwashima, M.; Turck, C. W.; Weiss, A., ZAP-70: a 70 kd protein-tyrosine kinase that associates with the TCR zeta chain. *Cell* **1992**, *71* (4), 649-62.
133. Bradshaw, J. M., The Src, Syk, and Tec family kinases: distinct types of molecular switches. *Cell Signal* **2010**, *22* (8), 1175-84.
134. Tsang, E.; Giannetti, A. M.; Shaw, D.; Dinh, M.; Tse, J. K.; Gandhi, S.; Ho, H.; Wang, S.; Papp, E.; Bradshaw, J. M., Molecular mechanism of the Syk activation switch. *J Biol Chem* **2008**, *283* (47), 32650-9.
135. Clark, P. M.; Rexach, J. E.; Hsieh-Wilson, L. C., Visualization of O-GlcNAc glycosylation stoichiometry and dynamics using resolvable poly(ethylene glycol) mass tags. *Curr Protoc Chem Biol* **2013**, *5* (4), 281-302.
136. Qin, W.; Qin, K.; Fan, X.; Peng, L.; Hong, W.; Zhu, Y.; Lv, P.; Du, Y.; Huang, R.; Han, M.; Cheng, B.; Liu, Y.; Zhou, W.; Wang, C.; Chen, X., Artificial Cysteine S-Glycosylation Induced by Per-O-Acetylated Unnatural Monosaccharides during Metabolic Glycan Labeling. *Angew Chem Int Ed Engl* **2018**, *57* (7), 1817-1820.

137. Rexach, J. E.; Clark, P. M.; Mason, D. E.; Neve, R. L.; Peters, E. C.; Hsieh-Wilson, L. C., Dynamic O-GlcNAc modification regulates CREB-mediated gene expression and memory formation. *Nat Chem Biol* **2012**, *8* (3), 253-61.
138. De Leon, C. A.; Levine, P. M.; Craven, T. W.; Pratt, M. R., The Sulfur-Linked Analogue of O-GlcNAc (S-GlcNAc) Is an Enzymatically Stable and Reasonable Structural Surrogate for O-GlcNAc at the Peptide and Protein Levels. *Biochemistry* **2017**, *56* (27), 3507-3517.
139. Maynard, J. C.; Burlingame, A. L.; Medzihradszky, K. F., Cysteine S-linked N-acetylglucosamine (S-GlcNAcylation), A New Post-translational Modification in Mammals. *Mol Cell Proteomics* **2016**, *15* (11), 3405-3411.
140. Xu, S.; Zheng, J.; Xiao, H.; Wu, R., Simultaneously Identifying and Distinguishing Glycoproteins with O-GlcNAc and O-GalNAc (the Tn Antigen) in Human Cancer Cells. *Anal Chem* **2022**, *94* (7), 3343-3351.
141. Thompson, J. W.; Griffin, M. E.; Hsieh-Wilson, L. C., Methods for the Detection, Study, and Dynamic Profiling of O-GlcNAc Glycosylation. *Methods Enzymol* **2018**, *598*, 101-135.
142. Schwein, P. A.; Ge, Y.; Yang, B.; D'Souza, A.; Mody, A.; Shen, D.; Woo, C. M., Writing and Erasing O-GlcNAc on Casein Kinase 2 Alpha Alters the Phosphoproteome. *ACS Chemical Biology* **2022**.
143. Borgo, C.; Ruzzene, M., Role of protein kinase CK2 in antitumor drug resistance. *J Exp Clin Cancer Res* **2019**, *38* (1), 287.
144. Gotz, C.; Montenarh, M., Protein kinase CK2 in development and differentiation. *Biomed Rep* **2017**, *6* (2), 127-133.
145. Meggio, F.; Pinna, L. A., One-thousand-and-one substrates of protein kinase CK2? *FASEB J* **2003**, *17* (3), 349-68.
146. Bodenbach, L.; Fauss, J.; Robitzki, A.; Krehan, A.; Lorenz, P.; Lozeman, F. J.; Pyerin, W., Recombinant human casein kinase II. A study with the complete set of subunits (alpha, alpha' and beta), site-directed autophosphorylation mutants and a bicistronically expressed holoenzyme. *Eur J Biochem* **1994**, *220* (1), 263-73.
147. Marchiori, F.; Meggio, F.; Marin, O.; Borin, G.; Calderan, A.; Ruzza, P.; Pinna, L. A., Synthetic peptide substrates for casein kinase 2. Assessment of minimum structural requirements for phosphorylation. *Biochim Biophys Acta* **1988**, *971* (3), 332-8.
148. Meggio, F.; Marin, O.; Pinna, L. A., Substrate specificity of protein kinase CK2. *Cell Mol Biol Res* **1994**, *40* (5-6), 401-9.
149. Sarno, S.; Vaglio, P.; Meggio, F.; Issinger, O. G.; Pinna, L. A., Protein kinase CK2 mutants defective in substrate recognition. Purification and kinetic analysis. *J Biol Chem* **1996**, *271* (18), 10595-601.
150. Meek, D. W.; Simon, S.; Kikkawa, U.; Eckhart, W., The p53 tumour suppressor protein is phosphorylated at serine 389 by casein kinase II. *EMBO J* **1990**, *9* (10), 3253-60.
151. St-Denis, N.; Gabriel, M.; Turowec, J. P.; Gloor, G. B.; Li, S. S.; Gingras, A. C.; Litchfield, D. W., Systematic investigation of hierarchical phosphorylation by protein kinase CK2. *J Proteomics* **2015**, *118*, 49-62.
152. Niefind, K.; Guerra, B.; Ermakowa, I.; Issinger, O. G., Crystal structure of human protein kinase CK2: insights into basic properties of the CK2 holoenzyme. *EMBO J* **2001**, *20* (19), 5320-31.
153. Nguyen le, X. T.; Mitchell, B. S., Akt activation enhances ribosomal RNA synthesis through casein kinase II and TIF-IA. *Proc Natl Acad Sci U S A* **2013**, *110* (51), 20681-6.
154. Donella-Deana, A.; Cesaro, L.; Sarno, S.; Ruzzene, M.; Brunati, A. M.; Marin, O.; Vilik, G.; Doherty-Kirby, A.; Lajoie, G.; Litchfield, D. W.; Pinna, L. A., Tyrosine phosphorylation of protein kinase CK2 by Src-related tyrosine kinases correlates with increased catalytic activity. *Biochem J* **2003**, *372* (Pt 3), 841-9.

155. Litchfield, D. W.; Luscher, B.; Lozeman, F. J.; Eisenman, R. N.; Krebs, E. G., Phosphorylation of casein kinase II by p34cdc2 in vitro and at mitosis. *J Biol Chem* **1992**, *267* (20), 13943-51.
156. Bosc, D. G.; Slominski, E.; Sichler, C.; Litchfield, D. W., Phosphorylation of casein kinase II by p34cdc2. Identification of phosphorylation sites using phosphorylation site mutants in vitro. *J Biol Chem* **1995**, *270* (43), 25872-8.
157. Shen, H.; Zhao, X.; Chen, J.; Qu, W.; Huang, X.; Wang, M.; Shao, Z.; Shu, Q.; Li, X., O-GlcNAc transferase Ogt regulates embryonic neuronal development through modulating Wnt/beta-catenin signaling. *Hum Mol Genet* **2021**.
158. Ge, Y.; Woo, C. M., Writing and erasing O-GlcNAc from target proteins in cells. *Biochem Soc Trans* **2021**.
159. Fridy, P. C.; Li, Y.; Keegan, S.; Thompson, M. K.; Nudelman, I.; Scheid, J. F.; Oeffinger, M.; Nussenzweig, M. C.; Fenyo, D.; Chait, B. T.; Rout, M. P., A robust pipeline for rapid production of versatile nanobody repertoires. *Nat Methods* **2014**, *11* (12), 1253-60.
160. Meggio, F.; Marin, O.; Boschetti, M.; Sarno, S.; Pinna, L. A., HIV-1 Rev transactivator: a beta-subunit directed substrate and effector of protein kinase CK2. *Mol Cell Biochem* **2001**, *227* (1-2), 145-51.
161. Poletto, G.; Vilardell, J.; Marin, O.; Pagano, M. A.; Cozza, G.; Sarno, S.; Falques, A.; Itarte, E.; Pinna, L. A.; Meggio, F., The regulatory beta subunit of protein kinase CK2 contributes to the recognition of the substrate consensus sequence. A study with an eIF2 beta-derived peptide. *Biochemistry* **2008**, *47* (32), 8317-25.
162. Bian, Y.; Ye, M.; Wang, C.; Cheng, K.; Song, C.; Dong, M.; Pan, Y.; Qin, H.; Zou, H., Global screening of CK2 kinase substrates by an integrated phosphoproteomics workflow. *Sci Rep* **2013**, *3*, 3460.
163. Rusin, S. F.; Adamo, M. E.; Kettenbach, A. N., Identification of Candidate Casein Kinase 2 Substrates in Mitosis by Quantitative Phosphoproteomics. *Front Cell Dev Biol* **2017**, *5*, 97.
164. Khan, D. H.; He, S.; Yu, J.; Winter, S.; Cao, W.; Seiser, C.; Davie, J. R., Protein kinase CK2 regulates the dimerization of histone deacetylase 1 (HDAC1) and HDAC2 during mitosis. *J Biol Chem* **2013**, *288* (23), 16518-16528.
165. Gavish-Izakson, M.; Velpula, B. B.; Elkon, R.; Prados-Carvajal, R.; Barnabas, G. D.; Ugalde, A. P.; Agami, R.; Geiger, T.; Huertas, P.; Ziv, Y.; Shiloh, Y., Nuclear poly(A)-binding protein 1 is an ATM target and essential for DNA double-strand break repair. *Nucleic Acids Res* **2018**, *46* (2), 730-747.
166. Szklarczyk, D.; Gable, A. L.; Lyon, D.; Junge, A.; Wyder, S.; Huerta-Cepas, J.; Simonovic, M.; Doncheva, N. T.; Morris, J. H.; Bork, P.; Jensen, L. J.; Mering, C. V., STRING v11: protein-protein association networks with increased coverage, supporting functional discovery in genome-wide experimental datasets. *Nucleic Acids Res* **2019**, *47* (D1), D607-D613.
167. Sarno, S.; Vaglio, P.; Marin, O.; Issinger, O. G.; Ruffato, K.; Pinna, L. A., Mutational analysis of residues implicated in the interaction between protein kinase CK2 and peptide substrates. *Biochemistry* **1997**, *36* (39), 11717-24.
168. Mochida, S., Regulation of alpha-endosulfine, an inhibitor of protein phosphatase 2A, by multisite phosphorylation. *FEBS J* **2014**, *281* (4), 1159-69.
169. Rowbotham, S. P.; Barki, L.; Neves-Costa, A.; Santos, F.; Dean, W.; Hawkes, N.; Choudhary, P.; Will, W. R.; Webster, J.; Oxley, D.; Green, C. M.; Varga-Weisz, P.; Mermoud, J. E., Maintenance of silent chromatin through replication requires SWI/SNF-like chromatin remodeler SMARCD1. *Mol Cell* **2011**, *42* (3), 285-96.
170. Lee, J. H.; Liu, R.; Li, J.; Zhang, C.; Wang, Y.; Cai, Q.; Qian, X.; Xia, Y.; Zheng, Y.; Piao, Y.; Chen, Q.; de Groot, J. F.; Jiang, T.; Lu, Z., Stabilization of phosphofructokinase 1 platelet isoform by AKT promotes tumorigenesis. *Nat Commun* **2017**, *8* (1), 949.

171. Li, X.; Sun, L.; Yan, G.; Yan, X., PFKF facilitates ATG4B phosphorylation during amino acid deprivation-induced autophagy. *Cell Signal* **2021**, *82*, 109956.
172. Mertins, P.; Qiao, J. W.; Patel, J.; Udeshi, N. D.; Clauser, K. R.; Mani, D. R.; Burgess, M. W.; Gillette, M. A.; Jaffe, J. D.; Carr, S. A., Integrated proteomic analysis of post-translational modifications by serial enrichment. *Nat Methods* **2013**, *10* (7), 634-7.
173. Dulla, K.; Daub, H.; Hornberger, R.; Nigg, E. A.; Korner, R., Quantitative site-specific phosphorylation dynamics of human protein kinases during mitotic progression. *Mol Cell Proteomics* **2010**, *9* (6), 1167-81.
174. Uberall, F.; Giselsbrecht, S.; Hellbert, K.; Fresser, F.; Bauer, B.; Gschwendt, M.; Grunicke, H. H.; Baier, G., Conventional PKC-alpha, novel PKC-epsilon and PKC-theta, but not atypical PKC-lambda are MARCKS kinases in intact NIH 3T3 fibroblasts. *J Biol Chem* **1997**, *272* (7), 4072-8.
175. Chen, X.; Rotenberg, S. A., PhosphoMARCKS drives motility of mouse melanoma cells. *Cell Signal* **2010**, *22* (7), 1097-103.
176. Pospisilova, S.; Brazda, V.; Kucharikova, K.; Luciani, M. G.; Hupp, T. R.; Skladal, P.; Palecek, E.; Vojtesek, B., Activation of the DNA-binding ability of latent p53 protein by protein kinase C is abolished by protein kinase CK2. *Biochem J* **2004**, *378* (Pt 3), 939-47.
177. Lee, Y. H.; Park, J. W.; Bae, Y. S., Regulation of protein kinase CK2 catalytic activity by protein kinase C and phospholipase D2. *Biochimie* **2016**, *121*, 131-9.
178. Bren, G. D.; Pennington, K. N.; Paya, C. V., PKC-zeta-associated CK2 participates in the turnover of free I $\kappa$ B $\alpha$ . *J Mol Biol* **2000**, *297* (5), 1245-58.
179. Jurkin, J.; Zupkovitz, G.; Lagger, S.; Grausenburger, R.; Hagelkruys, A.; Kenner, L.; Seiser, C., Distinct and redundant functions of histone deacetylases HDAC1 and HDAC2 in proliferation and tumorigenesis. *Cell Cycle* **2011**, *10* (3), 406-12.
180. Stemmer, C.; Schwander, A.; Bauw, G.; Fojan, P.; Grasser, K. D., Protein kinase CK2 differentially phosphorylates maize chromosomal high mobility group B (HMGB) proteins modulating their stability and DNA interactions. *J Biol Chem* **2002**, *277* (2), 1092-8.
181. Wu, L.; Luo, K.; Lou, Z.; Chen, J., MDC1 regulates intra-S-phase checkpoint by targeting NBS1 to DNA double-strand breaks. *Proc Natl Acad Sci U S A* **2008**, *105* (32), 11200-5.
182. Rehage, N.; Davydova, E.; Conrad, C.; Behrens, G.; Maiser, A.; Stehlein, J. E.; Brenner, S.; Klein, J.; Jeridi, A.; Hoffmann, A.; Lee, E.; Dianzani, U.; Willemsen, R.; Feederle, R.; Reiche, K.; Hackermuller, J.; Leonhardt, H.; Sharma, S.; Niessing, D.; Heissmeyer, V., Binding of NUFIP2 to Roquin promotes recognition and regulation of ICOS mRNA. *Nat Commun* **2018**, *9* (1), 299.
183. Bardoni, B.; Castets, M.; Huot, M. E.; Schenck, A.; Adinolfi, S.; Corbin, F.; Pastore, A.; Khandjian, E. W.; Mandel, J. L., 82-FIP, a novel FMRP (fragile X mental retardation protein) interacting protein, shows a cell cycle-dependent intracellular localization. *Hum Mol Genet* **2003**, *12* (14), 1689-98.
184. Woo, C. M.; Bertozzi, C. R., Isotope Targeted Glycoproteomics (IsoTaG) to Characterize Intact, Metabolically Labeled Glycopeptides from Complex Proteomes. *Curr Protoc Chem Biol* **2016**, *8* (1), 59-82.
185. Yang, B.; Li, R.; Liu, P. N.; Geng, X.; Mooney, B. P.; Chen, C.; Cheng, J.; Fritsche, K. L.; Beversdorf, D. Q.; Lee, J. C.; Sun, G. Y.; Greenlief, C. M., Quantitative Proteomics Reveals Docosahexaenoic Acid-Mediated Neuroprotective Effects in Lipopolysaccharide-Stimulated Microglial Cells. *J Proteome Res* **2020**, *19* (6), 2236-2246.
186. Zhong, J.; Martinez, M.; Sengupta, S.; Lee, A.; Wu, X.; Chaerkady, R.; Chatterjee, A.; O'Meally, R. N.; Cole, R. N.; Pandey, A.; Zachara, N. E., Quantitative phosphoproteomics reveals crosstalk between phosphorylation and O-GlcNAc in the DNA damage response pathway. *Proteomics* **2015**, *15* (2-3), 591-607.



187. Litchfield, D. W., Protein kinase CK2: structure, regulation and role in cellular decisions of life and death. *Biochem J* **2003**, 369 (Pt 1), 1-15.
188. Ong, Q.; Han, W.; Yang, X., O-GlcNAc as an Integrator of Signaling Pathways. *Front Endocrinol (Lausanne)* **2018**, 9, 599.
189. Li, X.; Gong, W.; Wang, H.; Li, T.; Attri, K. S.; Lewis, R. E.; Kalil, A. C.; Bhinderwala, F.; Powers, R.; Yin, G.; Herring, L. E.; Asara, J. M.; Lei, Y. L.; Yang, X.; Rodriguez, D. A.; Yang, M.; Green, D. R.; Singh, P. K.; Wen, H., O-GlcNAc Transferase Suppresses Inflammation and Necroptosis by Targeting Receptor-Interacting Serine/Threonine-Protein Kinase 3. *Immunity* **2019**, 50 (3), 576-590 e6.
190. Lin, Y., RIP1-Mediated Signaling Pathways in Cell Survival and Death Control. *Necrotic Cell Death* **2014**, 23–43.
191. Hadchouel, J.; Ellison, D. H.; Gamba, G., Regulation of Renal Electrolyte Transport by WNK and SPAK-OSR1 Kinases. *Annu Rev Physiol* **2016**, 78, 367-89.